THE HONG KONG
POLYTECHNIC UNIVERSITY
香港理工大學
Pao Yue-kong Library
包玉剛圖書館

Copyright Undertaking

This thesis is protected by copyright, with all rights reserved.

By reading and using the thesis, the reader understands and agrees to the following terms:

1. The reader will abide by the rules and legal ordinances governing copyright regarding the use of the thesis.
2. The reader will use the thesis for the purpose of research or private study only and not for distribution or further reproduction or any other purpose.
3. The reader agrees to indemnify and hold the University harmless from and against any loss, damage, cost, liability or expenses arising from copyright infringement or unauthorized usage.

IMPORTANT

If you have reasons to believe that any materials in this thesis are deemed not suitable to be distributed in this form, or a copyright owner having difficulty with the material being included in our database, please contact lbsys@polyu.edu.hk providing details. The Library will look into your claim and consider taking remedial action upon receipt of the written requests.

Pao Yue-kong Library, The Hong Kong Polytechnic University, Hung Hom, Kowloon, Hong Kong

http://www.lib.polyu.edu.hk

DEVELOPMENT OF ENCAPSULATION METHODS FOR ORGANIC-BASED PHASE CHANGE MATERIALS IN WATER

TAN SUQING

PhD

The Hong Kong Polytechnic University

2019

The Hong Kong Polytechnic University
Department of Applied Biology and
Chemical Technology

Development of Encapsulation Methods for Organic-based Phase Change Materials in Water

TAN SUQING

A thesis submitted in partial fulfilment for the requirements for the degree of Doctor of Philosophy

May 2019

Certificate of Originality

I hereby declare that this thesis is my own work and that, to the best of my knowledge and belief, it reproduces no material previously published or written, nor material that has been accepted for the award of any other degree or diploma, except where due acknowledgement has been made in the text.

Tan Suqing

(May 2019)

Abstract

Thermal energy storage becomes increasingly important as fossil fuel reserves diminish and renewable energy is still catching up. Phase change materials (PCM) can store and release substantial amounts of thermal energy (as high as 250 J/g) in response to temperature changes in its environment. In comparison to popular inorganic PCMs, organic PCMs possess several advantages such as negligible loss of latent heat over time and low supercooling. However, organic PCMs suffer from low thermal conductivity which increases the response time to temperature changes in the environment. Furthermore, high flammability of organic PCMs is also a concern which limits their applications as thermal storage materials. To address the above-mentioned drawbacks of organic PCMs, encapsulated-PCM (EPCM) in water has been developed by various research groups. However, the current methods still suffer some drawbacks such as PCM leaching, loss of heat storage over time and low PCM loading. The goal of this work is to develop an innovative approach to fabricate encapsulated-PCM (EPCM) in the aqueous system. It was anticipated that the EPCM with particle sizes in a nanoscale range may increase the heat transfer rate because of the increase of heat transfer area. At the same time, the dispersed EPCM in water would reduce flammability and enhance thermal conductivity.

The thesis begins by introducing the importance of thermal energy storage and the distinct types of PCM materials that have a solid-liquid phase transition taking place

at temperatures in the range of ±15 ˚C of human skin temperature. The current approaches used to synthesize EPCMs and their limitations are presented. The applications of low-temperature EPCMs are also highlighted.

In this work, two approaches to fabricate the EPCMs have been developed:

1) Fabrication of EPCMs in water through a Pickering emulsion template using poly(butyl acrylate)/chitosan nanoparticles as the shell material

In this approach Pickering emulsion was utilized as a template to prepare EPCMs in water. The shell material used was amphiphilic poly(butyl acrylate)/chitosan (PBA/CTS) nanoparticles consisting of hydrophobic poly(butyl acrylate) cores and water-soluble chitosan shells synthesized with core-shell particle platform technology developed by Li's group. The resultant PBA/CTS particles were characterized by dynamic light scattering, ξ -potential measurements at different pHs, Fourier-transform infrared spectroscopy (FTIR) and field emission scanning electron microscopy (FE-SEM). Encapsulation involved formation of a Pickering emulsion with PBA/CTS nanoparticles and an organic PCM, hexadecane, which has a melting point ranging from 16-18 ˚C, followed by crosslinking of functional groups on the PBA/CTS nanoparticle form a continuous polymer shell enclosing the PCM droplet. The effects of different monomer to chitosan ratio and different types of initiator were investigated to find out the optimal particle composition for stabilization of the dispersed PCM. To further optimize the emulsion stability, parameters such as solution pH, electrolyte concentration, and different types of surfactant were also examined. Furthermore, different crosslinking methods to form continuous shells of PBA/CTS nanoparticles were investigated. Phase change

performance and thermal properties of the EPCMs were also studied to evaluate stability of EPCMs after multiple phase change cycles. Results suggested that the encapsulation efficiency was as high as 91%. However, there was ~5% latent heat loss after 20 heat-freeze cycles due to the PCM leakage from the encapsulated PCM capsules. SEM images revealed that the capsules had diameters in the range of 3-5 μm but showed ruptures upon drying. In conclusion, the EPCMs in water have been successfully fabricated with high encapsulation efficiency. However, heat-freeze cycling capability was still unsatisfactory.

2) Synthesis of EPCMs via a coacervation using chitosan-co-poly(methacrylic acid) as a shell material

The coacervation approach is based on an aggregation process of a dissolved polymer chain to form a coating around the hydrophobic droplet by decreasing polymer solubility. The amphoteric water-soluble polymer, chitosan-co-poly(methacrylic acid) (CTS-co-PMAA) copolymer was synthesized as the shell material. The synthesis involved a two-step reaction: 1) The chitosan was first modified with methacrylic acid (MAA) through an amidation reaction between the amine group of the chitosan and double bond of the MAA to form MAA@CTS; 2) Free radical polymerization of remaining MAA to generate CTS-co-PMAA copolymer. The copolymer was characterized by dynamic light scattering, surface charge measurement, FTIR and FE-SEM. The fabrication of encapsulated PCMs through coacervation of CTS-co-PMAA was optimized by varying various factors which include: pH titration profiles, CTS to PMAA ratio in the copolymer, the shell rigidity and addition of the nucleating agent to reduce supercooling. The resultant EPCMs could be applied in three forms: 1) EPCMs dispersing in water. The water-

dispersible EPCMs showed up to 90% encapsulation efficiency, with little reduction in latent heat or leakage after 100 heat-freeze cycles. 2) Dried EPCM: The EPCMs were crosslinked with glutaraldehyde to form rigid shells, thus retaining their structure in the dried state. Results indicated that there was 5% PCM leakage after drying. SEM images of the dried EPCMs showed film structure encasing nodules of PCM which diameters ranging from 174 to 312 nm and latent heat of melting of 165 J/g. 3) Freeze-dried EPCM: The EPCMs dispersed in water were freeze-dried to remove water, giving a sponge-like structure with low density of 0.03 g/mL and latent heat of melting of 102 J/g. Finally, supercooling phenomena was reduced by the use of the nucleating agent, eicosane, which increased the onset freezing temperature (T_f) of the EPCMs from 5 to 10 ˚C. Overall, the coacervation approach presents a simple method to fabricate encapsulated nanosized PCM with high thermal energy storage and good phase change cycling that can be dispersed in water or used to form PCM composites which could potentially be used for thermoregulation.

List of publications

Conferences and Symposia

1. Suqing Tan, Albert Ping-Chuen Chan, and Pei Li*. "Novel micro-encapsulated phase change material for thermal regulation in personal cooling systems". *Abstract of Papers*. Second International Conference on Sustainable Urbanization (ICSU). Hong Kong, China, 7 to 9 January 2015.
2. Suqing Tan, Albert Ping-Chuen Chan, and Pei Li*. "Novel micro-encapsulated phase change material for thermal regulation in personal cooling systems". *Oral Presenter*. Second International Conference on Sustainable Urbanization (ICSU). Hong Kong, China, 7 to 9 January 2015.
3. Suqing Tan, Albert Ping-Chuen Chan, and Pei Li*. "Novel micro-encapsulated phase change material for thermal regulation in personal cooling systems". *Abstract of Papers*. The 22nd Chemistry Postgraduate Symposium. Hong Kong, 18 April 2015.
4. Suqing Tan, Albert Ping-Chuen Chan, and Pei Li*. "Novel micro-encapsulated phase change material for thermal regulation in personal cooling systems". *Abstract of Papers*. Polymer Colloid Group (IPCG) Research Conference. New Hamspshire, U.S., June 28 to July 3, 2015.

Acknowledgements

There are many people who have contributed and made an impact on this research project. First of all, I would like to thank my supervisors Prof Pei Li and Prof APC Chan. I specially thank my supervisor Prof Pei Li for her supervision in the past four years, her remarkable leadership, professional guidance, and valuable comments have made my study a rewarding experience. I would also like to thank my co-supervisor Prof APC Chan for his guidance and support.

I want to thank all the members of Prof. Pei Li's research group, foremostly Dr Yao Yuan for teaching me the synthesis of CTS-co-PMAA copolymer which is used extensively on this project, Dr Chen Liang Hui, Dr Niu Dechao, Dr Wang Xia, Dr. Edmond Kin Man Ho, Joyce Luo, Dr. Cheng Hao Lee, Yuen Shan Siu, Dr Yam Chun Ho and Dr Chun Him Wong, for continual support and interesting discussions.

I would also like to acknowledge Mr. Jimmy Ho for his valuable help with the DSC, elemental analysis, and TGA throughout my research project. I am also grateful to the staff in the Department of Applied Biology and Chemical Technology who had helped me a lot in various ways.

Thanks to Research Committee of the Hong Kong Polytechnic University and The Research Institute of Sustainable Urban Development (RISUD) for their financial support of my postgraduate study.

Table of Contents

Certificate of Originality ..... **ii**

Abstract **iii**

List of publications ..... **vii**

Acknowledgements ..... **viii**

Table of Contents ..... **ix**

List of Figures ..... **xiii**

Abbreviations and Symbols ..... **xix**

Chapter 1 Introduction to PCM based Thermal Energy Storage **1**

1.1 Importance of Thermal Energy Storage systems 1

1.2 Methods of storing thermal energy 3

1.3 Applications of PCM in thermal energy storage 5

1.3.1 Thermal protection of temperature sensitive materials 6

1.3.2 Space heating/cooling 7

1.3.3 Improved efficiency of solar heating systems 10

1.4 Applications and advantages of PCM microcapsules 12

1.4.1 PCM composites 13

1.4.2 PCM slurry 16

1.5 Types of PCM and their properties 20

1.5.1 Organic PCMs 21

1.5.2 Inorganic PCM 24

1.6 Current methods of PCM microencapsulation and their limitations 27

1.6.1 Physical 28

1.6.2 Chemical Synthesis of MEPCMs 34

1.6.3 Physico-chemical 50

Chapter 2 Research Objectives 65

Chapter 3 Development of Phase Change Material Microcapsules in Water with a Pickering Emulsion Technique using Amphiphilic Core-Shell Particles 68

3.1 Experimental 70

3.1.1 Materials 70

3.1.2 Experimental procedures 70

3.1.3 Measurement and Characterization 78

3.2 Results and Discussion 86

3.2.1 Properties of PBA/CTS nanoparticles 86

3.2.2 Pickering emulsion with PBA/CTS particles as the stabilizer 93

3.2.3 Chemical crosslinking of preformed Pickering emulsion 105

3.3 Conclusion 112

Chapter 4 Microencapsulation of Phase Change Materials through Coacervation Techniques 113

4.1 Experimental 115

4.1.1 Materials 115

4.1.2 Synthesis of chitosan-co-poly(methacrylic acid) copolymer 115

4.1.3 Synthesis of CTS-co-PMAA/C16 microcapsules 116

4.1.4 Measurement and Characterization 127

4.2 Results and Discussion 138

4.2.1 Synthesis of chitosan-co-poly(methacrylic acid) copolymer 138

4.2.2 Optimization of encapsulation of hexadecane through coacervation using CTS-co-PMAA as shell material 147

4.2.3 Characterization of CTS-co-PMAA/C16 Nanocapsules 180

4.2.4 Characterization of freeze-dried CTS-co-PMAA/C16 nanocapsules 190

4.2.5 Bulk synthesis and characterization of CTS-co-PMAA/C16 microcapsules 195

4.3 Conclusion 200

Chapter 5 Conclusion and Recommendations for Future Study 202

5.1 Conclusions 202

5.2 Recommendations for Future Study 203

5.2.1 Investigation of NEPCMs in water as heat transfer fluid 203

5.2.2 Encapsulation of fragrances or other volatile materials 204

Chapter 6 Appendix 206

6.1 DSC scan of PCM, hexadecane.....206

6.2 Thermal profiles of MEPCMs synthesized via crosslinking of C16-PBA/CTS emulsions.....207

References 211

List of Figures

Figure 1.1 World consumption of energy from 1998 to 2016.[2] (Y-axis unit: million ton oil) 1
Figure 1.2 Role of PCM in TES: a) temperature control and b) thermal energy storage[14] 5
Figure 1.3 Schematic of PCM encapsulated in insulated walls [33] 9
Figure 1.4 Cross-section of different MEPCM morphologies 13
Figure 1.5 PCM microcapsules as (a) textile coating ; (b) enclosed in textile fiber [74] 15
Figure 1.6 Energy density of different thermal fluids($\Delta T = 5°C$:) [78] 17
Figure 1.7. Types of PCM microencapsulation methods 27
Figure 1.8. Schematic of spray drying to produce MEPCMs[100] 29
Figure 1.9 SEM images of MEPCMs synthesized via spray drying: a) LDPE/EVA-Rubitherm@RT27 [102]; b) Gum arabic-ethyl hexanoate[103]; c) gelatin and acacia-paraffins [104] 30
Figure 1.10 Schematic diagram for fluidized bed [112] 31
Figure 1.11 Chemical structure of the poly(ethylene glycol) (PEG) 33
Figure 1.12 Chemical structure of (a) isophorone diisocyanate (IPDI); (b) tetraethylenepentamine (TEPA) and (c) Dibutyltin dilaurate (DBTDL) 38
Figure 1.13 Schematic diagram of the fabrication of monodisperse PCM@polyurea microcapsules in a tubular microfluidic device[116] 39
Figure 1.14 MEPCMs prepared by the interfacial polymerization (a) Octadecane/Polyurea MEPCMs (D_n, 1 micron)[128]; (b) Polyurea MEPCMs (D_n, 6.4 microns) [115]; and (c) Octadecane/Polyurea MEPCMs synthesized with tubular microfluidics (D_n 308 micron)[116] 39
Figure 1.15 Chemical structure of (a) Melamine; (b) Urea and (c) Formaldehyde 40
Figure 1.16 SEM images of MEPCM synthesized via in-situ polymerization: a) poly(urea-formaldehyde) shell with hexadecane core[119]; b) resorcinol modified poly(melamine-formaldehyde) shell with octadecane core[117];c) resorcinol modified poly(urea-formaldehyde) shell with tetradecane core[118] 42
Figure 1.17 Chemical structure of a) butyl stearate; b) divinyl benzene; c) poly(butyl acrylate); d) paraffin wax 43
Figure 1.18 SEM images of MEPCM synthesized with suspension polymerization: a) PS/Rubitherm 31 [133]; b) poly(ethylene glycol dimethacrylate) - Hexadecane[120] c) Poly(methyl methacrylate) -Rubitherm®27[121];d) Poly (butyl acrylate) crosslinked with divinyl benzene/Paraffin-Butyl stearate[122] 45
Figure 1.19 Schematic of encapsulation via emulsion polymerization[141] 46
Figure 1.20 Image of MEPCM synthesized with emulsion polymerization: PMMA/n-eicosane[90] 47
Figure 1.21 Image of MEPCM synthesized with emulsion polymerization:poly(butyl acrylate)/hexadecane[72] 48

Figure 1.22 Images of MEPCM synthesized with emulsion polymerization: Poly(methyl methacrylate)/Paraffin [65] 48
Figure 1.23 Images of MEPCM synthesized with emulsion polymerization: Poly(styrene) crosslinked with divinylbenzene-SiO_2/1-Dodecanol[124].....49
Figure 1.24 Schematic diagram of the coacervation process 52
Figure 1.25 SEM image of MEPCM prepared by coacervation: Gelatin/acacia - paraffin[104] 54
Figure 1.26 Image of MEPCM prepared by coacervation: Coco fatty acid-Gelatin-Gum Arabic shell[87].....55
Figure 1.27 Image of MEPCM prepared by coacervation: Urea formaldehyde – Octanoic acid with Tween40 as surfactant [146] 56
Loxley proposed a new method of synthesizing microcapsules based on phase separation to encapsulate n-hexadecane with a poly(methyl methacrylate) (PMMA) shell.[166] This method is commonly used to form MEPCMs with n-alkanes as the PCM core.[147, 167] The method is based on an oil in water emulsion. The oil phase is composed of the shell material, a good solvent for the shell material and a poor solvent for the shell material. The emulsion is formed with the aid of a homogenizer, and under reduced pressure. When the good solvent is removed, it causes precipitation of the shell material, which migrates towards the outer ring of the oil droplet. As more and more solvent is removed, the microcapsules are formed. The microcapsules formed possess shells with uniform thickness, and their diameter can approach 10 μm easily. Figure 1.28 illustrates the schematic formation of microcapsules with phase separation. 56
Figure 1.29 Schematic formation of microcapsules with phase separation (v.s.： volatile and good solvent for shell material; n.v.n.s.: non-volatile and poor solvent for shell material) [166].....57
Figure 1.30 Image of MEPCMs prepared by phase separation using acrylonitrile–styrene copolymer with n-tetradecane PCM core[147] 58
Figure 1.31 Schematic reaction of sol-gel encapsulation [148].....59
Figure 1.32 SEM image of MEPCM synthesized via sol-gel : Silica / n-octadecane (30/70 ratio) synthesized at pH 2.45 [148].....60
Figure 1.33 DSC of sodium silicate/n-octadecane MEPCM (35% PCM) over 100 thermal cycles.[149].....61
Figure 1.34 Images of MEPCM synthesized via sol-gel : Silicon oxide-expanded graphite / paraffin (Left:SEM; Right:TEM) [150].....62
Figure 1.35 SEM image of MEPCM synthesized via sol-gel: Silicon dioxide / stearic acid [151] 63
Figure 2.1 Simplified scheme for the synthesis of MEPCMs via Pickering emulsion template 65
Figure 2.2 Simplified scheme for the synthesis of MEPCMs via coacervation technique with CTS-co-PMAA as shell material 66
Figure 3.1 Chemical structures of emulsifiers 75
Figure 3.2 Chemical structures of a) glutaraldehyde; b) Sodium tripolyphosphate; c) boric acid 77

Figure 3.3 Example of an optical image (left) transformed to binary colors (right).....83
Figure 3.4 DSC scan of microencapsulated hexadecane (from 25 °C to -10 °C and -10 °C to 25 °C at a rate of 4 °C min¬¹).....84
Figure 3.5 Formation mechanism of amphiphilic core–shell particle via graft copolymerization of vinyl monomer from a water-soluble polymer containing amino group[176].....87
Figure 3.6 SEM image of PBA/CTS (2-1 H_2O_2) at magnification of 10,000 X 92
Figure 3.7 FTIR spectra of PBA/CTS (2-1, H_2O_2).....93
Figure 3.8 Optimum contact angle for oil in water emulsion: $70^\circ \leqslant \theta \leqslant 86^\circ$; water in oil emulsion: $94^\circ \leqslant \theta \leqslant 110^\circ$[178].....94
Figure 3.9 Thermal profile of MEPCMs synthesized via GAL crosslinking of Pickering emulsion formed with PBA/CTS Np and C16.....95
Figure 3.10 Pickering emulsions formed with PBA/CTS (2-1 H_2O_2) dispersions at different pH after 1 h (Conditions: Total Volume: 20ml; %vol PCM:20%; %SC of Np used: 0.5%).....96
Figure 3.11 *zeta*- Potential curve of PBA/CTS (2-1, H_2O_2).....97
Figure 3.12 Surface modification of modified PBA/CTS Np with T80 98
Figure 3.13 Effect of various types of emulsifiers on emulsion stability after 1 h. The emulsions were prepared by homogenizing the mixtures (10%vol PCM in 0.5% PBA/CTS at pH4.88 with 0.2 wt% different emulsifier) for 1 min at 11k rpm.....98
Figure 3.14 Optical image [left] and size distribution [right] of Pickering emulsion without emulsifier. Average diameter of droplets: 2.62±3.83 µm.....100
Figure 3.15 Optical image [left] and size distribution [right] of Pickering emulsion with 0.2 wt% Cremophor . Average diameter of emulsified droplets: 1.86±0.83 µm.....100
Figure 3.16 Optical image [left] and size distribution [right] of Pickering emulsion with 0.2 wt% T80. Average diameter of emulsified droplets: 3.34±0.79 µm.....101
Figure 3.17 Optical image [left] and size distribution [right] of Pickering emulsion with 0.2 wt% CTAB. Average diameter of emulsified droplets: 3.95±3.72 µm 101
Figure 3.18 Optical image [left] and size distribution [right] of Pickering emulsion with 0.2 wt% SDS. Average diameter of emulsified droplets: 7.40±03.84 µm.....102
Figure 3.19 Effect of different concentrations of $CaCl_2$. Pictures of emulsions were taken after 24 h (20%vol PCM in 0.5% PBA/CTS at pH4.88 and 0.2% Tween80) with different wt% $CaCl_2$ 104
Figure 3.20 SEM images of Pickering emulsion formed with T80 modified PBA/CTS Np and 0.04 wt% $CaCl_2$ (Sample was dispersed in ethanol then imaged with SEM) ; MEPCM Diameter = 1.16±0.37 µm; Wall thickness: 100 – 200 nm.....105
Figure 3.21 Hydration of glutaraldehyde 106
Figure 3.22 Reaction of glutaraldehyde with amine groups in acidic or neutral conditions.[181] 106
Figure 3.23 Crosslinking of boric acid and chitosan [185, 188] 107
Figure 3.24 Ionic crosslinking of chitosan and tripolyphosphate ion[192] 108
Figure 3.25 Optical images of EC-GAL (Size distribution: 2-120 µm) 110

Figure 3.26 Optical image [left] and size distribution [right] of EC-Borax (2.80±0.70 μm) 110
Figure 3.27 Optical image [left] and size distribution [right] of EC-TPP (3.30±1.70 μm) 111
Figure 4.1 Distribution of MEPCM after centrifugation 118
Figure 4.2 DSC scan of microencapsulated hexadecane (from 25 °C to -10 °C and -10 °C to 25 °C at a rate of 4 °C min¬¹) 131
Figure 4.3 Experimental setup to measure temperature history of samples at ambient temperatures of 42-43 °C and 2-3 °C 137
Figure 4.4 Synthesis of zwitterionic copolymer of CTS-co-PMAA via the two-step reaction: Step 1. Amidation reaction; 2) Polymerization 139
Figure 4.5 ^{1}H-NMR spectra in 2 wt%-d-Acetic acid in D_2O of MAA monomer, CTS, MAA-CTS and CTS-co-PMAA (*H1 peak is overlapped by solvent peak in the CTS spectra 140
Figure 4.6 FTIR spectra of chitosan, MAA modified chitosan and CTS-co-PMAA (synthesized with 1:1 w/w). 142
Figure 4.7 *zeta*-Potential curves of CTS-co-PMAA (PMAA:CTS=1:2 w/w), CTS-co-PMAA (PMAA:CTS=1:1 w/w) and CTS-co-PMAA (PMAA:CTS=2:1 w/w) 144
Figure 4.8 SEM image of CTS-co-PMAA (1:1) (Freeze dried) a) X1000; b) X20,000 magnification 145
Figure 4.9 TGA curve of CTS-co-PMAA (1:1) 146
Figure 4.10 TGA curve of CTS prior to PMAA modification 147
Figure 4.11 Surface tension of CTS-co-PMAA (pH 1.5) compared to conventional surfactants 148
Figure 4.12 Surfactant molecules oriented at the air-water interface 148
Figure 4.13 CTS-co-PMAA (1:1) at 80°C (left) cooled to room temperature (right) 149
Figure 4.14 Turbidity of CTS-co-PMAA vs temperature, measured with 633 nm laser at 173° 150
Figure 4.15 Hydrogen bonding between PMAA and CTS moiety in CTS-co-PMAA 151
Figure 4.16 Structure of CTS-co-PMAA stabilized emulsion droplet 151
Figure 4.17 DSC of aqueous CTS-co-PMAA/C16 coacervates (PMAA:CTS ratio = 1:1) before and after drying 153
Figure 4.18 Turbidity of CTS-co-PMAA as a function of pH. Blue: Absorbance intensity (abs) at 690 nm; and Black: Relative scattered light intensity (cps) at 90° with laser at 690 nm 154
Figure 4.19 CTS-CO-PMAA (0.5 wt%) at various pHs (From left to right: 1.3, 1.6, 1.9, 2.5, 3.0, 3.5, 4.1, 4.6, 5.0, 5.5, 6.0, 7.5) 155
Figure 4.20 DSC freezing profiles of CTS-co-PMAA/C16 coacervates synthesized with different titration profiles 158
Figure 4.21 Morphologies and particle sizes of encapsulated HD particles (CTS-co-PMAA-C16) observed with an optical microscopy. (Red Circles): Aggregation has occurred. (Red Arrows): Relatively fast flowing non-aggregated particles that couldn't be captured. 159

Figure 4.22 SEM image of dried CTS-co-PMAA/C16 coacervates synthesized with different titration profiles: a) XCTS (pH 10); b XCTS (pH 5.6) and c) XCTS(10→5.6) 160
Figure 4.23 Chemical reaction of GAL and CTS-co-PMAA 161
Figure 4.24 FTIR spectra of C16, CTS-co-PMAA and dried CTS-co-PMAA/C16 microcapsules crosslinked with GAL 162
Figure 4.25 SEM image of CTS-co-PMAA/C16 GAL:CTS ratio a) 5:1 (5X) b) 10:1 (10X) c) 15:1 (15X) and d) 20:1 (20X) (clockwise from top left) 163
Figure 4.26 DSC curves (TOP: cooling) and (BOTTOM: heating) of CTS-co-PMAA-C16-GAL coacervates crosslinked with various amounts of GAL 165
Figure 4.27 Size distribution (DLS) of the MEPCMs sample synthesized with method M1, M4 and M5. Figure 4.28 shows the SEM images of dried MEPCMs, M1, M4 and M5. Both samples of M1 and M4 show formation of a broken bubble structure. This is due to the deformation of the MEPCMs during evaporation of water, leading to coalescence of the MEPCMs and subsequent breakage of the shell releasing the core material. 169
Figure 4.28 SEM images of M1, M4 and M5 170
Figure 4.29 Summary of DSC results for M1, M4 and M5 172
Figure 4.30 Size distribution of MEPCMs with different amounts of nucleating agent measured with the Nanosight 173
Figure 4.31 SEM image of sample 3EI16 (Diameter: 220 ± 82 nm) 174
Figure 4.32 SEM images of 6EI16 (Diameter: 254±109 nm) 174
Figure 4.33 SEM image of 10EI16 (Diameter: 243 ± 69 nm) 175
Figure 4.34 DSC scan of MEPCMs synthesized with different amounts of nucleating agent 176
Figure 4.35 DSC freezing curves of XCTS/C16 with different nucleating agents 178
Figure 4.36 Schematic diagram of optimized synthesis of MEPCMs via coacervation of CTS-co-PMAA 180
Figure 4.37 Appearance of NEPCM a) dispersed in water ; b) dried powder 181
Figure 4.38 Size distribution of NEPCM measured by DLS 182
Figure 4.39 SEM images of NEPCM (Diameter: 243 ± 69 nm) 182
Figure 4.40 TEM images of NEPCM (Diameters between 90 and140 nm with shell thickness of 6-20 nm) 183
Figure 4.41 FTIR spectrum of C16 (Blue) and NEPCM (Red) 184
Figure 4.42 DSC curves and thermal characteristics of optimized NEPCMs (air dried) over 100 phase change cycles 186
Figure 4.43 Proposed encapsulation mechanism of CTS-co-PMAA/C16 nanocapsules 188
Figure 4.44 TGA curve of CTS-co-PMAA/C16 NEPCMs 190
Figure 4.45 Appearance of freeze-dried NEPCMs 191
Figure 4.46 SEM images of a) NEPCM (Diameter: 243 ± 69 nm) ; b) freeze dried NEPCM 192

Figure 4.47 Freezing curve of freeze dried NEPCMs and NEPCMs dried at room temperature.....193
Figure 4.48 DSC summary of optimized NEPCMs (freeze dried) over 100 heat-freeze cycles.....194
Figure 4.49 Appearance of C16/CTS-co-PMAA MEPCMs synthesized via bulk procedure.....195
Figure 4.50 (A) DLS of size intensity distribution of C16/CTS-co-PMAA microcapsules via bulk synthesis , (B) Optical images of MEPCM20X (Size distribution: 1.89±0.27 μm) 196
Figure 4.51 DSC of PCM encapsulated by CTS-co-PMAA using bulk synthesis method (Sample: MEPCM20X).....197
Figure 4.52 Temperature profile of hexadecane (C16) and MEPCM20X equilibrated at ~3 °C placed in ambient temperature of ~23 °C 198
Figure 4.53 Temperature profiles of hexadecane (C16) and MEPCM20X equilibrated at ~23 °C placed in controlled environment temperature of ~3 °C 199
Figure 6.1 DSC scan of hexadecane (from 25 °C to -10 °C and -10 °C to 25 °C at a rate of 4 °C min¬).....206
Figure 6.2 Thermal profile C16-PBA/CTS emulsions with no crosslinker added.....207
Figure 6.3 Thermal profile C16-PBA/CTS emulsions crosslinked with GAL (EC-GAL) 208
Figure 6.4 Thermal profile C16-PBA/CTS emulsions crosslinked with Borax (EC-Borax).....209
Figure 6.5 Thermal profile C16-PBA/CTS emulsions crosslinked with TPP (EC-TPP) 210

Abbreviations and Symbols

Abbreviation /Symbol	Definition
C16	Hexadecane
^{o}C	Celcius
%ee	Encapsulation efficiency
%PCM	Weight percentage of phase change material content in encapsulates
CTS	Chitosan
D_h	Hydrodynamic diameter
DLS	Dynamic Light Scattering
D_n	Number average hydrodynamic diameter
D_v	Volume average hydrodynamic diameter
EPCM	Encapsulated Phase Change Material
FTIR	Fourier-Transform Infrared spectroscopy
GAL	Glutaraldehyde
IEP	Isoelectric point
LH_f	Latent heat of freezing
LH_m	Latent heat of melting
MEPCM	Microencapsulated Phase Change Material
NMR	Proton nuclear magnetic resonance spectroscopy
o/w	Oil-in-water
PBA	Poly (butyl acrylate)
PCM	Phase Change Material
PDI	Polydispersity Index
SEM	Scanning Electron Microscopy
SEM	Field-emission scanning electron microscopy
TBHP	*tert*-butyl hydro peroxide
TEM	Transmission electron microscopy
T_f	Freezing temperature
T_g	Glass transition temperature

TGA	Thermogravimetry analysis
T_m	Melting temperature
T_{me}	Endset temperature of melting peak
T_{mo}	Onset temperature of melting peak
T_{mp}	Peak temperature of melting peak
T_{fe}	Endset temperature of freezing peak
T_{fo}	Onset temperature of freezing peak
T_{fp}	Peak temperature of freezing peak
v/v	Volume/Volume
w/o	Water-in-oil
w/w	Weight/Weight
wt%	Weight percentage
ΔT_f	Depression of freezing temperature

Chapter 1
Introduction to PCM based Thermal Energy Storage

1.1 Importance of Thermal Energy Storage systems

The world population is estimated to increase from the current 7.5 billion to 9 billion in twenty years.[1] **Figure 1.1** shows that the world's energy consumption from 1991 to 2016 increasing each year. This is because as buying power increases, so do standards of living, people will consume better goods, housing, safety, leisure, and material comforts. The projected population increase paired with higher living standards leads to higher energy consumption.

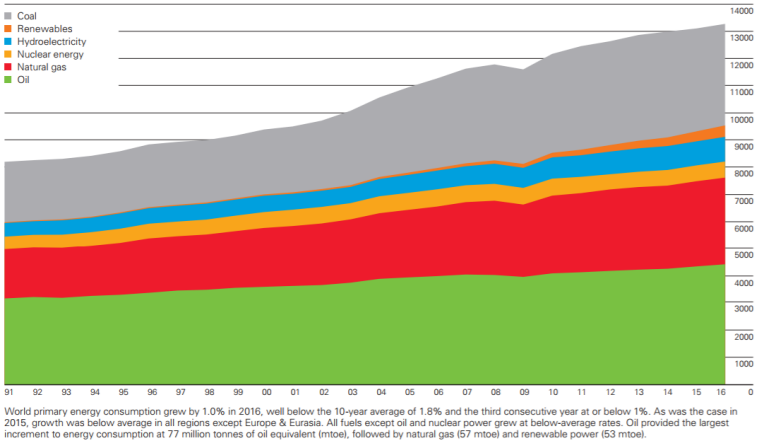


Figure 1.1 World consumption of energy from 1998 to 2016.[2] (Y-axis unit: million ton oil)

However, as of 2017, 76% of the world's annual energy consumption is still derived from depletable fossil fuels.[3] Studies show that under the assumption of constant production and consumption, the presently known reserves of oil will last around 41 years, natural gas 64 years, and coal 155 years.[4] Moreover, the market price of fossil fuels fluctuates greatly[2], and would predictably increase as reserves dwindle. Although renewable energy is making remarkable strides and the cost of photovoltaic energy is becoming comparable to that of energy from fossil fuel[5], there are still both technological and political barriers to overcome before renewable energy sources can replace fossil fuels. Even with the advent of cheap renewable energy, energy consumption inevitably leads to pollution of the environment regardless of its sources. Burning fossil fuels release carbon dioxide and other pollutants, which in turn leads to air pollution and global warming, of which have been shown to adversely affect crop yields[6-8]. Consumption of renewable energy such as solar energy requires the production of solar panels which likewise creates pollutants during production and bulk waste when they become obsolete. Thus, energy conservation methods which directly reduce energy consumption would serve as insulation against energy price fluctuations and indirectly reduce environmental pollution.

One of the ways to reduce energy consumption is through the use of thermal energy storage (TES) systems. The TES as its name implies are systems which can store thermal energy to be used at a later time or another location, much like the way battery stores electricity. An example of TES can be found in Persia 350 years ago when winter ice was harvested from lakes or mountains and stored underground for the coming

summertime. A more current example would be the use of TES to recover and store waste heat for other purposes.[9] For instance, the iron and steel industries use TES to recover waste heat from flue gases which is reused to preheat air to around 600°C for manufacturing steel.[10] Studies show that the use of TES in the iron and steel industry alone could potentially save up to 1.9 million barrels of oil per year.[11] Solar water heating, which stores solar energy in the form of thermal energy to heat water via a heat exchanger is also another example. This system has been shown to cut energy costs for water heating by 50-80%.[12]

In conclusion, with the projected increase in energy demands, methods of increasing energy efficiency will become increasingly important to meet these demands. Therefore, thermal energy storage (TES) methods as a means to increase energy usage efficiency will become increasingly important.

1.2 Methods of storing thermal energy

The thermal energy storage (TES) systems can store thermal energy in three ways: (1) Chemical storage: Thermal energy is stored/released during the formation/the breaking of chemical bonds in a chemical reaction. (2) Sensible heat storage: Thermal energy is absorbed/released when a material's temperature increases/decreases and can be quantified by the material's specific heat capacity, temperature raised/decreased and amount of material; (3) Latent heat storage: Thermal energy is absorbed/released when a material transitions to and from different phases, which can be solid-solid, solid-liquid,

solid-gas and liquid-gas. This phase change takes place at the material's phase transition temperature and is quantified by its latent heat/transition enthalpy and the amount of material. These materials are known as phase change materials (PCMs). The phase transition process involves certain complications, e.g., during liquid-gas and solid-gas transitions, a large volume and pressure change takes place and must be taken into consideration when designing the TES system. Solid-solid phase transitions involve changes of the crystalline structure from one lattice to another. This type of materials can be handled easily because they do not flow way and have the least volume change. However, they are undesirable as PCMs, as they have the lowest transition enthalpy. The most widely used PCMs are solid-liquid type, as the phase change volume and pressure are minimized while transition enthalpy remains high. However, they require a storage structure to prevent them from flowing away during phase transitions.

Among the three methods of thermal energy storage, storing thermal energy in the form of chemical energy is the least favorable due to high cost and low cycle stability as the storage capacity deteriorates rapidly over time. The sensible heat storage is a conventional method for thermal energy storage and is already well established.[13] However, compared to the sensible heat, the amount of latent heat stored by a PCM for the same amount of material is many times larger and requires a much narrower range of operating temperature. For example, the transition enthalpy of 1 kg of ice to water is equal to an increase of 80 kg of water by 1°C.

1.3 Applications of PCM in thermal energy storage

In TES systems, PCMs are used for the two main purposes: (1) Temperature control: To maintain a certain temperature. For example, PCMs of low thermal conductivity are desirable to insulate temperature sensitive cargo against temperature fluctuations. By selecting a PCM with a suitable transition temperature, the PCM stores/releases heat in response to the environmental temperature to delay overheating/undercooling (Figure 1.2); (2) Thermal energy storage: For storage/release of thermal energy, PCMs of higher thermal conductivity are desirable for faster response[14] and better storage efficiency.

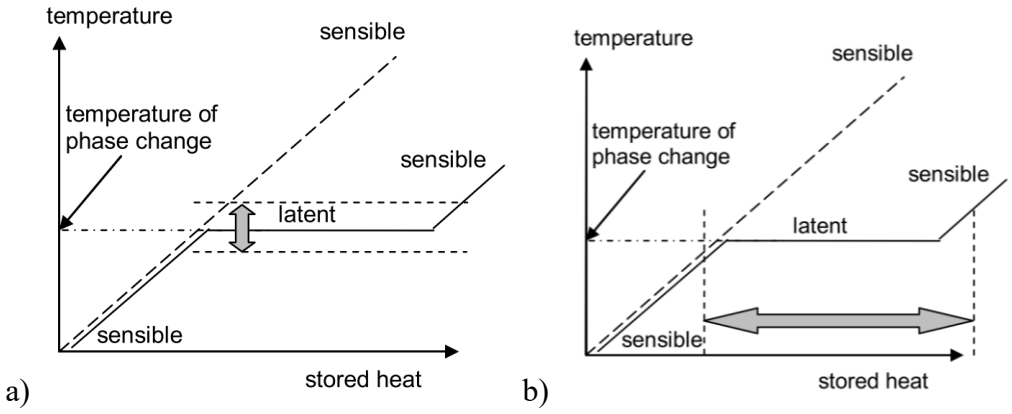


Figure 1.2 **Role of PCM in TES: a) temperature control and b) thermal energy storage[14]**

Examples of PCM-based low-temperature TES systems are listed in **Table 1.1**.Three of the most widely used applications of TES are 1) Thermal protection of heat sensitive materials; 2) Space heating and cooling; and 3) Improving efficiency of solar heating systems.

Table 1.1 **Examples of applications of PCM in low temperature TES**

PCM based TES Applications	Reference
Thermal protection of heat sensitive materials (e.g. medicine, food, organs) during transportation	[15-19]
Embedded in walls of refrigerated trucks as thermal buffer	[20, 21]
Reducing surface temperatures of asphalt roads to prevent overheating in the summer	[22]
Thermal control for large scaled chemical reactions during exothermic peak temperature	[23, 24]
Heat sink for thermoelectric refrigeration	[25-27]
Cooling overheated solar panels	[28]
Recycling waste heat	[11, 29-31]
Passive Space heating/cooling for thermoregulation	[32-34]
Off peak use of electricity (e.g. ice banks, paraffin banks)	[35-37]
Improving water heating efficiency	[38, 39]
Increasing the efficiency of solar collectors in solar water heating [40-42], greenhouses [43-45] and solar stills[46]	

1.3.1 Thermal protection of temperature sensitive materials

PCMs can be used to delay overheating or undercooling of temperature-sensitive cargo by absorbing or releasing substantial amounts of heat at their phase transition temperatures. Possibly the most common usage of PCM are during the transportation of temperature-sensitive cargo such as electronics[47, 48], frozen foods [18, 19] and biological

tissue [16, 17]. In these cases, uncontrollable circumstances such as failure of refrigeration, temperature fluctuation and delay in transportation would result in irreversible damage or losses. Thus, PCMs serve as a thermal buffer to protect the temperature-sensitive loads. It has been shown that PCM can delay overheating/undercooling for up to several hours depending on the heat capacity of the PCM.[20, 21] Also, the PCM responses directly to temperature changes in the environment and does not require any power source or mechanical systems.

In most cases, PCMs are packed into packets and stored together with temperature sensitive cargo. Another method is lining PCM directly inside the walls of a refrigerated truck, insulated casings or other systems. Studies carried out by Oro on a refrigerated truck showed an average reduction of 29.1% peak heat transfer rate and reduction of 16.3% total heat flow.[20] This would translate into energy saving for refrigerated trucks, reduced pollution, and lowered loads on refrigeration equipment. A similar study by Farid in the event of refrigeration failure also showed that the air temperature and the temperature of the frozen products remained lower for a longer time when PCM was used.[21] Therefore it is unsurprising how widely PCMs are used in the transportation of temperature-sensitive cargo.

1.3.2 Space heating/cooling

Thermal comfort is a subjective state where an individual is neither too hot nor too cold. The definition of thermal comfort based on energy is a state where there is no net heat being absorbed or lost between the body and the environment.[49] One of the methods

used in buildings to maintain thermal comfort for the occupants is through space heating/cooling.

In a report by the International Energy Agency, space heating/cooling accounts for 50% of the energy used in residential buildings.[32] This suggests an area for significant energy conservation. The thermoregulatory effect of PCMs can be used either *passive* (without energy input) or *active* (with energy input).

1.3.2.1 Passive Space Heating/Cooling

Temperature fluctuations in buildings have become more apparent as even lighter and stronger building materials are used. These buildings tend to have lower thermal masses and require higher heating/cooling power. Using PCM with an optimal melting temperature (T_m) is a passive method that does not require any input of energy. In the day time, the higher temperatures cause PCM to melt and store heat. At night, the lower temperatures cause PCM to solidify and release heat, thus levelling out temperature spikes in the building and therefore reducing space cooling/heating load. In 2005, Zhang et. al built test houses with insulated walls embedded with PCM containing pipes to compare the space cooling load over several days. A 10 wt% concentration of PCM (T_m between 20–30°C) in the walls (Figure 1.3) reduced the space cooling load by approximately 8.6%.[33] Macro-encapsulated PCM (T_m of 28 °C) manufactured by Rubitherm [50] lined on inner surface of walls and roof in test houses also showed a 17% reduction in the space cooling load for Mediterranean summer conditions.[34]

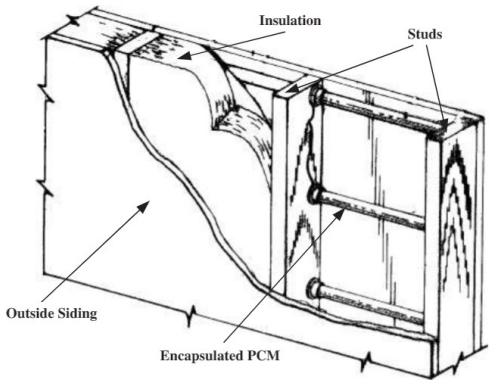


Figure 1.3 **Schematic of PCM encapsulated in insulated walls [33]**

1.3.2.2 Active Space Heating/Cooling

The cost of electricity is cheaper at night. The difference in cost is due to the electricity demand peaking during the day. The peak loads are two to three times higher than the average daily load.[10] To meet these demands, additional power generators have to be built and operated specifically for meeting peak loads, driving up the electricity cost. In 2004, a report by the U.S. Government Accountability Office estimated that the 100 highest priced hours in each year accounted for 10 to 20% of electricity costs for the 8766 hours in each year.[51] These 100 hours are the peak demand hours which occur during the hot summer afternoons.

As mentioned earlier, the largest portion of energy consumption of buildings is in the form of space cooling/heating. By using TES to store electricity in the form of thermal energy, the peak load can be reduced or shifted.[35-37, 52, 53] PCMs such as Water/ice, inorganic salt hydrates or paraffins are refrigerated and cooled at night and the cooling energy can be used the next day during the peak hours. This provides 1) reduced electricity

cost; 2) lower burden on the electric grid; 3) lower load for heating/cooling equipment; 4) Increased energy efficiency for cold TES during the night due to the lower temperature and 5) increased space due to smaller cooling/heating units.

Although there are considerations such as 1) initial capital costs; 2) long term payback period; and 3) stability of PCMs over the TES lifetime.[10] PCM-based TES systems remain an economic and ecological option for thermal energy storage.

1.3.3 Improved efficiency of solar heating systems

Solar heating systems collect solar energy in the form of thermal energy. The collected thermal energy can then be used to provide heat. The conventional solar heating systems collect solar energy in the form of sensible heat. However, recent studies have shown that incorporation of PCMs could improve the efficiency of these solar heating systems. Studies on various solar heating systems such as solar water heating [40-42], solar air heating [54, 55], solar stills [46] and greenhouses [43-45] have also reported higher efficiency when PCM is incorporated. In a study by Canbazoglu et.al[40], incorporation of salt hydrate PCMs into solar water-heating systems could increase total heat collected by 2.59-3.45 times, which increased hot water production. Besides solar water-heating systems, PCMs have also been shown to improve efficiency of solar stills. Solar stills produce freshwater through distillation of saline/salt water by solar energy. A study by Kabeel et. al in 2016 which compared solar stills with and without PCM (under Egyptian conditions) added to the base of the saline water reservoir exhibited an increased fresh water production of 67%.

Results show when PCM is used, there is 1) higher mass of freshwater produced throughout the day and 2) freshwater production after daylight hours (around 18:00) due to the PCM (T_m: 58 °C) continuously releasing heat as temperature drops[46]. To summarize, PCMs incorporated into solar heating systems have the following advantages: 1) increases the amount of solar energy collected in the form of latent energy which 2) can be used after daylight hours.

In summary, the advantages of using PCMs in TES are: 1) low environmental impact throughout their usage, PCM-based TES doesn't generate waste products during heat storage/release; 2) Reduced energy cost; 3) No power source or mechanical system such as compressors in cooling equipment or electrical heaters required for heat storage/release; 4) Low maintenance cost.

1.4 Applications and advantages of PCM microcapsules

As mentioned in the previous section, PCMs are widely used in TES due to their many advantages. However, PCMs possess limitations that need to be overcome before they can be used for practical applications. These include low thermal conductivity and volume change during phase transition. The phase transition itself also poses problems when designing TES, as liquid would flow away and properties such as viscosity, heat transfer characteristics differ in solid and liquid. One of the methods to overcome these issues are microencapsulation of PCM. The microencapsulation of PCM is the encapsulation of PCM material in a solid shell with diameters ranging from hundreds of nano- to micro-scale. Depending on the dimensions of the container, these capsules can be termed nanocapsules (diameterr <1 micron), microcapsules (diameter between 1 micron and 1mm) and macrocapsules (diameter > 1 mm).

There are five types of possible morphologies for microencapsulated PCMs (MEPCMs). Their cross-sectional structures are shown in Figure 1.4**.** (1) Mononuclear: Single PCM core surrounded by shell; (2) Polynuclear: Multiple PCM cores are dispersed in the shell material; (3) Matrix: The PCM is distributed in the shell material and there is no clearly defined shell. It is also known as form-stable PCM; (4) Multi-walled: The PCM is enclosed in more than one shell; (5) Irregular: The MEPCM has an irregular shape but is clearly defined.

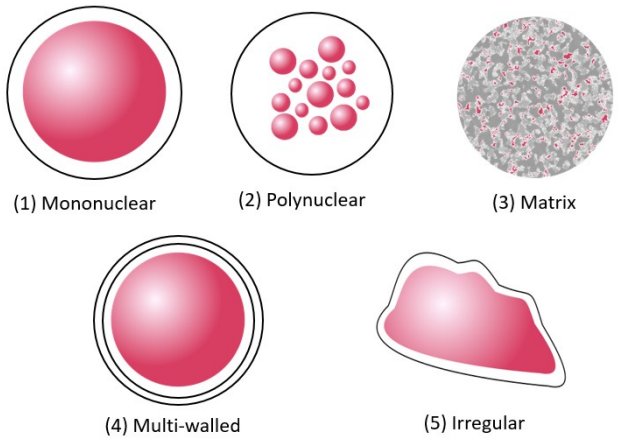


Figure 1.4 **Cross-section of different MEPCM morphologies**

MEPCMs can be used directly in the form of heat transfer media in a fluidized bed heat exchanger [56-59] and thermal storage media in direct contact heat exchangers [60]. MEPCMs can also be easily incorporated with other materials in the form of either 1) PCM composites or 2) PCM slurry.

1.4.1 PCM composites

PCM composites are solid materials that contain encapsulated PCM material. However, PCMs cannot be directly incorporated into materials due to the following reasons: 1) PCMs may interact with the materials and adversely affect them[61]; 2) The transition from solid to liquid during absorption/release of heat may lead to PCM leakage. Therefore, PCM needs to be encapsulated before the formation of the PCM composites. There are advantages in using MEPCM for PCM composites: 1) MEPCMs allow selection

of shell material that is compatible with the surrounding material, e.g., metal or polymer; 2) MEPCMs encasing PCMs in a solid shell prevent it from flowing away; 3) MEPCMs have much larger surface to volume ratio and thus larger heat transfer area which leads to higher heat transfer rate.

One of the applications of PCM composites is increasing the thermal mass of buildings, which means higher energy input is required to increase the buildings' temperature. MEPCMs are incorporated into building materials such as polyurethane[62], plaster[63], gypsum[64, 65], concrete[66-69] to build walls, ceilings and floors. The MEPCMs store heat during the day as PCMs melt, which can be released at night when the PCMs solidify due to temperature differences to provide a thermoregulatory effect. A study carried out in Spain compared two concrete cubicles, one built with MEPCM and the other without PCM. The walls containing MEPCM were made of concrete developed with 5 wt% of MEPCMs (T_m: 26 °C and latent heat of fusion 110 kJ/kg). The temperatures of the cubicle's walls herewere measured over a six-month period. It was found that there was no adverse effects on splitting strength or mechanical properties.[66] Results also showed that incorporation of MEPCM lowered the difference between minimum and maximum temperature by 3°C, and a delay of 2 h for the walls to reach the maximum temperature. Kuznik and Virgone also studied the differences in temperature of drywall that contained up to 60wt% MEPCM in three different climates: summer, winter and spring/autumn. Cubicles built with drywalls containing PCM was compared with cubicles without PCM. The maximum air temperature was reduced by 4.2°C compared with non-MEPCM containing wallboard.[70] The thermoregulatory effect of MEPCMs would not be enough to substitute air-conditioning. It would, however, delay the onset of peak temperature, thus

saving energy that would have been used to cool the building. There was no input of energy except for the initial infrastructure.

PCMs in textiles for thermal comfort is another example of PCM composites. Incorporation of MECPMs into textiles impart thermoregulatory properties to the textile. As seen in **Figure 1.5**, MEPCMs can be used as a textile coating or embedded within the fiber to make blankets, protective clothing, insulation and other items.[71, 72] In 2006, Wang et al. carried out studies to compare fabric with and without MEPCM on a bionic skin model which mimics the microclimate of human skin. In a controlled environment, it was found that PCM incorporation into textiles reduced energy used for temperature control processes by around 30%.[73] The commercial brand "Outlast", manufactures clothing with either a MEPCM coating or MEPCMs embedded in the textile fiber itself [74]. The MEPCMs used are 20-40 μm in diameter with 80-85% PCM loading.

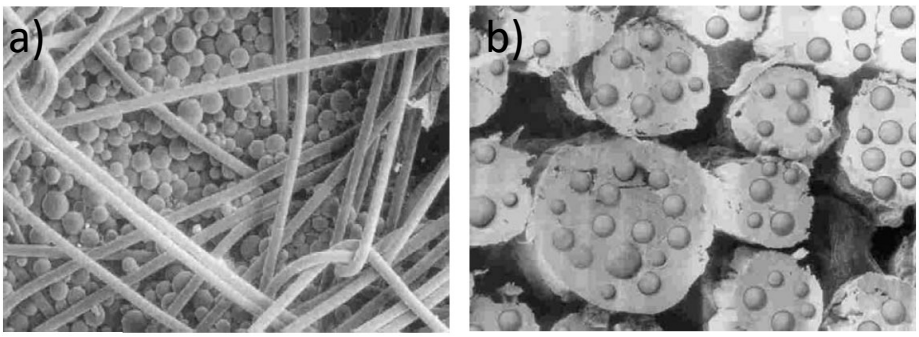


Figure 1.5 **PCM microcapsules as (a) textile coating ; (b) enclosed in textile fiber [74]**

1.4.2 PCM slurry

The PCM slurry is PCM dispersed in an aqueous medium. There are different types of PCM slurry: 1) Ice slurry: Ethylene glycol aqueous solutions supercooled to form fine particles of ice dispersed in water; 2) PCM microemulsion: Organic PCM dispersed in water and stabilized with emulsifiers; 3) MEPCM slurry: Organic PCM encapsulated in a tiny container and dispersed in water. Generally it requires fewer surfactants than PCM microemulsion for stabilization.[75]

The MEPCM slurry has some advantages over ice slurry and PCM microemulsion in the following two aspects: 1) a wider range of temperatures: Compared to ice slurry which only has T_m of 0 °C, organic PCMs have various T_m which can be selected based on TES application. For instance, ice slurries are not useful for space cooling as its T_m of 0 °C is much lower than the ambient temperature.[76] 2) Long-term stability: PCM microemulsions have lower stability than MEPCM slurries because the PCM particles are not encapsulated. This means that during thermal cycles of the PCM, melting and solidifying the PCM particles will coagulate or coalesce forming larger and larger PCM particles which lead to phase separation and possibly clogging in the pipes or pumps and reduced heat storage rate. [77]

PCM slurries can be used as thermal fluids to transport thermal energy from one location to another in the form of latent heat of PCMs. Figure 1.6 shows the energy storage density of PCM slurry comparing to water over a temperature gradient of 5 °C. A slurry containing 30 wt% PCM doubles the thermal storage capacity of the thermal fluid.[78] A

study of a TES system comprised of 10-30 micron PCM particles slurried in water and silicone oil in a heat exchange loop showed an increase of heat transfer rate and reduced system temperature compared to sensible heat thermal fluids.[79] The higher heat transfer rate of PCM slurry is also useful in applications which require thermal energy to be stored/released at faster rates. PCM slurries are used in waste heat recycling, where large amounts of waste heat, e.g. flue gas, waste water have to be recovered from the process stream in a short timeframe.[80] In conclusion, PCM slurries combine both 1) high thermal energy storage of PCM and 2) the ability to circulate or transport thermal energy via pipes; with 3) higher heat transfer rate.

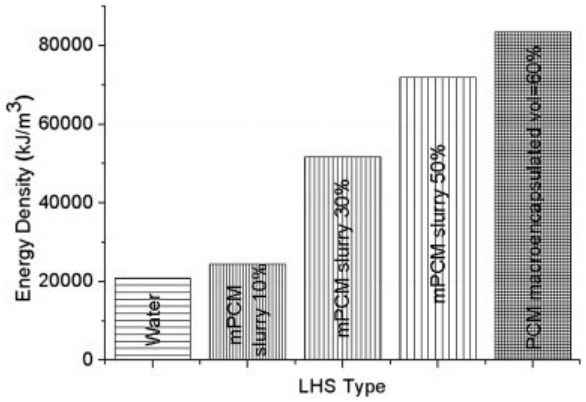


Figure 1.6 Energy density of different thermal fluids(ΔT = 5°C:) [78]

The properties of PCM slurry makes them useful in applications such as heat storage tanks and as thermal fluids.[75] At the Narita Airport in Tokyo, refrigerants have been replaced due to the chiller units were unable to meet peak demand periods. To resolve the problem without additional cooling equipment, Mitsubishi Heavy Industries installed a MEPCM slurry tank. The MEPCM slurry was cooled during off-peak hours,

and the cooling energy was used to meet peak demand periods. Although the storage density of the MEPCM slurry tanks was lower than that of an ice tank, it still is higher than that of water. Moreover, its coefficient of performance (COP) and operational costs were similar to a water tank and lower than those of an ice tank.[81] PCM slurry has been compared with water as heat transfer fluid in the chilled ceiling for space cooling. The PCM with a T_m of 18 °C was encapsulated to form 40 vol% PCM slurry and tested over four months in the chilled ceiling for space cooling. Compared with water, the PCM slurry requires 1) lower pumping rates due to its higher heat capacity and 2) reduced panel temperatures during the day.[82]

PCM slurry shows potential to enhance thermal energy transportation, thermal energy storage and heat transfer properties in heat exchangers. However, factors such as hydrodynamics[83, 84], heat transfer characteristics [85], heat capacity[86], the coefficient of performance, initial costs and long-term stability need to be considered before they can be used in practical applications.

In conclusion, Then MEPCMs offer the following advantages:

- Enable the PCM to be handled as either solid material or formulated into aqueous dispersions or powder, thus allowing easy handling.

- Preventing PCM from flowing away during its solid-liquid phase transition[87].

- Protecting PCMs from the external environment, e.g. contamination, chemical reactions, prevention of vaporization.

- PCMs have inherently low thermal conductivity (0.3-0.5 W/m ºC)[88]. The large surface area of the MEPCMs may allow faster response to changes in the environment's temperature, providing a thermoregulatory with better insulation and cooling effects.

- MEPCMs also show reduced volume change during phase transition, enhanced mechanical stability in heating-cooling cycles, reduced PCM toxicity and easy application. [89]

- MEPCMs dispersed in water have lowered viscosity[90] which aids heat transfer via convection.

1.5 Types of PCM and their properties

The criteria of PCM for optimal TES as defined by Dincer and Rosen[10] are:

1. High thermal storage per unit mass (kJ/kg)
2. High thermal storage per unit volume (kJ/m^3)
3. No loss of thermal storage capacity over time
4. The phase transition is reversible
5. Phase transition temperature is within the operating temperature range
6. Low or no supercooling (Supercooling is the phenomena where the freezing temperature is much lower than melting temperature)
7. Chemical stability without reaction with the container.
8. Small volume change during the transition
9. Low toxicity
10. Low cost in relation to the application

PCMs can be divided into two large classes, **organic** and **inorganic**. This section will discuss various PCMs that have a phase transition temperature in the range around ~32.5±15 °C which would be suitable for thermal comfort applications.

1.5.1 Organic PCMs

Organic PCMs can be divided into paraffins, fatty acids, polyethylene glycol and others. The advantages of organic PCMs are 1) low supercooling; 2) non-corrosive; 3) melt and freeze repeatedly without phase segregation; 4) little to no degradation of latent heat of fusion. The disadvantages compared to inorganic PCMs are 1) lower phase change enthalpy; 2) lower thermal conductivity; 3) flammability.[91, 92]

Paraffin waxes are one of the most important types of PCMs. They consist of a range of n-alkanes [CH_3-$(CH_2)_n$-CH_3], which have high latent heat storage capacities between 200 and 250 kJ/kg with various melting temperatures. As the number of carbons increase, the melting temperature increases as well. They are easily available, odorless, chemically inert, non-corrosive and non-toxic.[93] **Table 1.2** summarizes the melting points (T_m) and latent heats of fusion (LH_f) of some paraffin waxes.

Table 1.2. **Paraffines : T_m and LH_f** [91]

No. of carbon atoms	T_m (°C)	LH_f (kJ/kg)
16	16.7	237.1
17	21.7	213
18	28.0	244
19	32.0	222

20	36.7	246
21	40.2	200
22	44.0	249
23	47.5	232
24	50.6	255

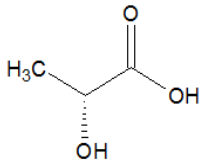
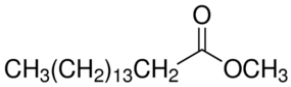
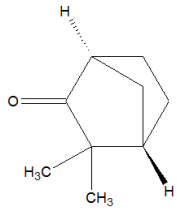
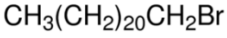
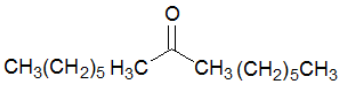
Fatty acids as shown in **Table 1.3** are usually derived from animal or plant fats and oils, and thus are considered a renewable and sustainable source of PCMs. The general chemical structure is $CH_3(CH_2)_n \cdot COOH$. They are biodegradable and non-toxic with good thermal and chemical stability. Some of the undesirable characteristics of fatty acids include their bad odour, corrosiveness and high sublimation rate. Different fatty acids can be mixed to form a eutectic mixture with a lower phase change temperature.[94, 95] Examples of eutectic fatty acid mixtures tested for thermal stability and reliability are lauric acid-myristic acid, lauric acid-palmitic acid and myristic acid-stearic acid.[95]

Table 1.3. **Fatty acids : : T_m and LH_f [91]**

Material	**Formula**	**T_m (°C)**	**Latent heat (kJ/kg)**
Caprylic acid	$CH_3(CH_2)_6COOH$	16.1	144
Acetic acid	CH_3COOH	16.7	184
Capric acid	$CH_3(CH_2)_8 \cdot COOH$	36	152
Eladic acid	$C_8H_7C_9H_{16} \cdot COOH$	47	218
Lauric acid	$CH_3(CH_2)_{16} \cdot COOH$	49	178

Other organic PCMs are a class of phase change materials which consist of sub-groups of paraffins, fatty acids, esters, alcohols and other organic compounds. Examples of these PCMs are shown in **Table 1.4**.

Table 1.4. **Other organic PCMs: : T_m and LH_f** [91]

Material	Structure	Melting	Laten
Glycerin		17.9	198.7
d-Lactic acid		26	184
Methyl palmitate		29	205
Camphenilone		39	205
Docosyl bromide		40	201
Caprylone		40	259
Phenol		41	120
Heptadecanone		41	201
1-Cyclohexylooctadecane		41	218

4-Heptadacanone	41	197
p-Joluidine	43.3	167
Cyanamide	44	209
Methyl eicosanate	45	230
3-Heptadecanone	48	218
2-Heptadecanone	48	218
Hydrocinnamic acid	48.0	118
Cetyl alcohol	49.3	141
α-Nepthylamine	50.0	93
Camphene	50	238

1.5.2 Inorganic PCM

Inorganic PCMs refer to salt hydrates and eutectic metals/salts. The advantages of inorganic PCMs over organic PCMs are 1) high volumetric heat capacity, 2) relatively higher thermal conductivity (compared to paraffins), 3) salt hydrates are inexpensive, 4) high availability, 5) eutectic metals/salts have higher working temperatures up to 832 ºC which is used to harvest concentrated solar energy used in solar power plants[96]. The drawbacks of salt hydrates include: 1) Incongruent melting wherein the dehydrated salt sinks, causing phase separation of the materials. This phase separation decreases the amount of dehydrated salt available for rehydration which leads to loss of latent heat of fusion over repeated melting and freezing; 2) Supercooling, wherein poor nucleating properties require temperatures lower than the melting point to initiate nucleation to release the stored heat; and 3) metal-corrosive which makes them incompatible with metal

containers. Salt hydrates have a general formula of $AB{\cdot}nH_2O$ where n molecules of H_2O are coordinated to the inorganic salt AB. When melting occurs, the salts release the coordinated water either partially or completely.

$$AB \cdot nH_2O \rightarrow AB \cdot (n-m)H_2O + mH_2O \quad \text{or} \quad AB \cdot nH_2O \rightarrow AB + nH_2O$$

Table 1.5 summarizes some common salt hydrates and their thermal properties.

Table 1.5: Salt hydrates: T_m and LH_f [91]

Material	T_m (°C)	LH_f (kJ/kg)
$K_2HPO_4{\cdot}6H_2O$	14.0	109
$FeBr_3{\cdot}6H_2O$	21.0	105
$Mn(NO_3)_2{\cdot}6H_2O$	25.5	148
$FeBr_3{\cdot}6H_2O$	27	105
$CaCl_2{\cdot}12H_2O$	29.8	174
$LiNO_3{\cdot}2H_2O$	30	296
$LiNO_3{\cdot}3H_2O$	30	189
$Na_2CO_3{\cdot}10H_2O$	32	267
$Na_2SO_4{\cdot}10H_2O$	32.4	241
$KFe(SO_4)_2{\cdot}12H_2O$	33	173
$CaBr_2{\cdot}6H_2O$	34	138
$LiBr_2{\cdot}2H_2O$	34	124
$Zn(NO_3)_2{\cdot}6H_2O$	36.1	134
$FeCl_3{\cdot}6H_2O$	37	223

$Mn(NO_3)_2 \cdot 4H_2O$	37.1	115
$Na_2HPO_4 \cdot 12H_2O$	40.0	279
$CoSO_4 \cdot 7H_2O$	40.7	170
$KF \cdot 2H_2O$	42	162
$MgI_2 \cdot 8H_2O$	42	133
$CaI_2 \cdot 6H_2O$	42	162
$K_2HPO_4 \cdot 7H_2O$	45.0	145
$Zn(NO_3)_2 \cdot 4H_2O$	45	110
$Mg(NO_3) \cdot 4H_2O$	47.0	142
$Ca(NO_3) \cdot 4H_2O$	47.0	153
$Fe(NO_3)_3 \cdot 9H_2O$	47	155
$Na_2SiO_3 \cdot 4H_2O$	48	168
$K_2HPO_4 \cdot 3H_2O$	48	99

1.6 Current methods of PCM microencapsulation and their limitations

In the previous section, it was mentioned that PCMs have high heat storage density. However, PCMs each have some technical difficulty which needs to be overcome before it can be incorporated into a PCM-based TES system. They include agglomeration, component separation, supercooling, large volume change during phase transition, low thermal conductivity, costly heat exchangers, possible corrosion to container walls and limited heat transfer area. However, some of these technical difficulties can be overcome with microencapsulation of the PCM.

The most common methods for synthesizing MEPCMs as reported in literature are spray drying, *in-situ* polymerization, interfacial polymerization, suspension polymerization and coacervation methods[97-101]. The following section will discuss the various methods of microencapsulation according to the type of process that takes place during encapsulation, namely physical, chemical or physico-chemical[89].

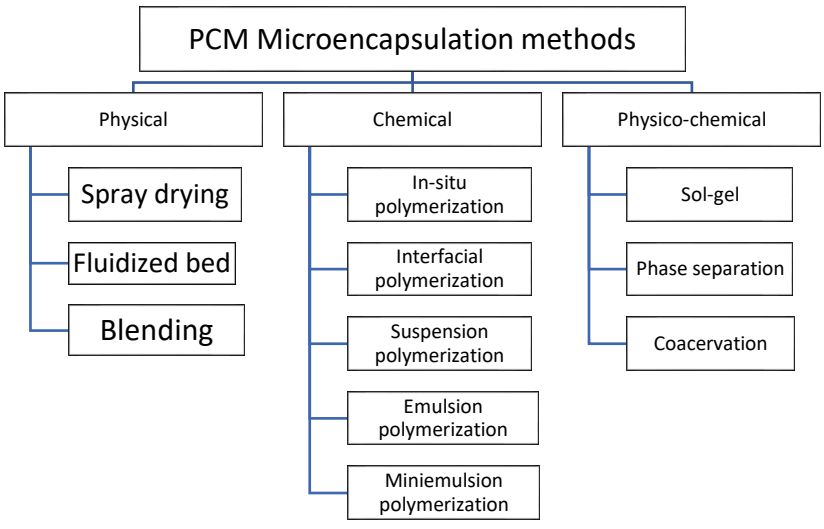


Figure 1.7. Types of PCM microencapsulation methods

1.6.1 Physical

Physical approaches used to synthesize the MEPCMs are spray drying, fluidized bed and blending. Table 1.6 shows examples of these MEPCMs synthesized with these methods and their properties.

Table 1.6 Examples of MEPCMs synthesized by physical methods and their properties

Method	Shell Material-PCM	Diameter (μm)	T_f (°C)/ T_m (°C)	Transition enthalpy (kJ/kg)	Encapsulation efficiency	%PCM	Thermal cycling
Spray drying	LDPE/EVA-Rubitherm@RT27 [102]	< 10 μm	28/29	98	63%	48%	N/A
	Gum Arabi c- ethyl hexanoate [103]	10-20 μm	N/A	N/A	90%	20%	N/A
	Gelatin and acacia - paraffins [104]	<1 μm	N/A	140-210	84-91%	66%	N/A
Blending	PEG - CEL [105]	-	35/60	127	-	75%	N/A
	PEG - CEL [106]	-	27/59	143	-	95%	N/A
	PEG - PMMA [107]	-	43/57	142	-	80%	N/A

(N/A: Data not available; - : Data is irrelevant)

1.6.1.1 Spray drying

Spray drying is commonly used in food processing and it can also be used to produce MEPCMs. The process requires formation of an oil-in-water emulsion wherein the oil phase is the PCM; and the aqueous phase is composed of the shell material and solvent. **Figure 1.8** shows a schematic diagram of the spray dry process, the emulsions are heated and fed to an atomizer where it is sprayed into the hot gas stream. The solvent is swiftly vaporizes as the droplets fall through the hot air (~150 ºC) to form the MEPCM.[103] The advantages of synthesized MEPCMs with spray drying are: high encapsulation efficiency, relatively easy scale-up for production and high thermal stability.

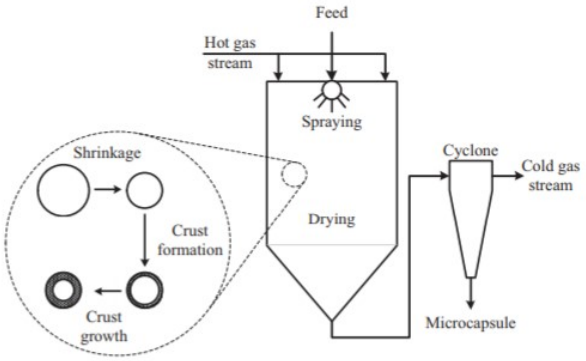


Figure 1.8. **Schematic of spray drying to produce MEPCMs[100]**

Borreguero[102] used spray drying to encapsulate Rubitherm@RT27(paraffin-based PCM) with a shell material: thermoplastic low density polyethylene (LDPE) and ethylvinylacetate copolymer (EVA) (LDPE/EVA-Rubitherm@RT27). The LDPE/EVA-Rubitherm@RT27 microcapsule had a matrix structure. Spray drying using gum arabic

as shell material and esters for core has also been reported with encapsulation efficiency of up to 90% and diameters of approximately 10-20 μm. However, leakage of PCM occurred at relative humidity exceeding 80% RH, possibly due to low rigidity or water solubility of the shell material.[103] Hawlader also utilized this method to form MEPCMs with gelatin and acacia as shell material and paraffins as PCM cores.[104] The paraffin emulsion was atomized with a centrifugal atomizer at 25,000 rpm with inlet and outlet temperatures of 130 and 80 °C, respectively. The product yield was up to 95%. Latent heat of fusion and melting were 221.52 J/g and 216.4 J/g respectively, which are comparable to bulk paraffin whose latent heat is in the range of 200-250 J/g. The properties of some MEPCMs synthesized by spray drying are shown in Table 1.6 and their respective morphologies are shown in Figure 1.9.

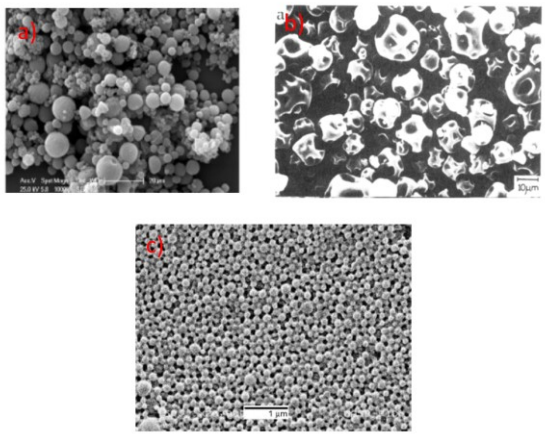


Figure 1.9 SEM images of MEPCMs synthesized via spray drying: a) LDPE/EVA-Rubitherm@RT27 [102]; b) Gum arabic-ethyl hexanoate[103]; c) gelatin and acacia-paraffins [104]

Diameters of the MEPCMs synthesized with spray drying range from 1-20 μm. This encapsulation method is also limited to PCMs with relatively high degradation

temperatures and high boiling points. Inlet and outlet air temperatures reach up to 150 ºC during spray drying[103, 108]. Therefore, this precludes encapsulation of PCMs such as fatty acids which have low boiling point and salt hydrates where high temperatures will evaporate the water of hydration.

1.6.1.2 Fluidized bed

Fluidized bed is another method than can be used to prepare MEPCMs. It is a common commercial method of encapsulation patented by Dr Wurster from 1957-1966.[109-111] The shell material is either a dissolved solution or a melt. It is sprayed either through the top or bottom of the atomized PCM suspended by hot gas flow. (see Figure 1.10) The shell is formed through either 1) The hot gas evaporates the solvent to form a solid shell over the atomized PCMs or 2) the melt proceeds to solidify onto the PCM cores. The hot gas flow is important for uniform circulation of the particles to achieve 1) uniform coating and 2) reduce agglomeration.

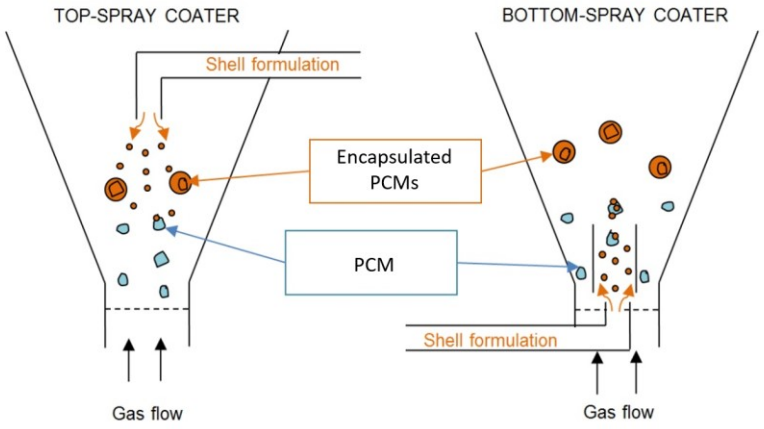


Figure 1.10 **Schematic diagram for fluidized bed** [112]

Chen used this method to encapsulate salt hydrates that were solidified at low temperature, and ground to become a flowable powder to be formed into pellets with a tableting machine. These pellets were then encapsulated via the fluidized bed. One of the encapsulated PCMs synthesized by Wurster was sodium sulfate decahydrate, $Na_2SO_4 \cdot 10H_2O$ in multilayer walls with shell materials such as asphalt; mica; butadiene-acrylonitrile and vinylidene chloride-acrylic copolymer. The encapsulated pellets were cylindrical, with a diameter of 125 mm and thickness around 9 mm. Concrete mortar brick with 30 wt% of the synthesized PCM capsules showed no fractures or leakage after several phase-change cycles.[113]

MEPCMs synthesized with fluidized bed are not water dispersible due to their large dimensions. However, this is possibly the only method which reports successful encapsulation of salt hydrates with repeated thermal cycling. Although it multiple shell layers (six in total) are required to prevent PCM salt hydrates from water loss which is the major technical difficulty for salt hydrate PCM encapsulation.

1.6.1.3 Blending

The PCM poly(ethylene glycol) can be modified by blending with another polymer to form a matrix structured MEPCM. The matrix MEPCMs is classified as solid-solid PCMs because the phase transition is from a crystalline state to an amorphous solid state without melting. Their advantages include having no shell structure enabling direct contact with the heat transfer medium, small volume change and no liquid phase.

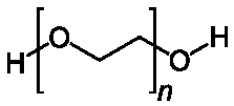


Figure 1.11 **Chemical structure of the poly(ethylene glycol) (PEG)**

Most modifications involve blending PEG with a rigid polymer that has hydroxyl groups to provide mechanical strength for a network structure to hold the PEG and hydroxyl groups for intermolecular interaction with the hydroxyl groups on PEG. Both these factors can result in restricting the movement of the PEG chains to prevent melting. Sari and Alkan[107] have studied blends of PEG/PMMA and found a maximum of 80% w/w of PEG in which no leakage of PEG occurred for 100 heating/cooling cycles. Liang[106] and Pliechowska[105] have both studied PEG blended with cellulose (PEG/CEL). The amount of transition enthalpy is directly related to the amount of PEG in the matrix (see Table 1.6). Matrix PCMs have low dispersibility in fluid, and need to be powdered followed by addition of stabilizers to form a stable dispersion.

1.6.2 Chemical Synthesis of MEPCMs

Chemical approaches used to synthesis the MEPCMs mainly involve the interfacial polymerization, *in-situ* polymerization, suspension polymerization, and emulsion polymerization. Table 1.7 shows examples of these chemical methods and their properties.

Table 1.7 **Examples of MEPCMs synthesized by chemical methods and their properties**

Method	**Shell Material-PCM**	**Diameter (μm)**	**Tf(°C) / T_m (°C)**	**Transition enthalpy (kJ/kg)**	**Encapsulation efficiency**	**%PCM**	**Thermal cycling**
Interfacial polymerization	Polyurea-butachlor	1-20	-	-	-	-	-
	Polyurea-octadecane[114]	1	20 / 31	112	75.4%.	65%	N/A
	Polyurea-30-C paraffin[115]	6.4	14-31 / 29-44	121	99%	88%	N/A
	Polyurea -Octadecane[116]	~308	25 / 29	198	~100%	84%	N/A
In-situ polymerization	Resorcinol modified poly(melamine formaldehyde)-Octadecane[117]	12	21-23 / 27	149	92%	69%	N/A

Table 1.7 **Examples of MEPCMs synthesized by chemical methods and their properties**

	Resorcinol modified poly (urea formaldehyde)-tetradecane[118]	100 nm	2-3 / 5-7	134	N/A	60%	N/A
	poly (urea formaldehyde)-hexadecane[119]	≤100	16 / 20	52	N/A	20%	N/A
Suspension polymerization	polystyrene -paraffin	D_n 14; D_v 278	N/A	135	N/A	68%	N/A
	poly(ethylene glycol dimethacrylate) Hexadecane[120]	4-11	1-8 /1 5	190-210	N/A	83-91%	N/A
	Poly(methyl methacrylate)/Rubitherm®27[121]	5-30	8 / 22	163	~100%	62%	N/A
	Poly (butyl acrylate) crosslinked with divinyl benzene/Paraffin-Butyl stearate[122]	10-80	28 / 26	86	N/A	46-68%	500 cycles; <4% enthalpy loss

Table 1.7 **Examples of MEPCMs synthesized by chemical methods and their properties**

Emulsion polymerization	Poly(methyl methacrylate)/Paraffin [123]	0.4-2.3	35 / 35	84-88	N/A	35%	5000 cycles; ~0% enthalpy loss
	Poly (butyl acrylate) crosslinked with allyl methacrylate/Paraffin microcapsules [72]	0.5-4	15 / 18	85	N/A	35%	-
	Poly(methyl methacrylate)/Paraffin [65]	0.5-2	25-27 / 24-33	101	83%	61%	200 cycles; 1% enthalpy loss
	Poly(styrene) crosslinked with divinylbenzene-SiO_2/1-Dodecanol[124]	10-200	16-18 / 24-25	125	94%	63%	2000 cycles; 6% enthalpy loss

(N/A: Data not available; -:Data is irrelevant)

1.6.2.1 Interfacial polymerization

Interfacial polymerization also known as polycondensation is one of the most common methods to synthesize MEPCMs. The size of microcapsules produced with the interfacial polymerization can be as small as 3-6 μm[89]. Encapsulation through interfacial polymerization involves dispersing the PCM in an oil-in-water emulsion. The microcapsule wall forms at the interface of the oil-in-water emulsion when the oil-soluble monomer (A) and the water-soluble monomer (B) react through interfacial polymerization to form A-B through the condensation reaction [100]. As the thickness of the AB polymer shell increases, diffusion of monomers is reduced thus slowing down the polymerization. Some examples of monomer pairs of (A) and (B) are isocyanates and polyalcohol (polyurethane shell), isocyanates and polyamines (polyurea shell), acid chlorides and polyamines (polyamides)[125]. Interfacial polymerization is a viable method to synthesize MEPCMs. There have been reports of synthesized microcapsules with high resistance towards thermal degradation which is a desirable feature for reducing flammability.[115, 126]

An early use of interfacial polymerization for microencapsulation can be found in the work of Yadav[127]. He synthesized microcapsules with a polyurea shell and a core of butachlor with diameters from 1-20 μm. He concluded that the stirring rate had little effect on the microcapsule size. Yadav also found that more time was needed to form microcapsules of larger size. The diffusion rate of each of the monomers (A) and (B) across the o/w interface through the partially formed polymer shell of the microcapsule is another key factor that affects the rate of the formation of the microcapsules.

MEPCMs with high uniformity were prepared with tubular microfluidics (Figure 1.13). The organic phase contains PCM, catalyst for interfacial polymerization, dibutyltin dilaurate (DBTDL) and isophorone diisocyanate monomer (IPDI). The continuous aqueous phase contains emulsifier, tetraethylenepentamine monomer (TEPA) and poly(vinyl alcohol) (PVA) as stabilizer. (Chemical structures shown in Figure 1.12) As the PCM containing organic phase is injected at a constant speed of 0.5 μL/s into the aqueous phase which flows at 8 μL/s, the difference in the velocities of the liquid causes the organic phase to break off into uniform droplets. The droplets are stabilized by the emulsifier in the aqueous phase, and interfacial polymerization takes place to form a polyurea shell. The MEPCMs synthesized by Lone had a 84% Loading, supercooling was ΔT_f -4.22 °C which was reduced to -2.65 °C through incorporation of Fe_3O_4 nanoparticles into the shell material. The Fe_3O_4 nanoparticles can act as nucleating sites due to their high crystallinity. These nucleating sites promote heterogeneous nucleation thus reducing supercooling phenomena.[116]

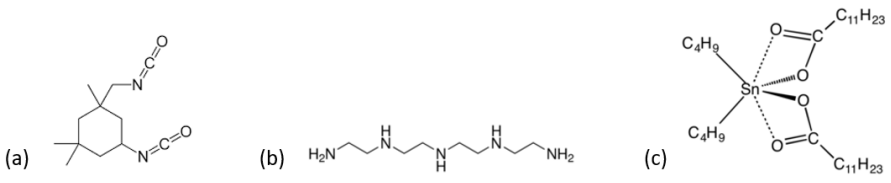


Figure 1.12 **Chemical structure of (a) isophorone diisocyanate (IPDI); (b) tetraethylenepentamine (TEPA) and (c) Dibutyltin dilaurate (DBTDL)**

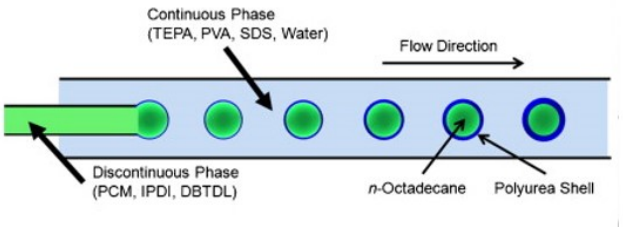


Figure 1.13 **Schematic diagram of the fabrication of monodisperse PCM@polyurea microcapsules in a tubular microfluidic device[116]**

Figure 1.14 shows some examples of MEPCMs prepared by interfacial polymerization :octadecane/polyurea MEPCMs (D_n 1 micron)[128], polyurea MEPCMs (Dn 6.4 microns) [115], and octadecane/polyurea MEPCMs (D_n 308 micron)[116]. The thermal properties of the MEPCMs shown are summarized in Table 1.7. It shows that MEPCMs synthesized via interfacial polymerization has higher transition enthalpy (>150 kJ/kg), but suffers from significant supercooling. At the same time, more studies on thermal energy storage over multiple cycles need to be carried out to evaluate MEPCMs for practical applications.

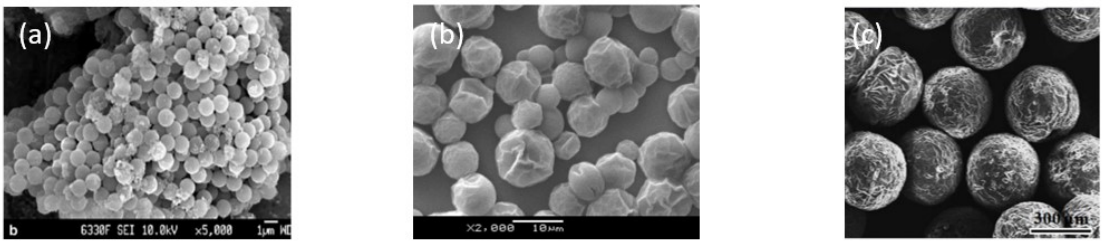


Figure 1.14 **MEPCMs prepared by the interfacial polymerization (a) Octadecane/Polyurea MEPCMs (D_n, 1 micron)[128]; (b) Polyurea MEPCMs (D_n, 6.4 microns) [115]; and (c) Octadecane/Polyurea MEPCMs synthesized with tubular microfluidics (D_n 308 micron)[116]**

1.6.2.2 In-situ polymerization

In-situ polymerization involves polymerization of water-soluble monomers, which precipitate onto oil droplets to form a shell. Various researchers have used this method to produce MEPCMs. [118, 129-131]. Melamine-formaldehyde and urea-formaldehyde are common monomer pairs for synthesizing MEPCMs and their respective chemical structures are shown in Figure 1.15. Synthesis of MEPCMs with in-situ polymerization requires the PCM and surfactant dispersed in water, followed by addition of monomers or a prepolymer. The pH is decreased to initiate the condensation reaction, polymerization occurs in the aqueous continuous phase to form a crosslinked polymer at reported temperatures of 45-75 °C. [129-132]As polymerization continues, the molecular weight of the crosslinked polymer increases, it becomes increasingly insoluble, precipitates out and deposits on a PCM oil droplet to form a shell.

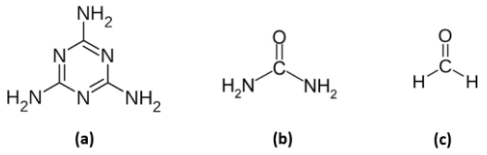


Figure 1.15 Chemical structure of (a) Melamine; (b) Urea and (c) Formaldehyde

The properties of three MEPCMs synthesized by in-situ polymerization are compared in Table 1.7 and their morphologies are shown in Figure 1.16. These include: a) Sarier and Onder have encapsulated various paraffins for textile applications.[119] b) Zhang [117] synthesized the MEPCMs with a poly(melamine-formaldehyde) shell with an octadecane core. c) Fang [118] also used urea-formaldehyde as shell material to encapsulate

PCM, tetradecane. Although all three MEPCMs were synthesized via in situ polymerization they varied in size (from 100 nm to 100 μm) and their surfaces from rough to smooth. This might be due to the different conditions for precipitation during shell formation, which could be influenced by temperature, surfactant, pH, electrolyte concentration, stirring rates, shell material etc. All three of the aforementioned MEPCMs used resorcinol as an additional crosslinker during polymerization. Perhaps, most intriguing is the minimal supercooling (2-3 °C) for MEPCMs with diameters as small as 100 nm without addition of nucleating agents which is singularly reported by Fang.[118] This is antithesis to supercooling phenomena which increases when MEPCMs get smaller, as seen in previous MEPCMs with diameters in the μm range exhibit much higher supercooling (~3-8 °C).

To summarize, the MEPCMs synthesized via in-situ polymerization have low supercooling, but at the same time have low transition enthalpy <150 kJ/kg with the encapsulation ratio of 20-70%. Furthermore, the shell materials have residual formaldehyde which poses an environmental and health concern. At the same time, more studies on thermal energy storage over multiple cycles need to be carried out to evaluate MEPCMs for practical applications.

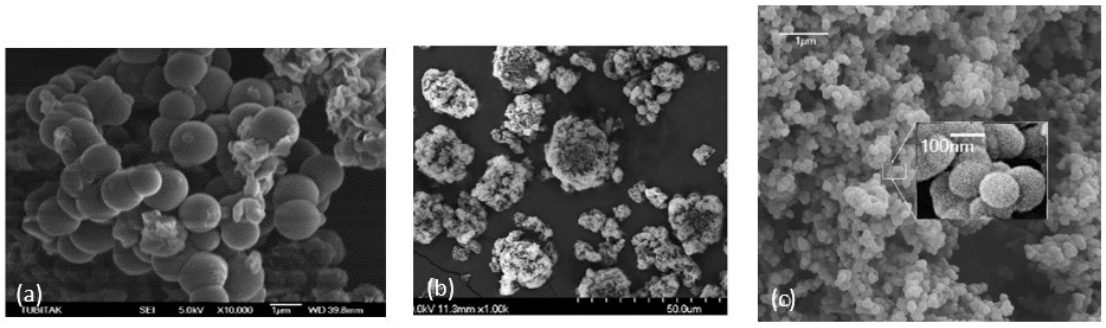


Figure 1.16 **SEM images of MEPCM synthesized via in-situ polymerization: a) poly(urea-formaldehyde) shell with hexadecane core[119]; b) resorcinol modified poly(melamine-formaldehyde) shell with octadecane core[117];c) resorcinol modified poly(urea-formaldehyde) shell with tetradecane core[118]**

1.6.2.3 Suspension polymerization

Suspension polymerization involves rigorous agitation to disperse the oil phase of PCM in an aqueous medium. The aqueous medium is composed of stabilizers for the suspension. The oil phase is composed of the PCM together with a monomer(s) and an initiator. When the monomer to PCM ratio is too large, the polymerization might take place in the oil phase, forming homopolymer dispersed in the PCM core of the microcapsule. On the other hand, if monomer to PCM ratio is too small, the PCM core might not be fully encased.[133]

Sánchez-Silva employed this method to prepare microcapsules with polystyrene as shell material and a PCM core of Rubitherm® RT31. A study of different suspension stabilizers including polyvinylpyrrolidone (PVP), Arabic gum, polystyrene, poly(vinyl alcohol) (PVA) and gelatin was carried out. Results showed that stabilizers strongly affected the properties of the microcapsules including size and size distribution, encapsulation efficiency, thermal energy storage and morphology. For example, the MEPCMs synthesized with Arabic gum showed the highest %loading of up to 68% with a number average diameter of 13.5 μm, and volume average diameter of 278 μm.[133] Ma reported a PCM mixture comprised of butyl stearate and paraffin with similar melting

points mixed in 1:1 ratio and encapsulated with poly (butyl acrylate) crosslinked with divinylbenzene. Figure 1.17 shows their respective chemical structures. The MEPCMs had minimal supercooling exhibited only as broadening of the freezing peak. PCM loading of 68% showed a transition enthalpy of 89 kJ/kg. Ma also reported that samples subjected to 500 thermal cycles of freezing and melting had as little as 4% PCM loss.[122]

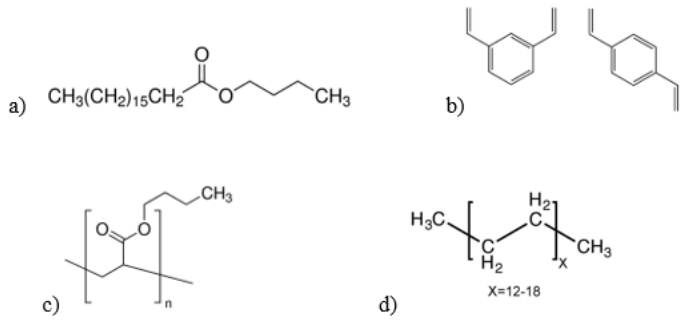


Figure 1.17 **Chemical structure of a) butyl stearate; b) divinyl benzene; c) poly(butyl acrylate); d) paraffin wax**

Micro-suspension polymerization is a modified version of suspension polymerization. Like suspension polymerization, the initiator is soluble in the monomer droplets. But it also uses a surfactant to reduce the size of the monomer droplet to produce sizes ranging from 1-20 micron. This approach often exhibits the kinetics of both emulsion and suspension polymerization. However, when monomer droplet size is decreased <20 micron, both the suspension and emulsion polymerizations take place, leading to different particle sizes and composition. The reason both kinetics takes place is because of solubility of the monomer and initiator in the aqueous phase which however small would lead to nucleation of emulsion particles. To avoid the formation of any undesirable by-

products, initiators and monomers with low water solubility are employed. Cunningham compared MMA micro-suspension polymerization with azobisisobutyronitrile (AIBN) and lauryl peroxide (LPO). The LPO showed reduced formation of the emulsion polymer[134]. Other methods to reduce emulsion polymerization kinetics are addition of water soluble inhibitors to quench radicals in the aqueous phase[135], and iodine transfer agent which increases water insolubility of the radical in the monomer droplet, thus reducing its diffusion into the aqueous phase.[136] Micro-suspension polymerization has been used for encapsulation of TiO_2 which is used in electrophoretic display screens such as Kindle[137], pigments[138] and finally PCMs.

Chaiyasat reported MEPCMs synthesized with micro-suspension polymerization with a water domain formed in the PCM core during the cooling of the MEPCMs after synthesis. There was increased supercooling presumably due to the PCM in direct contact with the water domain inside the MEPCM. [139] Okubo's group synthesized MEPCMs through micro-suspension polymerization with different polymer shells of increasing polarity and larger MEPCM diameter to reduce supercooling. In most cases, the freezing temperature of PCM is lowered drastically due to microencapsulation.[120] Poly(methyl methacrylate)/Rubitherm®27 (PMMA/RT27) MEPCMs were synthesized with micro-suspension polymerization and used iodine transfer agents to suppress radical exit from the monomer droplet and benzoyl peroxide as initiator.[121]

The properties of the MEPCMs synthesized with suspension polymerization or micro-suspension polymerization are summarized in Table 1.7 and selected SEM images are shown in Figure 1.18. The formation of emulsion nuclear particles is a problem. These

polymers do not contribute to the PCM encapsulation and decrease the heat storage capacity. During synthesis, radical scavengers have to be added to the aqueous phase[140] or iodine transfer polymerization can be used to reduce radical solubility in water.[121, 136]

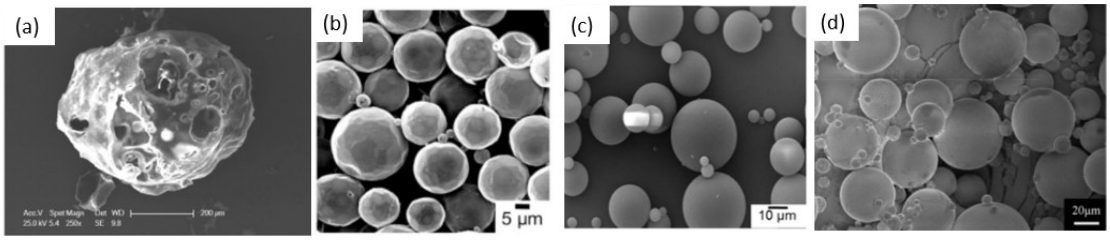


Figure 1.18 **SEM images of MEPCM synthesized with suspension polymerization: a) PS/Rubitherm 31 [133]; b) poly(ethylene glycol dimethacrylate) - Hexadecane[120] c) Poly(methyl methacrylate) -Rubitherm®27[121];d) Poly (butyl acrylate) crosslinked with divinyl benzene/Paraffin-Butyl stearate[122]**

1.6.2.4 Emulsion polymerization

Emulsion polymerization is used for fabricating MEPCMs with sizes ranging from 500 nm to hundreds of microns.[65, 72, 123, 124] The first step in emulsion polymerization is the formation of an oil-in-water emulsion. Unlike suspension polymerization and interfacial polymerization, the oil phase containing PCM and monomer(s) is stabilized with emulsifiers through the formation of micellar structure and uses a water-soluble initiator. There are only a few literatures which have reported emulsion polymerization as a means to fabricate MEPCMs, possibly due to formation of secondary particles without PCM inside as a result of particle nucleation taking place in the aqueous phase.

The encapsulation process via emulsion polymerization is best described by Mcdonald's research on voided particles[141]. Figure 1.19 shows the schematic of encapsulation proposed by Mcdonald which starts with an o/w dispersion of monomer dissolved in PCM droplets stabilized by surfactant, the PCM being a non-solvent for the polymer. As polymerization progresses, the oligomers become less soluble in the PCM/monomer droplet and phase separation occurs primarily at the droplets' interface which has the lowest interfacial energy in the system. The water-soluble initiator generates aqueous phase radicals, which adsorb onto the surface of the dispersion. The droplet surface serves as the primary site for polymerization with the monomer concentration being replenished by diffusion through both the continuous phase of the emulsion and the PCM/monomer droplet. This interfacial polymer also serves as the polymerization locus for the further monomer or crosslinker charge for formation of the network polymer shell.

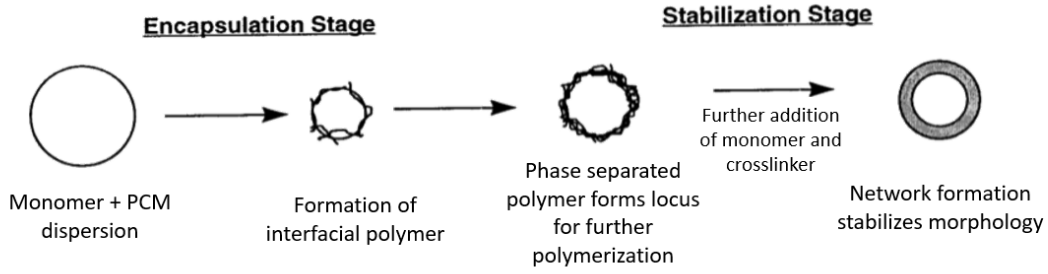


Figure 1.19 **Schematic of encapsulation via emulsion polymerization[141]**

Sari and Alkan's group reported the synthesis of MEPCM with emulsion polymerization.[90, 142] In accordance with traditional emulsion polymerization, they used TritonX100 as surfactant, and ferrous ammonium sulphate solution to form an emulsion with the oil phase via stirring at a high speed of 2000 rpm. The oil phase was composed of the monomer methyl methacrylate (MMA), allyl methacrylate and the PCM. After

stirring for half an hour in a nitrogen a$T_m$osphere, above the melting temperature of the PCM, a water soluble initiator, tertbutyl hydroperoxide was charged to the system. The final product can be seen in Figure 1.20. It shows the presence of many smaller secondary particles. The loading percentage was 35% and ΔT_f was +1.5 °C indicating that the freezing temperature increased upon encapsulation. This might be due to the incorporation of the ferrous ammonium sulphate crystals into the crosslinked poly (methyl methacrylate) shell or the PCM core which acted as nucleation sites for solidfication. Tests to determine the thermal cycling stability of the MEPCMs (thermal storage capability changes over melting and freezing cycles) were carried out. Thermal profiles of the MEPCMs subjected to 5000 thermal cycles showed no decrease in latent heat or changes in chemical structure.

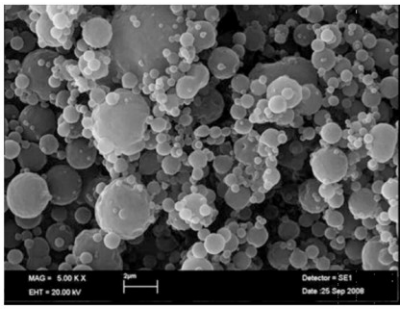


Figure 1.20 Image of MEPCM synthesized with emulsion polymerization: PMMA/n-eicosane[90]

Alay synthesized poly(butyl acrylate) MEPCMs for encapsulation of hexadecane. Three crosslinkers were compared: allyl methacrylate, ethylene glycol dimethacrylate, and glycidyl methacrylate. The optimized product was incorporated into a cotton/polyester blend fabric via pad-cure method. The fabric showed 29 kJ/kg transition enthalpy which could be used in thermoregulatory clothing.[72]

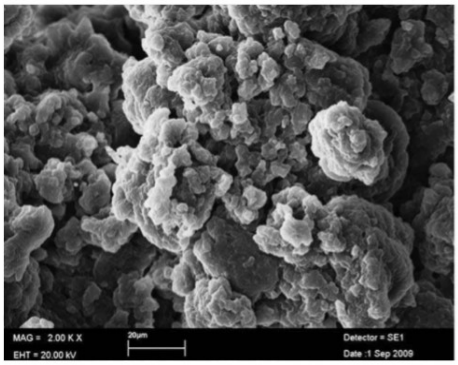


Figure 1.21 Image of MEPCM synthesized with emulsion polymerization:poly(butyl acrylate)/hexadecane[72]

Ma prepared poly(methyl methacrylate)/paraffin MEPCMs via emulsion polymerization initiated by UV irradiation. MEPCM diameter was shown to decrease with increasing emulsifying power during emulsion formation. The MEPCMs were tested with 200-1000 thermal cycles of freezing and melting and thermal profiles showed little to no enthalpy loss.[65]

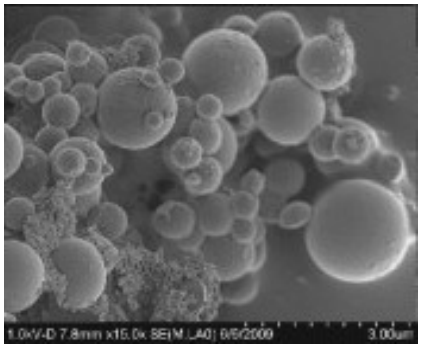


Figure 1.22 Images of MEPCM synthesized with emulsion polymerization: Poly(methyl methacrylate)/Paraffin [65]

Yin prepared MEPCMs with shell composed of SiO_2 and poly(styrene) crosslinked with divinylbenzene to encapsulate 1-dodecanol. The PCM emulsion was

stabilized with SiO_2 particles followed by polymerization to form a continuous shell. MEPCMs were subjected to 2000 thermal cycles with 5.8% enthalpy loss[124].

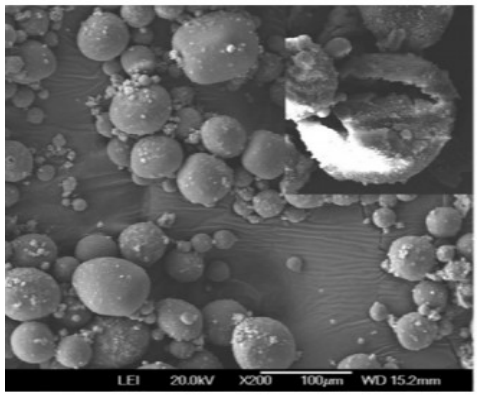


Figure 1.23 **Images of MEPCM synthesized with emulsion polymerization: Poly(styrene) crosslinked with divinylbenzene-SiO_2/1-Dodecanol[124]**

The properties of the MEPCMs synthesized with emulsion polymerization are summarized in Table 1.7. From Table 1.7, we see the MEPCMs have low transition enthalpy (<150 kJ/kg) and low encapsulation ratio. Percentage PCM is < 80% of the MEPCMs. Also, monomer to crosslinker ratio as high as 1:1 was required for successful encapsulation to form network polymer.[72, 90, 122, 142, 143] At the same time, polymerization might not take place at the o/w interface leading to the formation of emulsion nuclear particles that do not contribute to PCM encapsulation. To circumvent this, emulsion polymerization has been carried out with oil-soluble initiators.[144]

1.6.3 Physico-chemical

Table 1.8 lists selected examples of MEPCMs prepared by physic-chemicl methods including coacervation, phase separation and sol-gel.

Table 1.8 **Examples of MEPCMs synthesized by physico-chemical methods and their properties**

Method	Shell Material-PCM	Diameter (μm)	T_f(°C) / T_m (°C)	Transition enthalpy (kJ/kg)	Encapsulation efficiency	%PCM	Thermal cycling
Coacervation	gelatin-acacia/paraffin [145]	<1	N/A	234-240	80-92%	N/A	N/A
	gelatin-gum Arabic/coco fatty acid [87]	1-1000	N/A / 29-31	N/A	N/A	N/A	50 cycles; No significant change to heating temperature profile
	Poly (urea-formaldehyde)/ decanoic acid[146]	200 nm – 1.5	5.1 / 13.9	94	N/A	59%	N/A

Table 1.8 **Examples of MEPCMs synthesized by physico-chemical methods and their properties**

Method	Shell Material-PCM	Diameter (µm)	T_f(°C) / T_m (°C)	Transition enthalpy (kJ/kg)	Encapsulation efficiency	%PCM	Thermal cycling
Phase separation	acrylonitrile–styrene copolymer / n-tetradecane[147]	< 1	1.5 / 4.3	142	N/A	84.5%	N/A
Sol-gel	Silicon dioxide / n-octadecane [148]	8-11	20, 22 / 28	185	N/A	77%	N/A`
	Sodium silicate / n-octadecane [149]	8	24,22 / 28	85	N/A	35%	100 cycles; Slow leaching
	Silicon dioxide-expanded graphite / paraffin [150]	-	N/A / 28	104	N/A	50%	N/A
	Silicon dioxide / stearic acid [151]	20-30	53 / 54	171	N/A	91%	N/A

(N/A: Data not available; -:Data is irrelevant)

1.6.3.1 Coacervation

The term coacervation was first coined in 1929 by Bungenburg[152]. It describes the aggregation process of a dissolved polymer chain as it crosses the solubility phase boundary to form a coating around hydrophobic centers, either oil droplets or solid particles. This method is commonly used to synthesize microcapsules[153-161] for active ingredients such as drugs[162], fragrances, ink[163] and other active ingredients.

Simple coacervation uses only one polymer as the coating material. Examples include gelatin, agar and milk. Complex coacervation uses two polymers with opposite charges, e.g. gelatin-acacia[104, 164], gum arabic-gelatin[87, 119] and chitosan-alginate[165]. The core PCM material is first dispersed in an aqueous medium containing the colloidal material. Then the coating material deposits on the surface of PCM cores through decrease in solubility of the polymer/polymers. If necessary, the coacervates are usually further rigidized through cross-linking.

There are three steps in coacervation:[153]

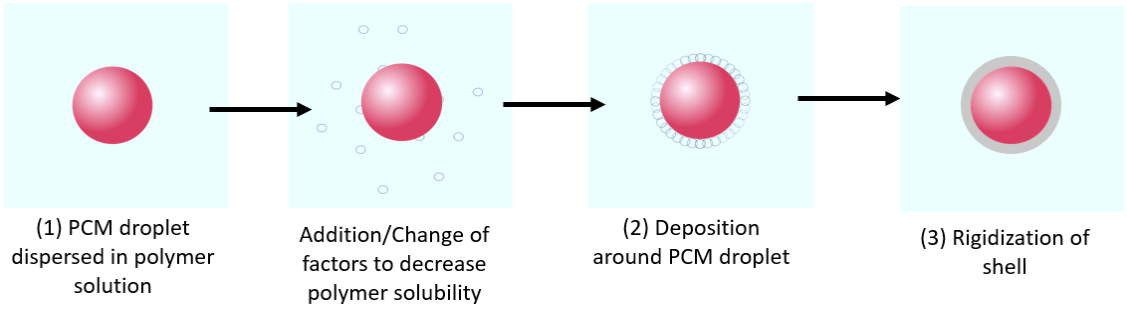


Figure 1.24 **Schematic diagram of the** coacervation process

1) **Core** material is dispersed into the coating material;

The three immiscible phases are, the polymer used as coating material, the solvent used to dissolve the polymer and the core material which is immiscible in either the polymer or the solvent. The coating material is dissolved in the solvent to form a solution. The core material which is immiscible with the solvent is dispersed in the polymer solution.

2) Deposition of coating material

As dissolution of the coating material is gradually increased, there are increased interactions between the polymer and the immiscible core particles. Dissolution of the coating material can be achieved by varying factors such as changing pH, increasing salt content, addition of a polyelectrolyte to neutralize charge on the polymer, changing temperature and addition of a non-solvent for the coating material. This leads to the formation of coacervate nuclei, concentrated polymer droplets. These droplets deposit onto the oil droplet interface. The resulting solution has two phases, one is the relatively polymer-concentrated coacervated nuclei droplets, and the other is the relatively lower polymer-concentrated phase. The coacervated nuclei adsorb onto the core/solvent interface, and in the absence of stabilizers they continue to aggregate and finally form a shell.

3) Rigidization of coating.

Rigidization of the coating can be carried out by adding chemical crosslinkers, or gelation of the polymer by lowering temperature.

The process describes above is simple coacervation, where only one polymer is used. When, two polymers of opposing charges are used to form the shell, the process is called complex coacervation. Instead of changing temperature or pH, a polymer of oppose charge is added to the soluble to neutralize the charges of the polymer and precipitate both to form the shell around the core material.

Coacervation has also been used in the encapsulation of PCM. Hawlader[104] has demonstrated preparation of paraffin MEPCMs with a gelatin-acacia shell via coacervation. PCM core to shell ratios as high as 2:1 were prepared. The paraffin was melted and dispersed via homogenization (10k rpm) in 10 wt% gelatin solution at 65 °C during which 10 wt% acacia solution was added dropwise. Rigidization of the shell was carried out by crosslinking with glutaraldehyde/formaldehyde. The resultant MEPCMs have latent heat of melting and fusion close to 240 J/g and 234 J/g, respectively. The diameter of the MEPCMs shown in Figure 1.25 were close to 1 μm or smaller.

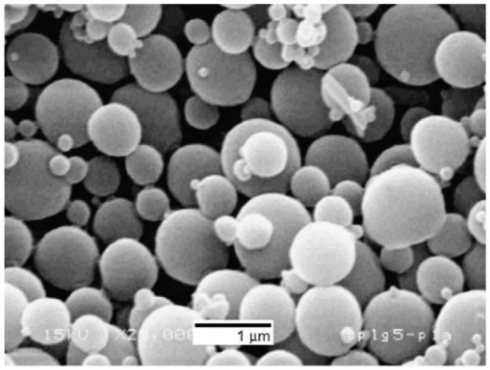


Figure 1.25 **SEM image of MEPCM prepared by coacervation: Gelatin/acacia - paraffin[104]**

Ozonur[87] prepared the MEPCMs using a natural coco fatty acid mixture as the PCM core. Gelatin-gum Arabic was found to be the best shell material. Diameters of the MEPCM depending on stirring speed and time, the MEPCM sizes ranged from 1 micron to 1 mm. The melting temperatures of the MEPCMs is in the range of 29–31°C, which is 7 °C higher than that of bulk coco fatty acid (22–24°C). This might be due to the temperature differences between the MEPCM shell and the core where the PCM resides. MEPCMs were subjected to 50 melt-freeze cycles and retain their geometrical profiles.

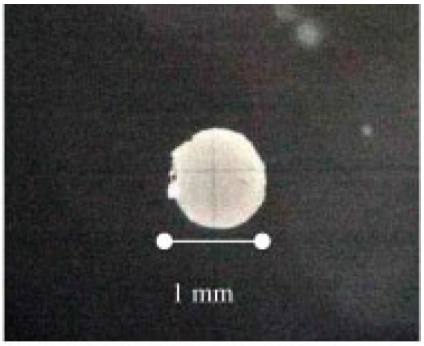


Figure 1.26 **Image of MEPCM prepared by coacervation: Coco fatty acid-Gelatin-Gum Arabic shell[87]**

Konuklu[146] also synthesized MEPCMs with a method similar to Ozonur's. They too tested a similar variety of shell materials to encapsulate octanoic acid (OA) but with the addition of non-ionic surfactants. The optimum MEPCM they synthesized was OA with urea-formaldehyde shell using the surfactant Tween 40. The MEPCMs had a melting and freezing temperatures of 13.9 and 5.1 °C respectively (T_m and Tf of OA were determined as 15.4 and 9.3 °C). The latent heats of melting and freezing for the MEPCMs was 93.9 and −106.1 J/g respectively (LHm and LHf for OA are 158.4 and −162.3 J/g). Figure 1.27 shows SEM images of the coacervates, diameters of the MEPCM was estimated to be from 200 nm to 1.5 μm.

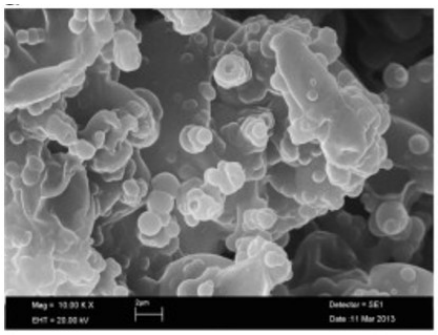


Figure 1.27 **Image of MEPCM prepared by coacervation: Urea formaldehyde – Octanoic acid with Tween40 as surfactant** [146]

Coacervation is a viable method to synthesize MEPCMs. Its advantages include: 1) Green chemistry, non-toxic shell materials and mild synthesis conditions. 2) The PCM encapsulation ratio can exceed 90% easily. However, coacervation also has some drawbacks: 1) broad size distribution ranging from micron to mm. 2) Rigidization via chemical crosslinking of the shell is necessary. Although coacervation is well-known and widely used for encapsulation, reports of MEPCM synthesis via coacervation are few and lack data on thermal properties.

1.6.3.2 Phase separation

Loxley proposed a new method of synthesizing microcapsules based on phase separation to encapsulate n-hexadecane with a poly(methyl methacrylate) (PMMA) shell.[166] This method is commonly used to form MEPCMs with n-alkanes as the PCM core.[147, 167] The method is based on an oil in water emulsion. The oil phase is composed of the shell material, a good solvent for the shell material and a poor solvent for the shell material. The emulsion is formed with the aid of a homogenizer, and under reduced pressure. When the good solvent is removed, it causes precipitation of the shell material,

which migrates towards the outer ring of the oil droplet. As more and more solvent is removed, the microcapsules are formed. The microcapsules formed possess shells with uniform thickness, and their diameter can approach 10 μm easily. Figure 1.28 illustrates the schematic formation of microcapsules with phase separation.

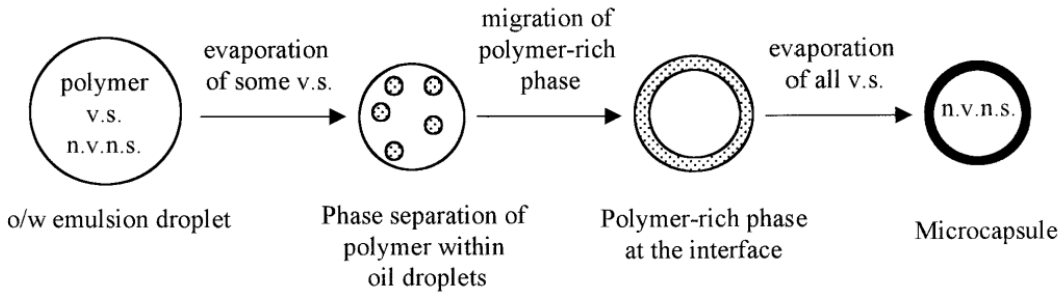


Figure 1.29 **Schematic formation of microcapsules with phase separation (v.s.: volatile and good solvent for shell material; n.v.n.s.: non-volatile and poor solvent for shell material)** [166]

Yang used a phase separation method to synthesize MEPCMs using different shell material including: acrylonitrile–styrene copolymer (AS), acrylonitrile–styrene–butadiene copolymer (ABS) and polycarbonate (PC). MEPCMs using AS as shell material had the highest %PCM of 84.5%. The effect of molecular weight on encapsulation efficiency was also studied. The studies showed that copolymer with lower molecular weight yielded higher encapsulation efficiency. Figure 1.30 shows SEM image of MEPCMs: Acrylonitrile-styrene copolymer - n-tetradecane. [146]

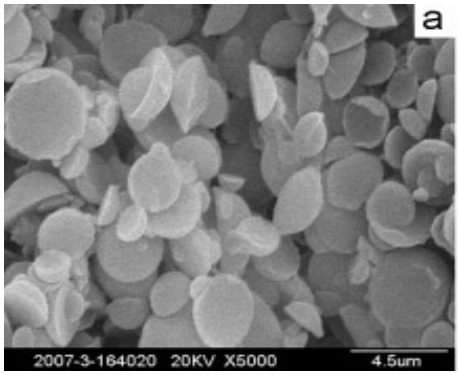


Figure 1.30 **Image of MEPCMs prepared by phase separation using acrylonitrile–styrene copolymer with n-tetradecane PCM core**[147]

1.6.3.3 Sol-gel

Figure 1.24 shows the PCM encapsulation process using the sol-gel method. This method can be used for w/o (water in oil) and o/w (oil in water) emulsions, the latter being more widely used in commercial applications for cosmetics and medications where water-based products are preferred.[168] PCM is first dispersed in the continuous phase to form an emulsion stabilized with surfactant to form PCM micelles. The orthosilicates are (1) hydrolyzed in the presence of an acid catalyst to form silanols (aka silica precursors or sol solution) which are then added to the PCM emulsion. The silanols are attracted to the surfactants at the o/w interface via hydrogen bonding, and (2) condensation (either removal of ROH or H_2O) is catalyzed by base or increase in pH past the isoelectric point of silica (around pH 2). The reaction forms oxo bridges (-O-) between silica atoms which leads to formation of a silica shell around the PCM.

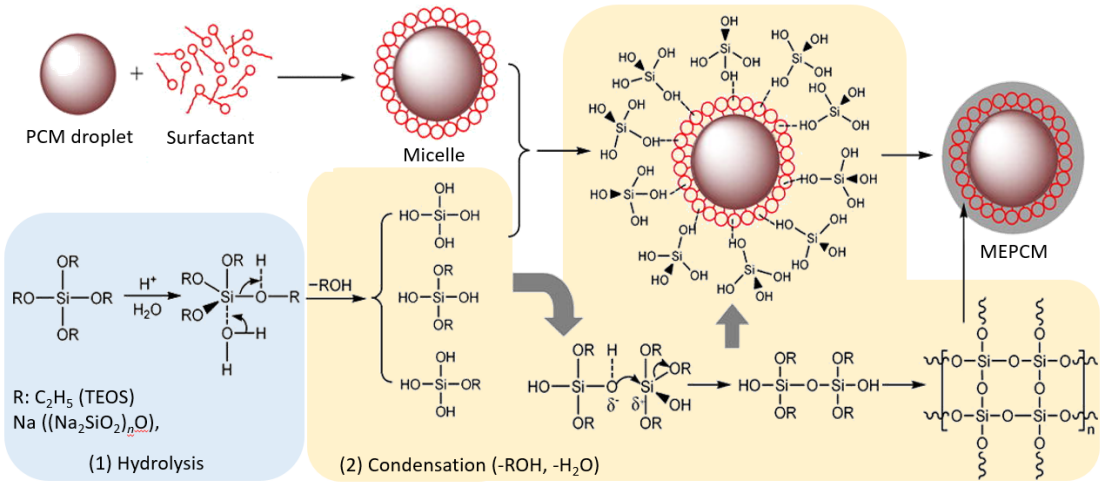


Figure 1.31 **Schematic reaction of sol-gel encapsulation** [148]

In 2010, Wu's group successfully synthesized a series of n-octadecane MEPCMs with pHs ranging from 2.26 to 2.89 through an o/w sol-gel process.[148] The optimum pH was found to be pH 2.45. The synthesis used non-ionic surfactant, n-octadecane was stirred for 3 h to form o/w emulsion. TEOS was dissolved in water and stirred at 35 °C with HCl as the acidic catalyst to form a homogenous solution, signifying the hydrolysis to form silanol precursors was complete. The silanol precursors were then added dropwise to the emulsion, and stirred for 24 h. The product was a white powder collected via filtration and washed with DI water. Finally, the obtained MEPCMs were washed with ethanol to effectively remove residual surfactants and dried at 40 °C overnight. The diameter of the MEPCMs ranged from 7-16 μm and its morphology is shown in Figure 1.32. Thermal studies showed that the MEPCMs had a latent heat of fusion of 185.6J/g and latent heat of melting 184.9 J/g with increased thermal conductivity of 0.456 $Wm^{-1}K^{-1}$ compared with the pure PCM (0.12 $Wm^{-1}K^{-1}$ (l) at 40 ºC)[169]. The MEPCMs had two T_c at 22 and 20 ºC. This Tc is lower than bulk n-octadecane (T_m 28 ºC)[91] thus the freezing temperature was depressed by -6 ºC.

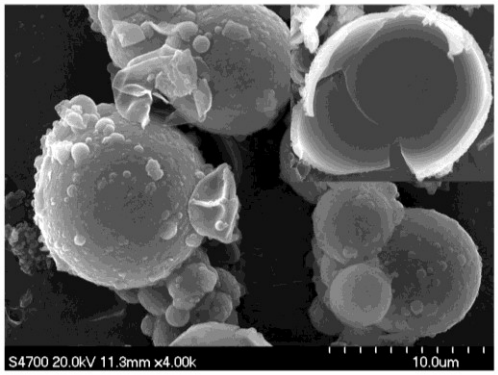


Figure 1.32 **SEM image of MEPCM synthesized via sol-gel : Silica / n-octadecane (30/70 ratio) synthesized at pH 2.45** [148]

In 2014, Wu's group also synthesized n-octadecane MEPCMs using sodium silicate ($(Na_2SiO_2)nO$) which improved thermal conductivity of the PCM from 0.153 to 0.85 W $m^{-1}K^{-1}$.[149] However the percentage PCM in the MEPCM was only 35%, which was considerably lower than the one in their previous study. Figure 1.33 shows the MEPCMs' thermal profile over 100 thermal cycles. The latent heat which is quantified by the area under freezing and melting peaks continually drops. This is probably due to the volume change during phase transition.

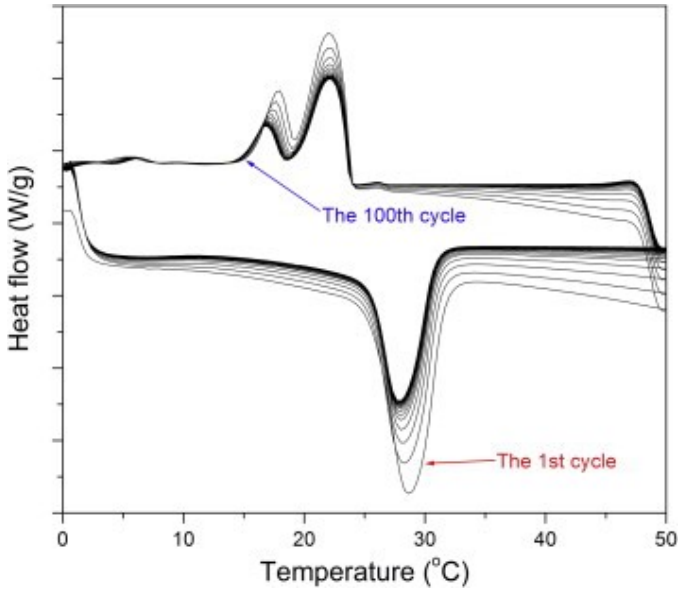


Figure 1.33 **DSC of sodium silicate/n-octadecane MEPCM (35% PCM) over 100 thermal cycles.[149]**

Matrix MEPCMs were also prepared with this method by Li[150]. Two composites of SiO_2/paraffin and SiO_2 with expanded graphite/paraffin were prepared. The thermal conductivity of the paraffin was increased by 28% and 95%, respectively. Both composites showed decrease of the T_m from 29˚C to 28˚C which was possibly due to the higher thermal conductivity. As exhibited by the TEM image in Figure 1.34, the MEPCMs are a continuous phase with graphene sheets interspersed and no core/shell structure is present.

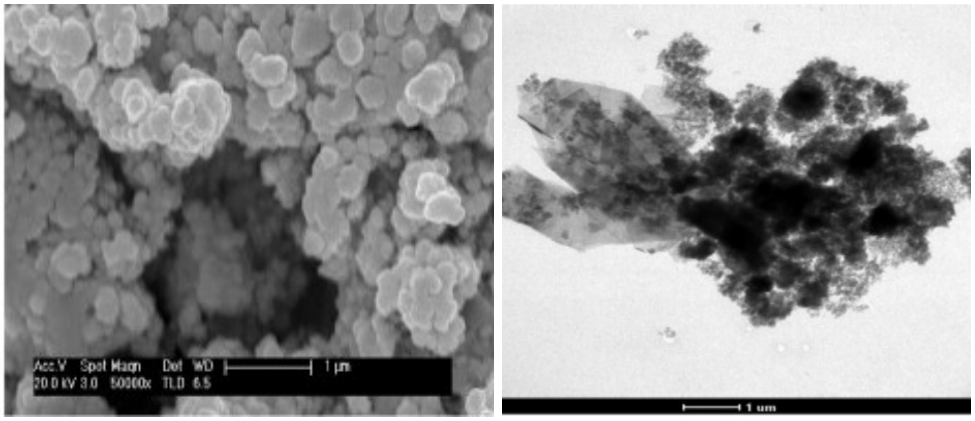


Figure 1.34 **Images of MEPCM synthesized via sol-gel : Silicon oxide-expanded graphite / paraffin (Left:SEM; Right:TEM)** [150]

Chen[151] synthesized MEPCMs with a high PCM loading of 90% using the sol gel method. The synthetic procedures involved the formation of stable emulsion with sodium dodecyl sulfate (SDS) with stirring at 800 rpm for 1h at 75 °C. The silica precursors/sol solution was added drop by drop into the emulsion and stirred at 300 rpm for 2 h in a water bath at 70°C. After polymerization, the MEPCMs were washed with DI water and dried in a vacuum oven at 50 °C for 24 h. Thermal profile of the MEPCMs showed reduced supercooling due to SiO_2 shells which acted as a nucleating agent. Figure 1.35 shows the MEPCMs were irregular in shape and had rough surfaces. Possibly, the sol precursors did not adhere to the emulsion droplet followed by condensation polymerization to form a continuous shell. Instead, condensation polymerization occurs in the aqueous phase followed by precipitation onto the PCM droplet as the molecular weight increased.

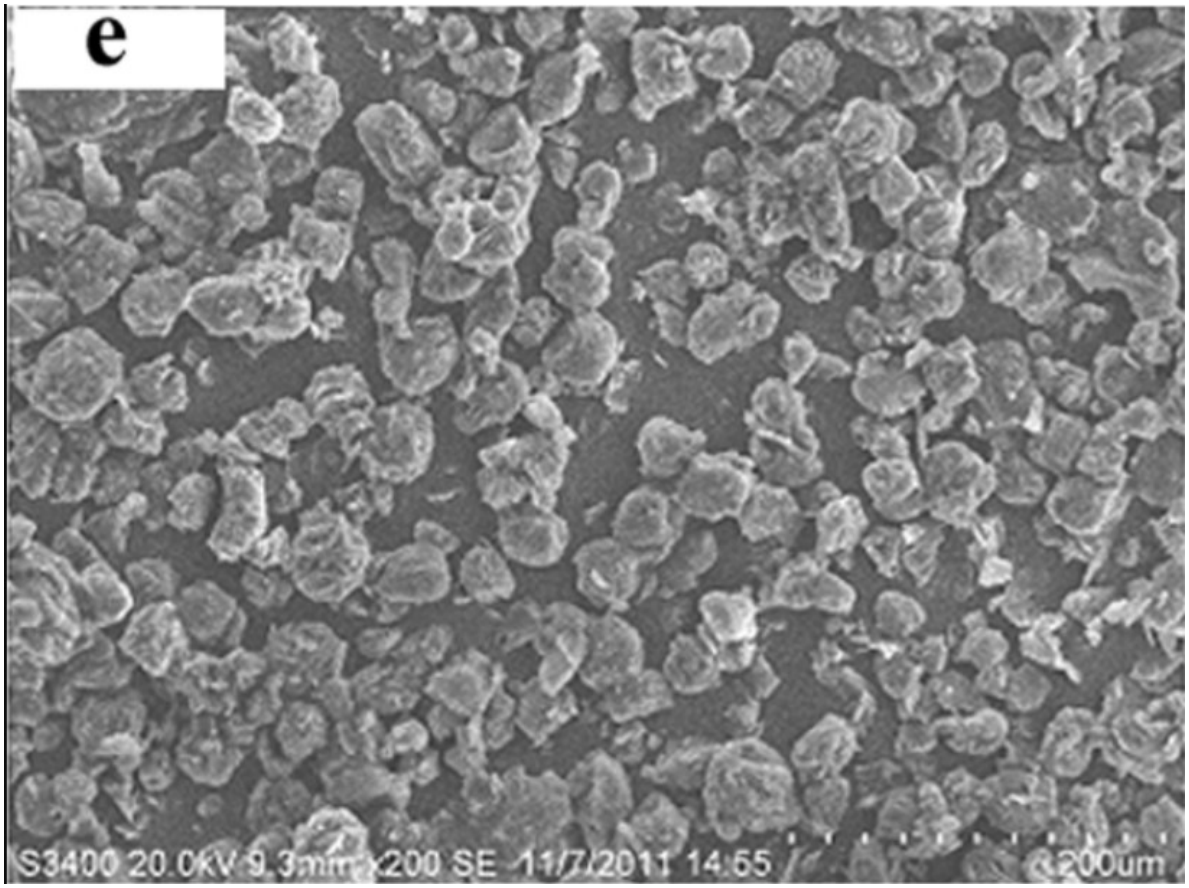


Figure 1.35 **SEM image of MEPCM synthesized via sol-gel: Silicon dioxide / stearic acid [151]**

The properties of the MEPCMs described are summarized in Table 1.8. In conclusion, MEPCMs with high latent heat and increased thermal conductivity can be synthesized via the sol gel process. At the same time, the silicate shells show decreased MEPCM flammability due to formation of charred carbonaceous-silicate built up on the MEPCMs' surface when temperatures increase.[151, 170] The high crystallinity of the silica shells may also act as a nucleating agent to reduce supercooling. [148, 149, 151]

In conclusion, there is a variety of methods for synthesizing MEPCMs with various thermal and mechanical properties. However, most MEPCMs have not been subjected to stability tests for long term use. In addition, encapsulated PCMs exhibit supercooling which decreases the efficiency of the thermal energy storage (TES) system which must be minimized for practical application. MEPCMs with sizes as large as ~30 μm have shown highly depressed freezing temperature, with ΔT_f close to -10 °C. In most cases, a nucleating agent must be added or in some cases the shell material is sufficiently crystalline to act as a catalyst for nucleation

Chapter 2

Research Objectives

The research work aims to develop new methodologies to prepare encapsulated PCM particles dispersed in water. Two different encapsulation approaches have been explored:

I. Synthesis and characterization of PCM microcapsules in water with a Pickering emulsion technique using poly(butyl acrylate)/chitosan (PBA/CTS) particles as shell material. A simplified scheme of the encapsulation process is displayed in Figure 2.1.

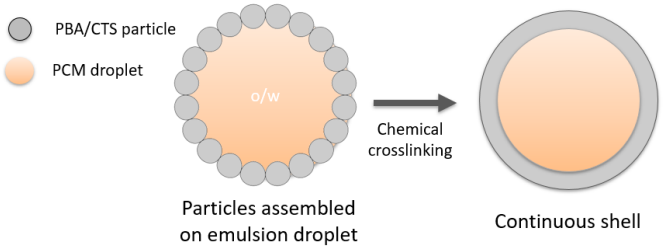


Figure 2.1 **Simplified scheme for the synthesis of MEPCMs via Pickering emulsion template**

The work includes the following specific objectives:

1) Synthesis and characterization of two types of PBA/CTS nanoparticles with different properties
2) Optimization of Pickering emulsion of hexadecane stabilized by PBA/CTS nanoparticles

3) Crosslinking of final optimized Pickering emulsion with various reagents

4) Thermal analysis and characterization of the MEPCMs formed from crosslinking of the Pickering emulsion droplets stabilized by PBA/CTS nanoparticles

II. Synthesis and characterization of PCM microcapsules in water with coacervation technique using water-soluble, amphoteric chitosan-co-poly(methacrylic acid) (CTS-co-PMAA) copolymer as shell material. A simplified scheme of the encapsulation process is displayed in Figure 2.2.

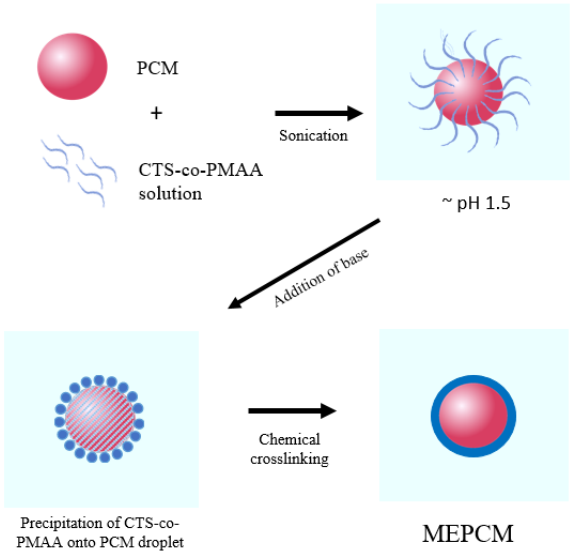


Figure 2.2 **Simplified scheme for the synthesis of MEPCMs via coacervation technique with CTS-co-PMAA as shell material**

The work includes the following specific objectives:

1) Synthesis and characterization of three types of amphoteric CTS-co-PMAA copolymer

2) Optimization of encapsulation of hexadecane with CTS-co-PMAA using coacervation to increase encapsulation efficiency and decrease supercooling
3) Thermal analysis and characterization of the optimized CTS-co-PMAA/C16 MEPCMs

Chapter 3

Development of Phase Change Material Microcapsules in Water with a Pickering Emulsion Technique using Amphiphilic Core-Shell Particles

This chapter describes the synthesis of microencapsulated phase change materials (MEPCMs) via a Pickering emulsion technique. Amphiphilic core-shell particles, namely, poly(butyl acrylate)/chitosan (PBA/CTS) were synthesized and then used to form a Pickering emulsion with the PCM material, hexadecane. The nanoparticles are then crosslinked to form a continuous polymer shell enclosing the PCM droplet to form MEPCMs.

The PBA/CTS particles were synthesized using the core-shell particle platform technology developed by Li's group. Synthesis of core-shell particles with different ratios of monomer to chitosan and different initiator were carried out to select the optimal recipe for stabilization of the dispersed PCM. The synthesized PBA/CTS particles were characterized by dynamic light scattering, ξ-potential measurements at different pHs, Fourier-transform infrared spectroscopy (FTIR) and field emission scanning electron microscopy (FE-SEM). Bottle tests were used to observe emulsion stability for signs of

creaming after selected periods of time. To further optimize emulsion stability, parameters such as solution pH, electrolyte and emulsifier concentrations were also studied. Various crosslinkers to crosslink PBA/CTS particles to form a continuous shell were evaluated and their thermal properties were studied by differential scanning calorimetry (DSC).

3.1 Experimental

3.1.1 Materials

The inhibitor present in the butyl acrylate monomer (Sigma) was removed by washing with 10% KOH solution, followed by multiple washings with deionized water (DI water). Chitosan was obtained from AKBIO (Low molecular weight with degree of deacetylation of 72.5%) and characterized with elemental analysis to confirm the degree of deacetylation (refer to Section 3.1.3.1). Hexadecane, calcium chloride ($CaCl_2$), glutaraldehyde (50 wt%), borax and sodium tripolyphosphate were all obtained from Aldrich and used as is. Dispersing medium used was Milli-Q purified DI water.

3.1.2 Experimental procedures

3.1.2.1 Synthesis of poly(butyl acrylate)/chitosan particles

The poly(n-butyl acrylate)/chitosan (PBA/CTS) particles were synthesized according to the following procedure: Chitosan (CTS) was dissolved in a 0.6% acetic acid solution and transferred to a water jacketed reactor. The chitosan solution was then stirred at 500 rpm and purged with nitrogen for 20 min at 60 ^{o}C. Purified and degassed butyl acrylate (BA) monomer was added dropwise to the chitosan solution, followed by charging a diluted *t*-butyl hydroperoxide (TBHP) solution to initiate polymerization. The polymerization was carried out for 3 h at 80 ^{o}C with a continuous stirring speed of 500 rpm. The product was then sieved to remove precipitates, and the solid content of the

crude product was determined by drying in an oven at 80 ºC. The particles were purified by repeated centrifugation at 15,000 rpm or 45,000 rpm for 2 h depending on particle size. The supernatant was discarded and the pellet was re-dispersed in the 0.6% acetic acid through mixing and sonication. This process was repeated thrice.

3.1.2.1.1 Effect of weight ratio of monomer to chitosan

The PBA/CTS particles with various BA to CTS ratios were synthesized according to the synthesis procedure described in 3.1.2.1 using the recipes shown in Table 3.1

Table 3.1 **Recipes of PBA/CTS particles synthesized with different BA to CTS ratios**

Ingredient (g)	BA:CTS=2:1	BA:CTS=4:1	BA:CTS =6:1	BA:CTS =8:1
Chitosan	1.67	1	0.71	0.56
Acetic acid (99%)	0.6	0.6	0.6	0.6
Butyl Acrylate (purified)	3.33	4	4.29	4.44
TBHP (100 mM)	1.0	1.0	1.0	1.0
Water	93.4	93.4	93.40	93.40
Total volume	100 ml	100 ml	100 ml	100 ml

3.1.2.1.2 Effect of type of initiator

The PBA/CTS particles were synthesized according to the general synthesis procedure in 3.1.2.1 except the initiator used was changed to hydrogen peroxide (H_2O_2). The amount of materials used in the synthesis is listed in the Table 3.2.

Table 3.2 **Recipes of PBA/CTS particles synthesized with different BA to CTS weight ratios using H_2O_2 as the initiator**

Ingredient (g)	**BA:CTS=2:1**	**BA:CTS=4:1**	**BA:CTS =6:1**	**BA:CTS =8:1**
Chitosan	1.67	1.00	0.72	0.56
Acetic acid (99%)	0.6	0.6	0.6	0.6
BA (purified)	3.33	4.00	4.28	4.44
H_2O_2 (100mM)	1	1	1	1.00
Water	93.4	93.4	93.4	93.4
Total volume	100 ml	100 ml	100 ml	100 ml

3.1.2.2 Formation of Pickering emulsion using PBA/CTS nanoparticles as stabilizer

3.1.2.2.1 General formation of Pickering emulsion

Pickering emulsions were formed by adding hexadecane (C16) and 0.5 wt% PBA/CTS nanoparticle dispersion in a centrifuge tube. The mixture was homogenized (IKA T18 Ultra Turrax) at 11,000 rpm for 1 min. The emulsions were placed in transparent scintillation flasks and observed for phenomena including creaming, sedimentation and phase separation after 2 h.

3.1.2.2.2 Synthesis of MEPCMs with PBA/CTS nanoparticles and GAL crosslinking

PBA/CTS nanoparticles (0.5 wt%, 16 ml) was homogenized with hexadecane (4 ml) at 11 krpm for 1 min. The resulting emulsion was diluted with DI water to 80 ml. A 0.2% GAL crosslinker solution (20 ml) was then added dropwise at a rate of 1 drop/sec with gentle stirring.

3.1.2.2.3 Effect of pH on PBA/CTS nanoparticle dispersion on Pickering emulsion stability

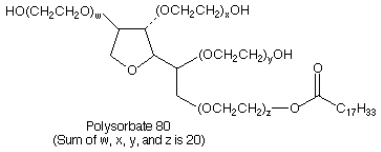
Pickering emulsions were formed according to 3.1.2.2.1 using PBA/CTS nanoparticle dispersions with pH adjusted from pH 3 to 10 using HCl or NaOH accordingly.

Table 3.3 Recipe for PBA/CTS-C16 emulsions stabilized with PBA/CTS Np dispersions of various pH

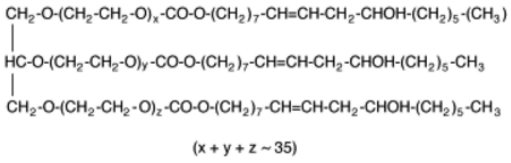
Ingredient	Volume (ml)
PBA/CTS Np dispersions (0.5 wt%)	16
C16	4

3.1.2.2.4 Effect of addition of emulsifier on Pickering emulsion stability

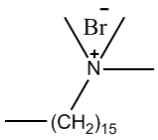
Pickering emulsions were formed according to 3.1.2.2.1 with the addition of various emulsifiers Tween 80 (T80), cremophor, sodium dodecyl sulfate (SDS) and cetrimonium bromide (CTAB). Their chemical structures are shown in Figure 3.1**.** The emulsifier was dissolved in the PBA/CTS nanoparticle dispersion to obtain concentration of 0.2 wt%



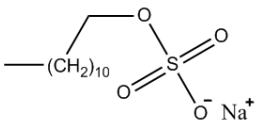
Tween80 (T80)



Cremophor EL[171]



CTAB



SDS

Figure 3.1 **Chemical structures of emulsifiers**

Table 3.4 Recipe for PBA/CTS-C16 emulsions with addition of emulsifiers

Ingredient	Amount
PBA/CTS Np dispersions (0.5 wt%)	16 ml
C16	4 ml
Emulsifier	0.4 g

3.1.2.2.5 Effect of electrolyte concentration on Pickering emulsion stability

Pickering emulsions were formed according to 3.1.2.2.1 with the addition of various amounts of $CaCl_2$ to PBA/CTS dispersions to obtain concentrations from 0%, 0.04%, 0.06% 0.08% and 0.1%.

Table 3.5 Recipe for PBA/CTS-C16 emulsions with addition of $CaCl_2$

Ingredient	Amount
PBA/CTS Np dispersions (0.5 wt%)	16 ml
C16	4 ml
T80	0.4 g
$CaCl_2$	0 / 0.0064 g / 0.0096 g / 0.0128 g / 0.016 g

3.1.2.2.6 Chemical crosslinking of pre-formed PCM Pickering emulsion

A 16 ml solution consisting of Tween80 (0.2 wt%), $CaCl_2$ (0.04 wt%) and PBA/CTS nanoparticles (0.5 wt%) was prepared in a scintillation flask. Table 3.4 lists actual weights of each ingredient used. Hexadecane (4 ml) was added to the solution followed by homogenization at 11 krpm for 1 min. The resulting emulsion was diluted with DI water to 80 ml. A crosslinker solution (20 ml) was then added dropwise at a rate of 1 drop/sec with gentle stirring. Three types of crosslinker solutions have been used including 0.2% glutaraldehyde (GAL), 0.5% borax solution and 1.4% sodium tripolyphosphate solution (TPP) (Figure 3.2). Stirring was continued for 24 h. The samples were then washed with hexane to remove unencapsulated hexadecane.

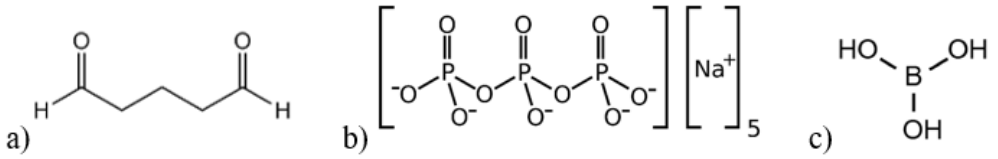


Figure 3.2 **Chemical structures of a) glutaraldehyde; b) Sodium tripolyphosphate; c) boric acid**

Table 3.6 Recipe for PBA/CTS-C16 emulsions with addition of crosslinker

Ingredient	Amount
PBA/CTS Np dispersions (0.5 wt%)	16 ml
C16	4 ml
T80	0.4 g
$CaCl_2$	0.0064 g
Crosslinker solution **0.2% GAL / 0.5% borax / 1.4% TPP**	20

3.1.3 Measurement and Characterization

3.1.3.1 Determination of degree of deacetylation of chitosan

The elemental composition of chitosan (obtained from AKBIO) was determined using an Elemental Analyzer (vario MICRO select). 0.2 g CTS was added to 50 ml of 0.6% acetic acid, stirred and heated to 60 ^{0}C until the CTS dissolved completely. The CTS was precipitate by addition of base followed by extraction with high speed centrifugation (20,000 rpm for 2 h) and washing with DI water. The CTS was freeze dried to remove water for 2 days at -60 ^{0}C at <10 Pa (LAB-KITS FD-12-MR). The freeze dried samples are stored in a dried box prior to measurement to prevent moisture absorption. The degree of acetylation was calculated from the carbon/nitrogen ratio (C/N). C/N ratio varies from 5.145 in 100% deacetylated chitosan ($C_6H_{11}O_4N$ repeat unit) to 6.861 in chitin ($C_8H_{13}O_5N$ repeat unit). The degree of deacetylation (DDA) was therefore calculated with the equation below:

$$\boldsymbol{DDA = 1 - \frac{C/N - 5.145}{6.861 - 5.145}} \qquad \textbf{Equation 3.1}^{[172]}$$

The C/N ratio of the CTS samples were measured twice, average obtained was 5.6011 with standard deviation of 0.24%. The degree of deacetylation calculated was 72.5%.

3.1.3.2 Determination of monomer conversion

The monomer conversion of the PBA/CTS nanoparticle synthesis was determined gravimetrically. After the reaction, the total weight of the crude PBA/CTS nanoparticle dispersion (Wt_{cr}) was measured with a balance. 1-2 ml of the unpurified PBA/CTS dispersion is placed in an aluminum pan .and weighed using a mass balance accurate up to 4 decimal places. The pan was placed in an oven and dried overnight at 80 ºC for 2 days to remove moisture and other volatile molecules. The percentage solid content of the crude product ($\%SC_{cr}$) was calculated with the equation below:

$$\%\mathbf{SC} = \frac{\mathbf{Weight\ of\ pan\ with\ dried\ sample - Weight\ of\ pan}}{\mathbf{Weight\ of\ sample}} \times \mathbf{100}\% \qquad \textbf{Equation 3.2}$$

The monomer conversion (%conv) was calculated with the equation below:

$$\%\mathbf{conv} = \frac{(\%\mathbf{SC}_{\mathbf{cr}} \times \mathbf{Wt_{cr}}) - \mathbf{Wt_{CTS}}}{\mathbf{Wt_{monomer}}} \times \mathbf{100\%} \qquad \textbf{Equation 3.3}$$

$\%SC_{cr}$: %SC of the crude product assuming all unreacted monomer has evaporated.
Wt_{cr} : Total weight of the crude product
Wt_{CTS} : Weight of chitosan added
$Wt_{monomer}$: Weight of monomer added

3.1.3.3 Determination of %CTS in particle

The actual ratio of PBA to CTS in PBA/CTS nanoparticle was determined with elemental analysis according to the procedure below: Purified nanoparticle samples were freeze dried in a scintillation flask to remove water. Elemental analyzer (Vario MICRO

select) was used to determine the C/N ratio for the nanoparticle (NP) samples. Molecular weight of butyl acrylate (BA) is 128.17. Average molecular weight of each unit in the chitosan polymer (DDA=72.5%) is 172.5. The molar ratio of PBA to CTS in the nanoparticle can be calculated from the equations below:

$$\textbf{Ratio of BA to CTS in particle } (n_{BA}/n_{CTS}) = \frac{C/N_{NP} - C/N_{CTS}}{\#\text{ of C in monomer}} \qquad \textbf{Equation 3.4}$$

C/N_{NP}: Carbon to nitrogen ratio in the PBA/CTS nanoparticles

C/N_{CTS}:Carbon to nitrogen ratio in CTS previously determined with elemental analysis was 6.07

The number of BA repeating units to 1 CTS unit (n_{BA}/n_{CTS}) in the PBA/CTS core-shell particles was calculated with the equation below. The number of carbons of the PBA polymer contributing to the C/N ratio was calculated by subtracting the C/N ratio of the chitosan polymer. By dividing the carbon number of the BA monomer, 7, the number of BA repeating units to 1 CTS is obtained.

$$\%\boldsymbol{CTS\ in\ particle} = \frac{n_{CTS} \times 172.5}{n_{CTS} \times 172.5 + n_{BA} \times 128.1} \times 100\% \qquad \textbf{Equation 3.5}$$

3.1.3.4 Fourier transform infrared spectroscopy

The chemical composition of PBA/CTS nanoparticles was characterized with a Fourier transform infrared spectroscopy (FTIR). The PBA/CTS nanoparticle samples were dried overnight in a vacuum oven prior to measurement. Spectrum was recorded on

a Nicolet Avatar 360 FT-IR spectrophotometer using the Attenuated Total Reflectance (ATR) sample holder with ZnSe plate which is suitable for samples to be examined directly in the solid or liquid state. Spectrum was recorded from the mid-infrared (4000 to 400 cm^{-1}) at 4 cm^{-1} resolution.

3.1.3.5 Particle size and size distribution

Dynamic light scattering (DLS) measurements were performed with a Delsa Nano Particle Analyzer (Beckman Coulter, Brea, CA, USA) using a photon correlation spectroscopy with electrophoretic dynamic light scattering (a two-laser diode light source with a wavelength of 658 nm at 30 mW). Fluctuations in back scattered light was detected at an angle of 165°. Each sample was diluted to 200-500 ppm, 60 runs were performed, and repeated three times to obtain the intensity size distribution and the polydispersity index (PDI) at 25 ℃.

3.1.3.6 zeta-potential measurements

Samples for *zeta*-potential measurements were diluted to 500 ppm in 1 mM NaCl solution and measured at room temperature with Delsa Nano C Particle Analyzer (Beckman Coulter, Brea, CA, USA). The *zeta*- potential measurement was measured with a monochromatic laser beam at 658 nm. The size range for *zeta*-potential measurements was between 0.6 nm and 30 µm. Prior to the measurement, samples pH was adjusted to pH 7. For each sample, the measurements were repeated thrice at 25 ℃.

3.1.3.7 Scanning electron microscopy

10-20 µL of diluted particle dispersions (50-100 ppm) was spread onto a glass substrate affixed to the sample holder with conducting tape. The samples were left to air dry overnight in a dust free environment followed by coating with a thin layer of gold. SEM images were taken on a JEOL SM-31010 with an accelerating voltage of 5 kV.

3.1.3.8 Optical microscope

The diameter of the microcapsules or emulsion droplets can be measured from optical images taken with a microscope or SEM. The image was optimized with the software ImageJ. Selection of droplets are based on circularity (>0.8) and size range was determined with some initial measurements by hand. The software analyzed and calculated the area of each black spot and the radius was obtained.

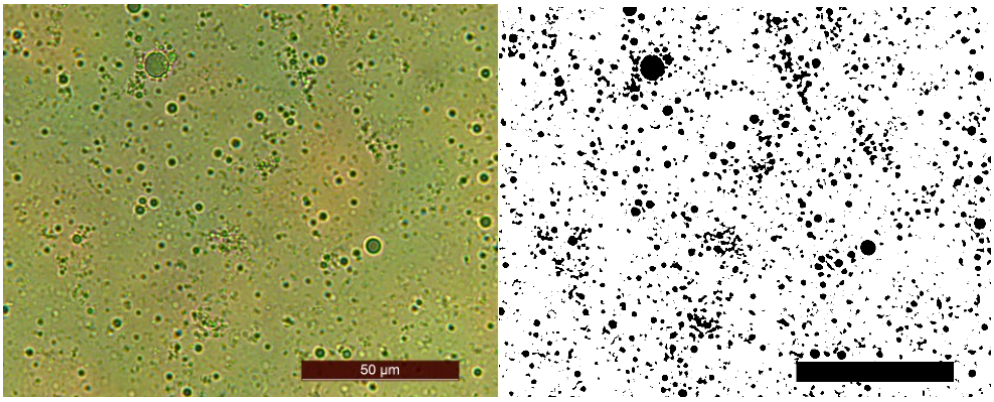


Figure 3.3 **Example of an optical image (left) transformed to binary colors (right)**

3.1.3.9 Differential Scanning Calorimetry

Samples were analyzed with a Differential Scanning Calorimetry (DSC) if product yield (calculated gravimetrically) exceeded 40%. Temperature profile used in the DSC scan was from 25°C to -10°C and -10°C to 25°C at a rate of 4°C min $^{-1}$. This temperature range encompasses the temperature range of freezing and melting of the hexadecane. A known weight of the sample (1-30 mg) was hermetically sealed in an aluminum pan and placed in the sample holder inside the DSC (Mettler Toledo, 822e). An empty Al pan was used as reference. Nitrogen was, passed through the sample chamber at 20 ml/min for protection. Indium was used to calibrate the temperature and latent heat. From the thermal profile of the MEPCM, we could determine the following properties: 1) Encapsulation efficiency (%ee); 2) Depression of freezing temperature (ΔT_f) and 3) %ee of MEPCM after multiple phase change cycles

3.1.3.9.1 *Encapsulation efficiency (%ee)*

Encapsulation efficiency of the MEPCM is the amount of PCM encapsulated divided by the amount of PCM added.(refer to Equation 3.6)The amount of PCM encapsulated is obtained by calculating the %PCM in the sample times total weight of the

sample. The %PCM in the sample is obtained from the thermal profile of the MEPCM (An example is shown in Figure 3.4). The area under the freezing curve of the encapsulated PCM divided by latent heat of hexadecane which is 249.14 J/g using Equation 3.7.

$$\%\text{Encapsulation efficiency} = \frac{\%\text{PCM} \times \text{Total Weight}}{\text{initial PCM added}} \qquad \textbf{Equation 3.6}$$

$$\%\text{PCM} = \frac{\text{Latent heat of sample}}{249.14} \qquad \textbf{Equation 3.7}$$

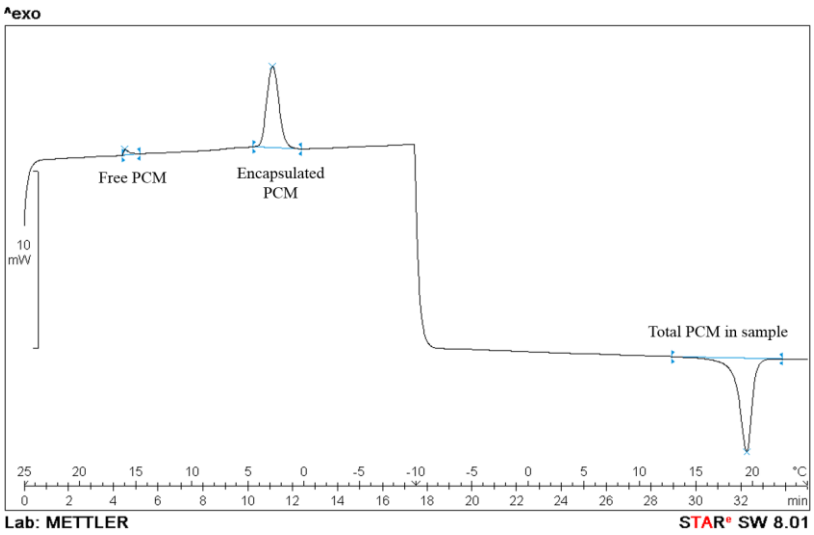


Figure 3.4 **DSC scan of microencapsulated hexadecane (from 25 °C to -10 °C and -10 °C to 25 °C at a rate of 4 °C min⁻¹)**

3.1.3.9.2 Depression of freezing temperature

Supercooling occurs in MEPCMs and can be measured by calculating the depression of freezing temperature. Depression of freezing temperature (ΔT) is the difference between the onset freezing temperature of MEPCMs (T_{fo} [$MEPCM$]) and the PCM (T_{fo} [$C16$]:15.81 ℃).

$$\boldsymbol{\Delta T = 15.81 - T_{fo}\,[MEPCM]} \qquad \textbf{Equation 3.8}$$

3.1.3.9.3 Encapsulation efficiency of MEPCM after multiple phase change cycles

MEPCMs are used for thermal energy storage. They need to maintain their thermal storage capacity without PCM leakage over many cycles of storage/release of thermal energy. This means that the MEPCM shell needs to withstand the volume changes when the PCM undergoes solidification and melting. To assess this ability, the MEPCMs were freeze and thawed from 25 to -10 °C and -10 to 25°C, repeatedly, at a rate of 20 °C min $^{-1}$ over 20 cycles using DSC (Mettler Toledo, 822e). . The encapsulation efficiency (%ee) before and after the multiple phase change cycles was compared to assess thermal capacity loss of the MEPCM or leakage of the PCM.

3.2 Results and Discussion

3.2.1 Properties of PBA/CTS nanoparticles

3.2.1.1 Mechanism of particle formation

Amphiphilic core-shell nanoparticles were synthesized in the absence of emulsifiers. Chitosan, a water soluble polymer containing amino groups can undergo graft copolymerization with butyl acrylate according to the method developed by Li's group.[173-175] The general formation mechanism in depicted in Figure 3.5. Typically, the reaction involves a water-soluble polymer rich in amino groups, a hydrophobic vinyl monomer and an alkyl hydroperoxide redox initiator. During initiation, the peroxide group (ROOH) interacts with the amino group on the water soluble polymer to form a redox pair, an electron transfer taking place from the amino nitrogen to ROOH forms cationic nitrogen radicals ($\cdot NH_2$) and alkoxyl radicals (RO·). Subsequent proton transfer leads to the formation of a macro amino radical which initiates the polymerization of vinyl monomer dissolved in the water to form a graft copolymer with hydrophobic and hydrophilic domains. As the vinyl polymer side chains grow, the graft copolymer reaches a hydrophobic-hydrophilic balance which induces the self-assembly of several copolymers to form micelle-like microdomains. These microdomains serve as loci for subsequent polymerization of vinyl monomer which is similar to emulsion polymerization. Simultaneously, alkoxyl radicals can initiate homopolymerization of the vinyl monomers within the micelles to form homopolymer. Alternatively, alkoxyl radicals can form macro

radicals through hydrogen abstraction from the backbone of the water-soluble polymer which is also able to initiate graft copolymerization of the vinyl monomer onto the polymer backbones. At the end of the polymerization, monodispersed amphiphilic core shell nanoparticles with a hydrophobic core and a hydrophilic shell can be obtained.

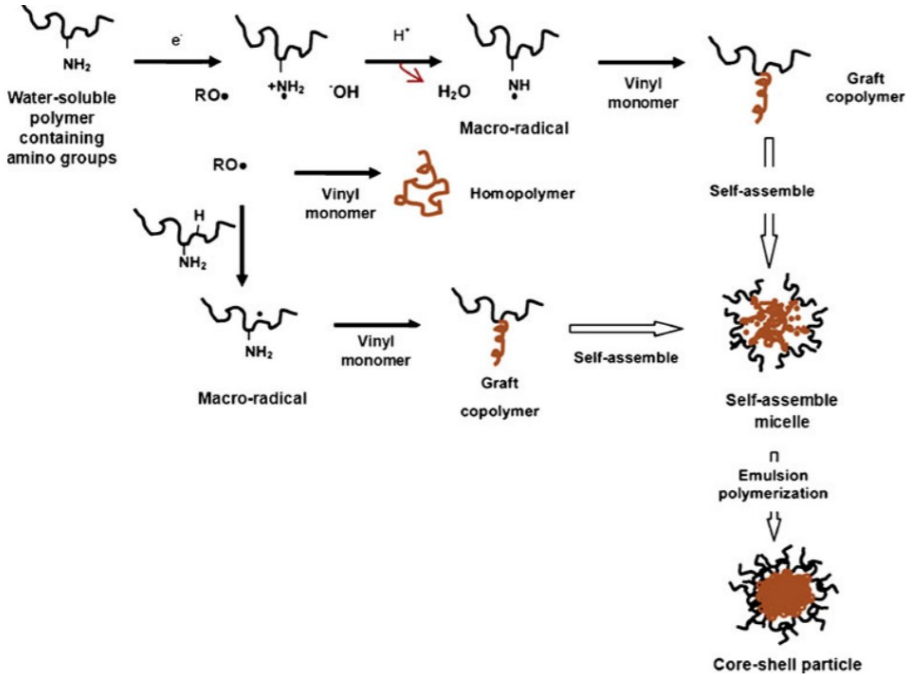


Figure 3.5 **Formation mechanism of amphiphilic core–shell particle via graft copolymerization of vinyl monomer from a water-soluble polymer containing amino group**[176]

3.2.1.2 Synthesis

For this study, poly(butyl acrylate)/chitosan (PBA/CTS) nanoparticles were synthesized using various monomer ratios and two types of hydroperoxide as initiators, namely t-butyl hydroperoxide, $(CH_3)_3COOH$, (TBHP) and hydrogen peroxide (H_2O_2).

The various properties of the PBA/CTS nanoparticles synthesized with different monomer to chitosan weight ratios using TBHP are summarized in Table 3.7. It was found that increasing the BA:CTS ratio to 8:1 had low monomer conversion (~60%) which was possibly due to the depletion of amino radicals before polymerization of all the monomers. The hydrodynamic diameter of the particles ranges from 700 nm to 1.49 μm and the polydispersity index (PDI >0.1) indicates a fairly large distribution. The %CTS reacted could not be measured as purification of PBA/CTS nanoparticles involves centrifugation which caused part of the sedimented to meld together due to the soft PBA core. This lead to loss of PBA/CTS particles. Thus the %CTS reacted could not be estimated from elemental analysis. The %CTS reacted also could not be determined with gravimetric measurements from supernatant obtained during purification of the PBA/CTS particles. The calculations indicated that solids in the supernatant exceeded the amount of CTS added during the reaction. This indicates the presence of either PBA homopolymer or CTS-g-PBA graft copolymer in the supernatant. Thus, we were unable to calculate the %CTS reacted. %CTS in the PBA/CTS particles was estimated from elemental analysis, all PBA/CTS particles showed very low amounts of %CTS, the highest not exceeding 6%.

Table 3.7 Properties of PBA/CTS nanoparticles synthesized with different BA toCTS ratios using TBHP as initiator

Properties	BA:CTS 2:1	BA:CTS 4:1	BA:CTS 6:1	BA:CTS 8:1
%conv	76%	99%	90%	60%
D_h	1490 (PDI 0.18)	720.4 (PDI 0.175)	804 nm (PDI 0.100)	1243 nm (PDI 0.195)
%CTS in particle	6.0 wt%	18 wt%	1.4 wt%	N/A

Another initiator, hydrogen peroxide, was used to synthesize PBA/CTS nanoparticles instead of TBHP. The various properties of the PBA/CTS nanoparticles synthesized with different monomer to chitosan weight ratios using the hydrogen peroxide as initiator are summarized in Table 3.10. Table 3.8.shows that PBA/CTS particles synthesized with H_2O_2 as initiator show smaller size (< 400 nm) and higher monodispersity (PDI<0.1) compared to PBA/CTS particles synthesized with TBHP as initiator. An explanation could be the H_2O_2 initiator generates 2 OH· radicals upon decomposition, while TBHP generates one tBuO· and one OH· radical. The more hydrophilic OH· radicals will be more likely to extract hydrogens from the hydrophilic CTS backbone to form graft copolymers as opposed to reacting with the hydrophobic monomer to form homopolymers. In that case, there are a higher number of PBA branches on the CTS backbone which

might lead to self-assembly of smaller particles. The %CTS in the particle was highest in PBA/CTS particles synthesized with monomer ratio of BA:CTS=2:1 which was 33% while other PBA/CTS particles had %CTS < 6%.

Table 3.8 **Properties of PBA/CTS nanoparticles synthesized with different BA:CTS ratios using H_2O_2 as initiator**

Properties	**BA:CTS 2:1**	**BA:CTS 4:1**	**BA:CTS 6:1**
%conv	94%	95%	97%
D_h	193 nm (PDI 0.074)	287 nm (PDI 0.094)	297 nm (PDI 0.057)
%CTS in particle	33.3 wt%	4.1 wt%	1.2 wt%

The chitosan content in the PBA/CTS particles (BA:CTS = 4:1) synthesized with TBHP is close to the theoretical %CTS. Whereas the chitosan content in PBA/CTS particles (BA:CTS = 2:1) synthesized with H_2O_2 also reached the theoretical %CTS . This indicates that there may be an optimum monomer ratio which affects %CTS in particle based on the initiator.

As high %CTS content is important for 1) stabilize hexadecane in water via the formation of Pickering emulsions, and 2) chemical crosslinking of functional groups

located on the chitosan shell. Therefore, the PBA/CTS particles with the highest CTS content in particle, PBA/CTS (2-1 H_2O_2) are used for subsequent studies.

3.2.1.3 Particle size and morphology

Figure 3.6 shows the morphology of the PBA/CTS particles PBA/CTS (2-1 H_2O_2). Statistical analysis of the image showed the PBA/CTS (2-1 H_2O_2) have an average size of 159 ± 22 nm which is smaller than the measured hydrodynamic diameter of 193 nm (PDI 0.074) which may be due to drying which causes chitosan shell to shrink. The SEM image shows that some of the PBA/CTS particles have fused together. As water is removed during drying of the sample, the electrostatic repulsion forces between particles drop down to zero. The polymer PBA has a low glass transition temperature, -54 °C[177], which means it will deform easily at room temperature, which leads to coalescence of the PBA/CTS particles, and fusing of the particles. In cases where the dispersion concentration was > 100 ppm, no individual particles could be observed as it had formed a continuous film.

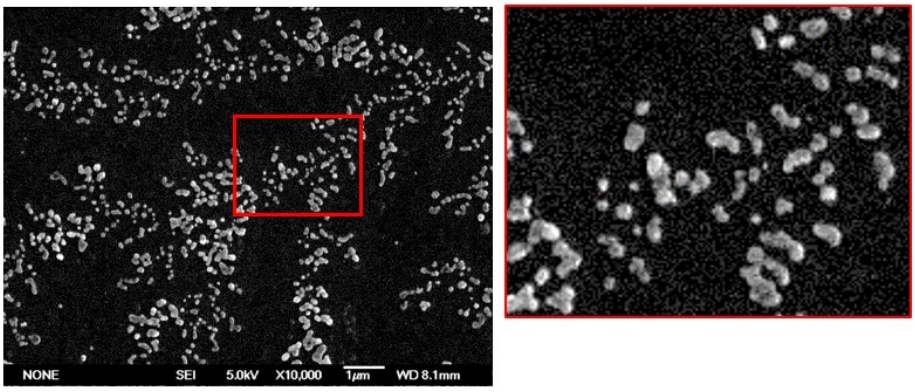


Figure 3.6 **SEM image of PBA/CTS (2-1 H_2O_2) at magnification of 10,000 X**

3.2.1.4 Chemical composition of the PBA/CTS particles

Figure 3.7 shows the FTIR spectra of PBA/CTS (2-1 H_2O_2) *The* FTIR shows PBA/CTS particles possess the characteristic peaks of PBA: C=O group [1731 cm^{-1}], (sp3) C-H peaks [2958 cm^{-1} to 2873 cm^{-1}] and C-O peak [1158 cm^{-1}] and of CTS: OH group and primary amine group [3269 cm^{-1}], amide group [1635 cm^{-1}].

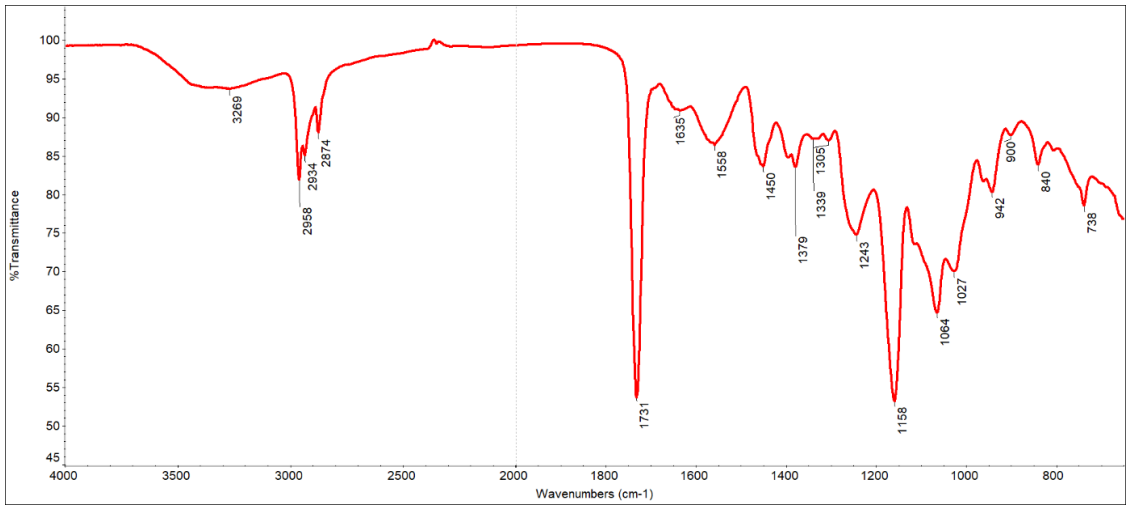


Figure 3.7 **FTIR spectra of PBA/CTS (2-1, H_2O_2)**

3.2.2 Pickering emulsion with PBA/CTS particles as the stabilizer

The ability of a solid particle to stabilize an oil droplet in an emulsion depends on the solid particle's ability to adhere to the oil-water interface. When solid particles adhere to the oil-water interface of the oil droplets, they replace the oil-water interface with a particle-water and particle-oil, thereby reducing the surface free energy. They serve as a

barrier to coalescence, giving a stable emulsion. The adherence depends on the particle's wettability or hydrophobicity/hydrophilicity property. The particle is able to be partially wetted by both the oil and water, if contact angle is approaching 90º (Figure 3.8).[178] To optimize the adhesion of PBA/CTS particles on hexadecane/water interface, various effects have been studied including pH of PBA/CTS particles, addition of various types of emulsifiers and the presence of electrolyte in the aqueous phase.

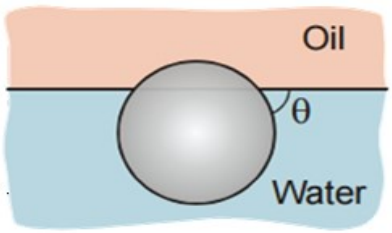


Figure 3.8 **Optimum contact angle for oil in water emulsion: $70^\circ \leq \theta \leq 86^\circ$; water in oil emulsion: $94^\circ \leq \theta \leq 110^\circ$**[178]

MEPCM was synthesized via formation of Pickering emulsion with PBA/CTS Np followed by GAL crosslinking (Detailed procedures in Section 3.1.2.2.2). Their thermal properties were evaluated based on procedures in Section 3.1.3.9. From the DSC scan (Figure 3.9), the percentage encapsulation efficiency(%ee) (based on peak at 3°C) was 77 This result suggests that PCM can be encapsulated with PBA/CTS Np followed by GAL crosslinking. However, the encapsulated PCM was unable to withstand 20 phase change cycles as exhibited by change in the morphology of the exothermic peak at 3 °C. Thus, further optimization was required. Various effect studies to improve the stability of the Pickering emulsion formed with PBA/CTS Np prior to crosslinking were carried out.

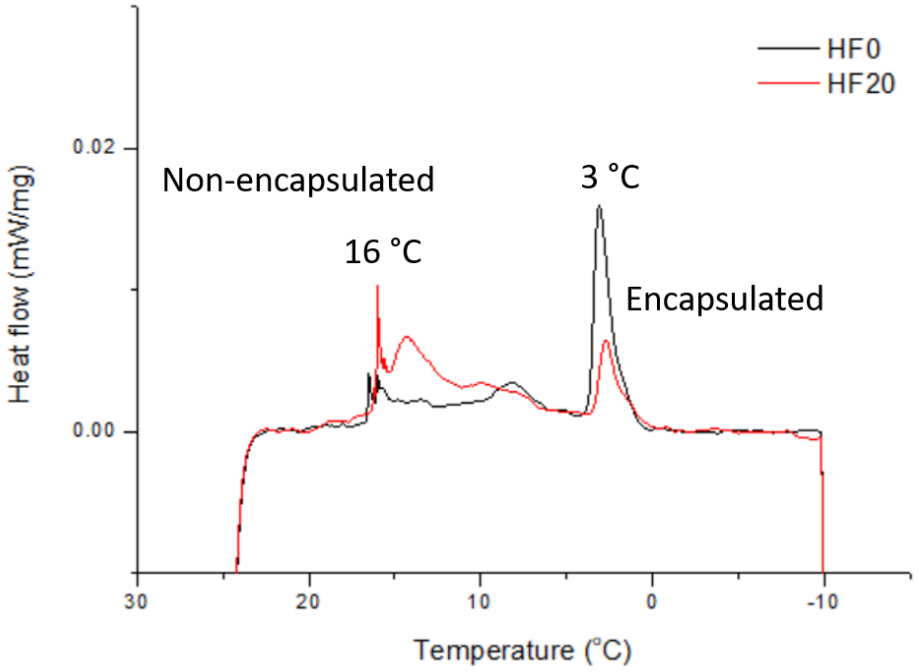


Figure 3.9 Thermal profile of MEPCMs synthesized via GAL crosslinking of Pickering emulsion formed with PBA/CTS Np and C16.

HF0: Thermal profile of MEPCMs after 1 phase change cycles

HF20 : Thermal profile of MEPCMs after 20 phase change cycles

3.2.2.1 Effect of solution pH on the Pickering emulsion of hexadecane

The ability of PBA/CTS (2-1 H_2O_2) (0.5 %SC) to stabilize 20 vol% hexadecane over a range of pHs is evaluated using a bottle test. Figure 3.10 show the emulsions after a period of 1 h which were prepared with PBA/CTS (2-1 H_2O_2). The emulsions formed with PBA/CTS (2-1 H_2O_2) dispersions from pH 4-12 in o/w emulsions. The emulsions formed with PBA/CTS (2-1 H_2O_2) dispersions at pH < 6.5 showed no creaming,

indicating more stable emulsion**.** Figure 3.11 shows *zeta*-potential as a function of pH. Increasing the solution pH from pH 4-10 steadily decreased *zeta*-potential value from > +40 mV to near zero after pH > 10. This is due to the deprotonation of the amino groups of chitosan which likely increases the hydrophobicity of the particles. As a result, solution pH is able to cause the change in stability of the emulsions.

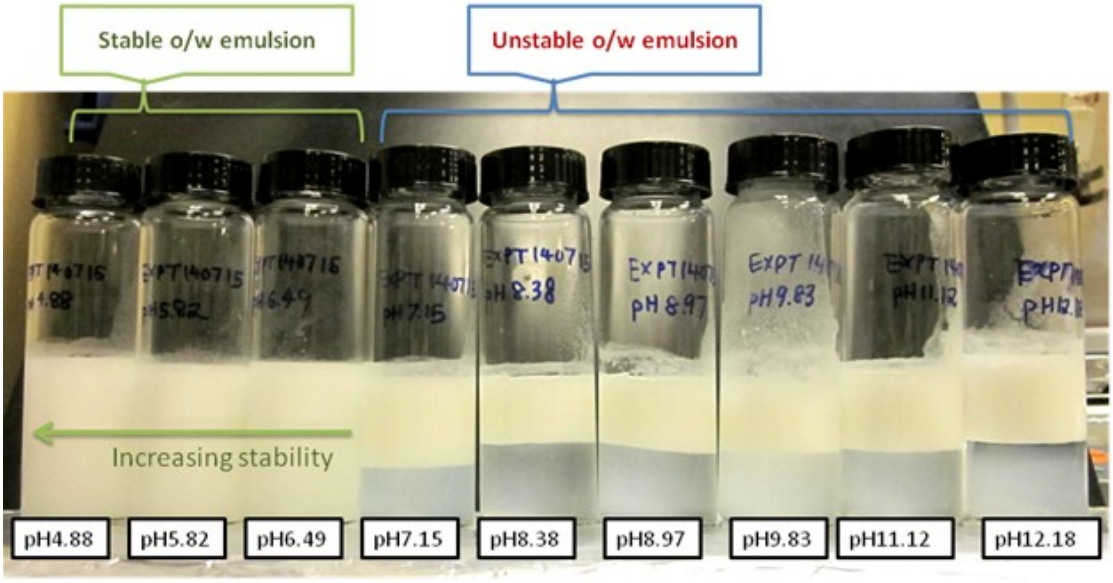


Figure 3.10 **Pickering emulsions formed with PBA/CTS (2-1 H_2O_2) dispersions at different pH after 1 h (Conditions: Total Volume: 20ml; %vol PCM:20%; %SC of Np used: 0.5%)**

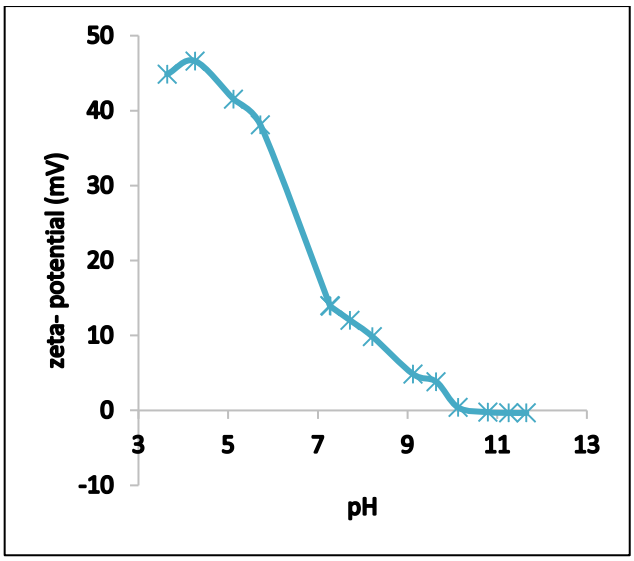


Figure 3.11 ***zeta*- Potential curve of PBA/CTS (2-1, H_2O_2)**

In conclusion, PBA/CTS (2-1 H_2O_2) particles form more stable Pickering emulsions at pH 4.88. However, when left overnight the emulsions showed phase separation. Thus further optimization of the Pickering emulsion was carried out in the next section.

3.2.2.2 Effect of emulsifiers on stability of the Pickering emulsion

To enhance the stability of the PBA/CTS particles, different types of emulsifiers have been investigated. The aim is to modify the surface properties of PBA/CTS Np through adsorption of the emulsifier on to the particle (as shown in Figure 3.12). Figure 3.13 shows the Pickering emulsions prepared with various emulsifiers after resting for 1 h. Emulsions stabilized by the nonionic emulsifiers, Tween80 and Cremophor show the

least amount of creaming, followed by cetrimonium bromide (CTAB) and sodium dodecyl sulfate (SDS) and finally emulsions with no emulsifier.

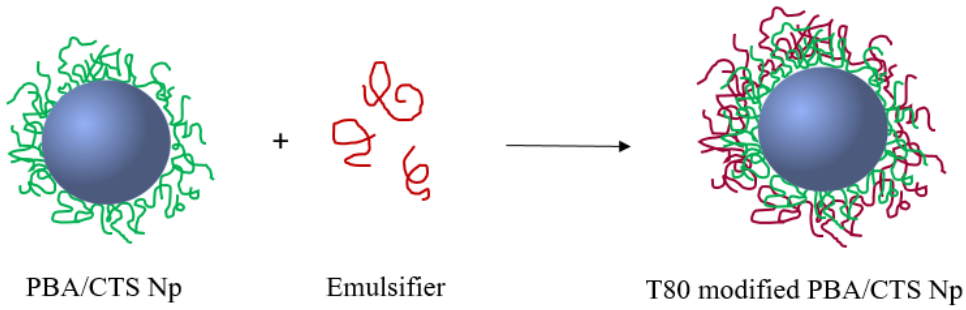


Figure 3.12 Surface modification of modified PBA/CTS Np with T80

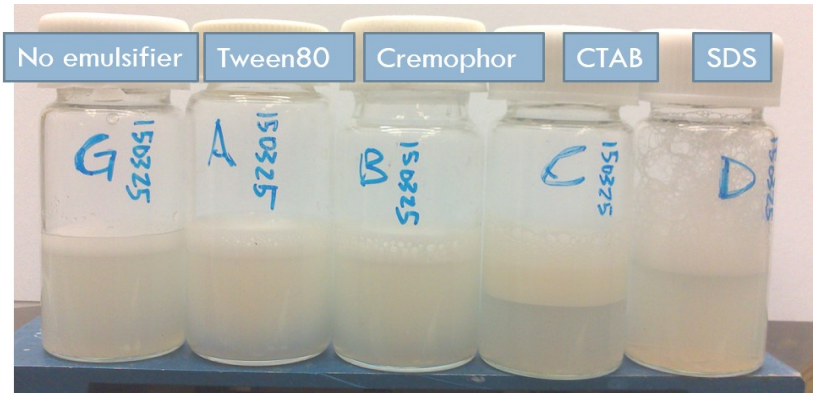


Figure 3.13 **Effect of various types of emulsifiers on emulsion stability after 1 h. The emulsions were prepared by homogenizing the mixtures (10%vol PCM in 0.5% PBA/CTS at pH4.88 with 0.2 wt% different emulsifier) for 1 min at 11k rpm.**

Optical images of the emulsions prepared using different emulsifiers are shown in Figure 3.14 to Figure 3.18. The Pickering emulsion prepared with no emulsifier shows

coalescence, giving large emulsion droplets up to 28 μm (Figure 3.14). Figure 3.15 and Figure 3.16 show that the emulsions using nonionic emulsifiers have fairly homogenous droplet sizes comparable to that without emulsifier but with little aggregation, signifying successful modification of the surface properties of the particles. Figure 3.17 shows that emulsions using the cationic emulsifier CTAB have larger droplet size with a broader distribution but also no aggregation, signifying some of the emulsion droplets were stabilized with the emulsifier, CTAB, and others with the Np However, in Figure 3.18, emulsions using anionic emulsifier SDS show aggregation of the emulsion droplets possibly due to neutralization of the positive charges on PBA/CTS particles. SDS likely formed a complex with PBA/CTS Np, with the hydrophilic head interacting with the NH^{3+}, thus increasing hydrophobicity of the PBA/CTS Np, which led to significant air bubble formation.

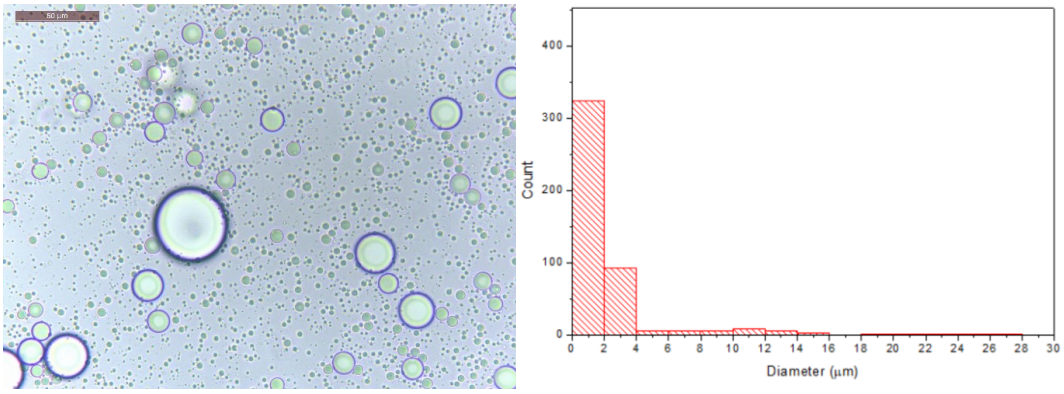


Figure 3.14 **Optical image [left] and size distribution [right] of Pickering emulsion without emulsifier. Average diameter of droplets: 2.62±3.83 μm**

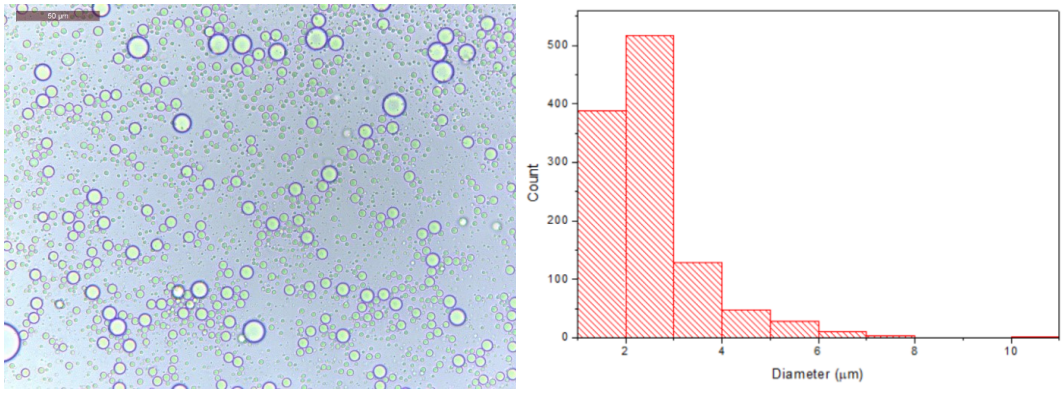


Figure 3.15 **Optical image [left] and size distribution [right] of Pickering emulsion with 0.2 wt% Cremophor . Average diameter of emulsified droplets: 1.86±0.83 μm**

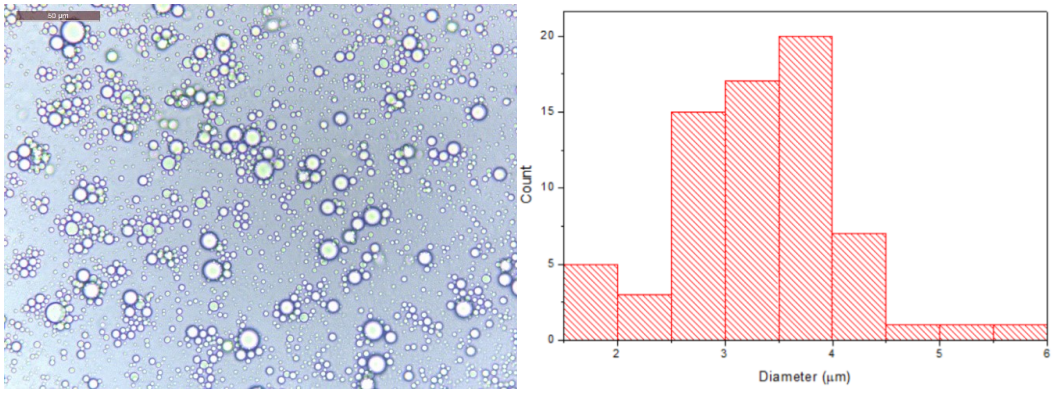


Figure 3.16 **Optical image [left] and size distribution [right] of Pickering emulsion with 0.2 wt% T80. Average diameter of emulsified droplets: 3.34±0.79 µm**

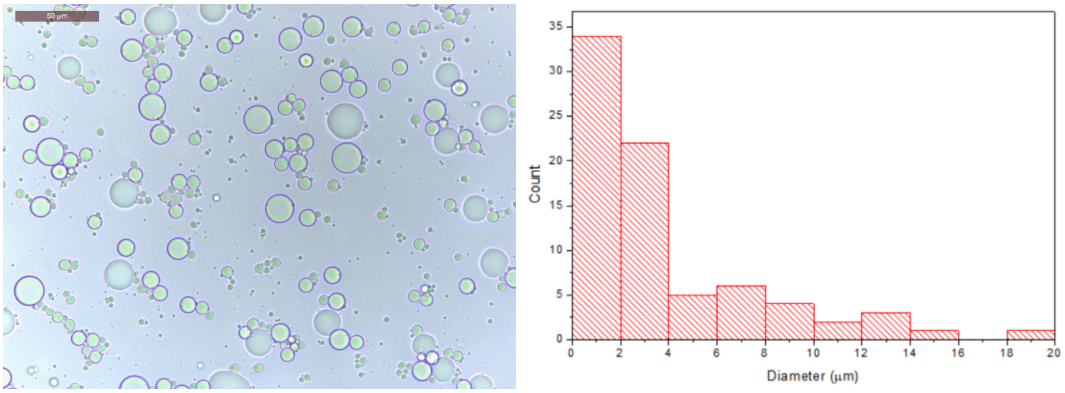


Figure 3.17 **Optical image [left] and size distribution [right] of Pickering emulsion with 0.2 wt% CTAB. Average diameter of emulsified droplets: 3.95±3.72 µm**

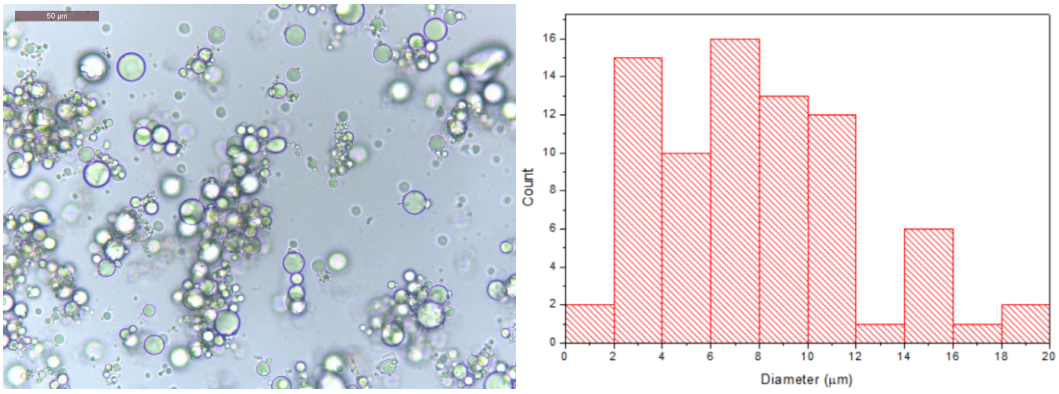


Figure 3.18 **Optical image [left] and size distribution [right] of Pickering emulsion with 0.2 wt% SDS. Average diameter of emulsified droplets: 7.40±03.84 µm**

Table 3.9 shows a summary of the droplet size of the emulsified PCM stabilized with PBA/CTS with various emulsifiers based on above optical images. The emulsion prepared with Tween80 shows least coalescence with the smallest percentage of standard derivation (%stdev), and therefore the highest stabilityThis is due to the abundance of hydroxyl groups in T80 which allowed it to adsorb onto the CTS shell of the PBA/CTS Np. As a result, the Tween80 was selected for further studies.

Table 3.9 **Summary of droplet size of emulsions prepared with various emulsifiers**

Sample	Droplet size	%stdev
No emulsifier	2.62±3.83 µm	146%
Tween80	3.34±0.79 µm	24%
Cremophor	1.86±0.83 µm	45%

CTAB	3.95±3.72 μm	52%
SDS	7.40±03.84 μm	94%

3.2.2.3 Effect of electrolyte concentration on stability of Pickering emulsion

The presence of electrolytes could shield the surface charge, thus modifying particle hydrophobicity for better adsorption to the o/w interface and possibly optimizing the contact angle of the PBA/CTS particles on the oil-water interface.[179]. The systems with 0.5 wt % PBA/CTS particles (pH 4.88) yielded emulsions which showed creaming after 2 h. Figure 3.19 shows obvious creaming after 24 h in all samples except sample containing 0.04 wt% $CaCl_2$. Table 3.10 shows a statistical analysis of droplet sizes of emulsions using different concentrations of $CaCl_2$ from the optical images of the samples. Results indicate that using 0.04 wt% $CaCl_2$ gives the lowest standard deviation.

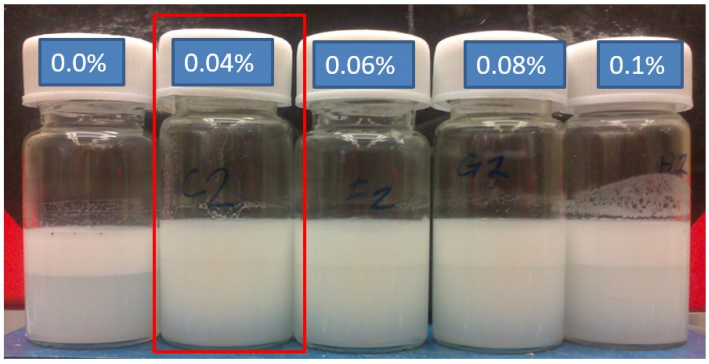


Figure 3.19 **Effect of different concentrations of $CaCl_2$. Pictures of emulsions were taken after 24 h (20%vol PCM in 0.5% PBA/CTS at pH4.88 and 0.2% Tween80) with different wt% $CaCl_2$**

Table 3.10 **Summary of emulsion droplet size of with addition of $CaCl_2$**

$CaCl_2$ (wt%)	**Droplet size**	**%stdev**
0.00	2.1±1.1	52
0.04	2.37±0.3	13
0.06	2.64±0.37	14
0.08	2.45±0.49	20
0.10	3.39±0.9	27

Figure 3.20 shows SEM images of the optimized PBA/CTS Np encapsulated PCM emulsion. A collapsed colloidosome structure with particle diameter of 1.16±0.37

μm with wall thickness ranging from 100 to 200 nm This result indicate that the T80 modified Np is able to adsorb onto the o/w interface.

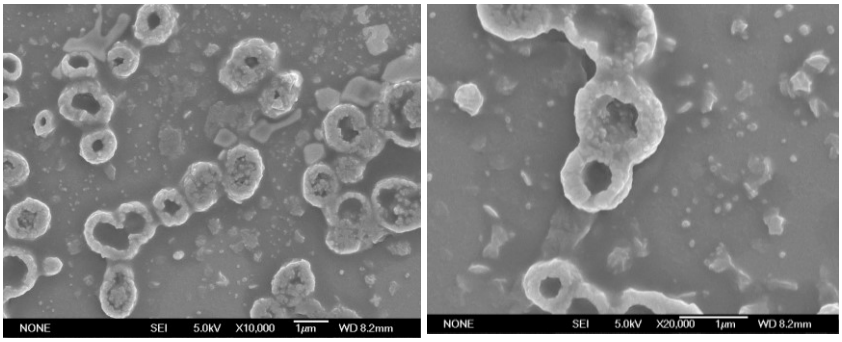


Figure 3.20 SEM images of Pickering emulsion formed with T80 modified PBA/CTS Np and 0.04 wt% $CaCl_2$ (Sample was dispersed in ethanol then imaged with SEM) ; MEPCM Diameter = 1.16±0.37 μm; Wall thickness: 100 – 200 nm

3.2.3 Chemical crosslinking of preformed Pickering emulsion

The PCM droplets are stabilized in water through adsorption PBA/CTS particles at the o/w interface. Crosslinking the functional groups on the PBA/CTS particles to form a continuous shell with the following chemical crosslinkers glutaraldehyde (EC-GAL), borax (EC-Borax) and sodium tripolyphosphate (EC-TPP) have been carried out.

EC-GAL

Monteiro's group has reported that suitable pH range for crosslinking of chitosan with glutaraldehyde is between pH 3 and 4.[180] In aqueous solution, multiple forms of glutaraldehyde co-exist in, monomeric hydrates, dimers, trimers and polymers formed from condensation (Figure 3.21). Because of this, the exact structure of the crosslinked product is not determinable. Under acidic or neutral conditions, the main crosslinking reactions is aldol condensation of the hydrated glutaraldehyde form and amine group in chitosan.[181] (Figure 3.22)

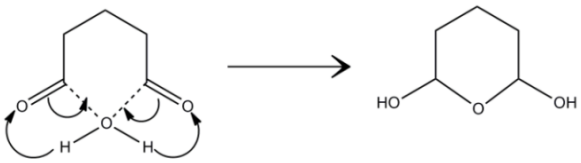


Figure 3.21 **Hydration of glutaraldehyde**

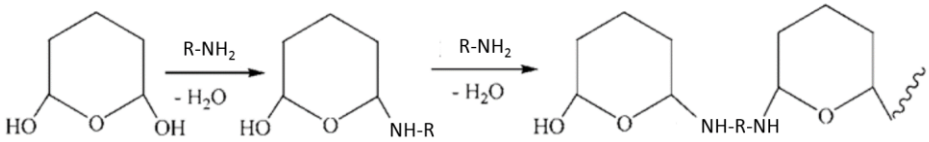


Figure 3.22 **Reaction of glutaraldehyde with amine groups in acidic or neutral conditions.[181]**

EC-Borax

Borate ions have been reportedly used to crosslink diols [182], starches such as chitosan[183-185], guar gum[186], poly(vinyl alcohols)[183, 187] which contain the alcohol group

under neutral conditions. Figure 3.23 shows the intramolecular crosslinking of boric acid and chitosan.

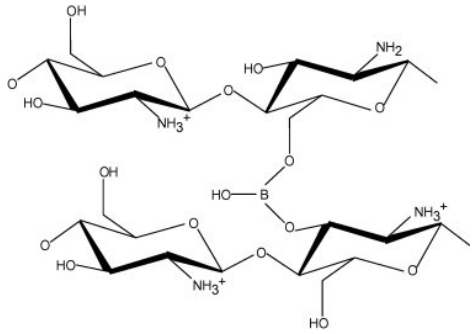


Figure 3.23 **Crosslinking of boric acid and chitosan** [185, 188]

EC-TPP

Chemical structure of the tripolyphosphate anion is shown in Figure 3.24. It is a negatively charged molecule which is able to crosslink chitosan of the PBA/CTS particles through electrostatic interaction with protonated amine group of chitosan. [189-191]

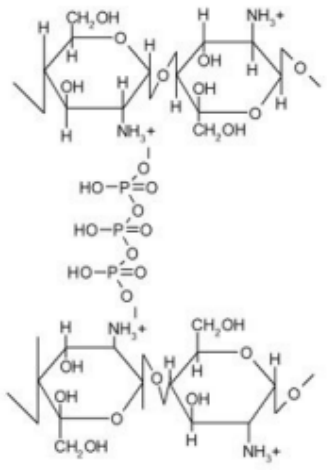


Figure 3.24 Ionic crosslinking of chitosan and tripolyphosphate ion[192]

3.2.3.1 Phase change performance

Table 3.11 shows the summary of the encapsulation efficiency (%ee) MEPCMs before and after crosslinking and the decrease in %ee after 20 heat freeze cycles. Detailed thermal profiles of the MEPCMs can be found in the Appendix, pg 207. The encapsulation efficiency of the MEPCMs have increased from 62% close to 100% with addition of crosslinkers. At the same time, crosslinking has significantly increased the thermal cycling stability of the encapsulated PCM (with the exception of borax). there was less than 5% decrease in %ee after 20 heat freeze cycles compared to 14.5% without crosslinking. The leakage of the PCM might be due to PCM escaping through the interstices between the PBA/CTS particles, caused by the volume expansion of the PCM during thermal cycling.

Table 3.11 **Phase change performance of crosslinked C16-PBA/CTS emulsions**

Code	%ee[1]	Decrease in %ee (HF20[2])	ΔT_f[3]
No crosslinker	62%	14.5%	-5.8
EC-GAL	100%	2.4%	-11.9
EC-Borax	98%	16.2%	-11.8
EC-TPP	97%	4.6%	-12.5

[1] Encapsulation efficiency (%ee)

[2]HF20: 20 heat freeze cycles

[3] Depression of freezing temperature

3.2.3.2 Morphology

Optical images of the MEPCMs show that EC-GAL possess a large size distribution spanning from 2-120 μm (Figure 3.25). This means that coalescence has taken place in EC-GAL. **Figure 3.26** and Figure 3.27 show that EC-Borax and EC-TPP have a more uniform distribution of 2.80±0.70 μm and 3.30±1.70 μm, respectively.

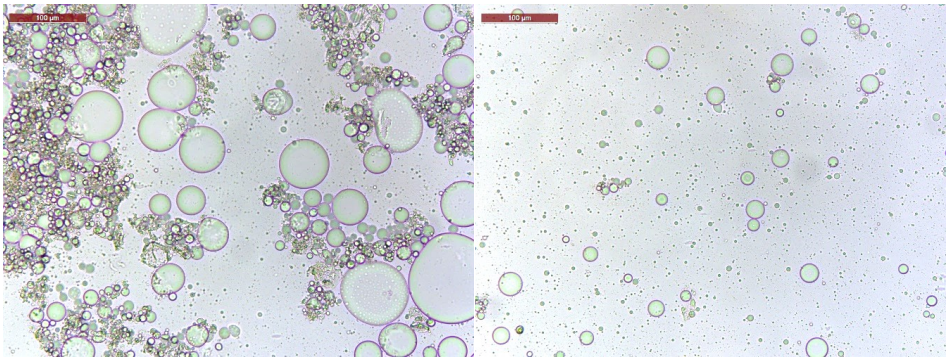


Figure 3.25 **Optical images of EC-GAL (Size distribution: 2-120 µm)**

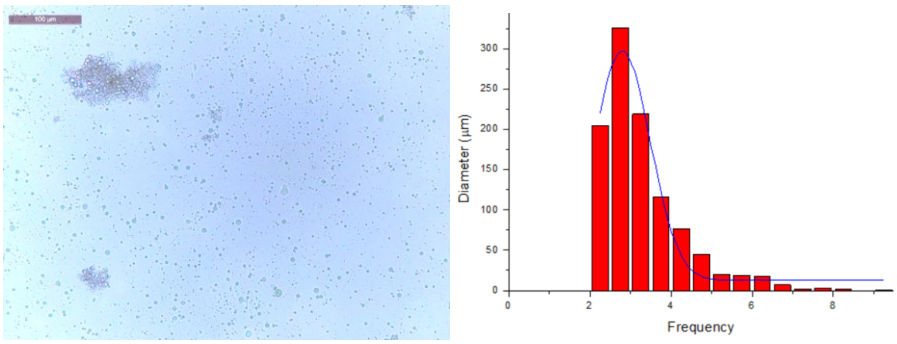


Figure 3.26 **Optical image [left] and size distribution [right] of EC-Borax (2.80±0.70 µm)**

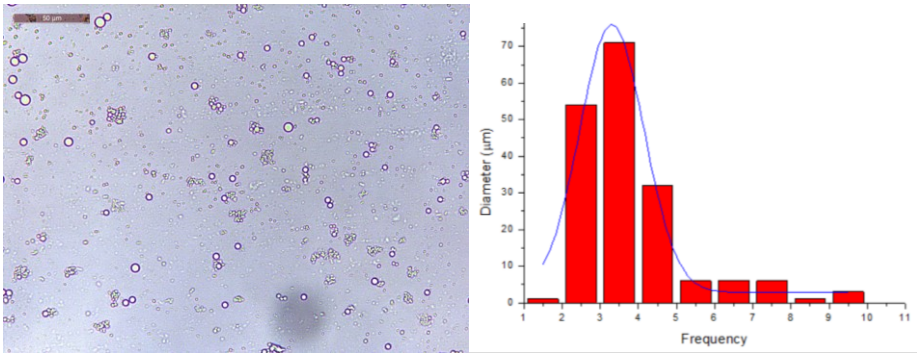


Figure 3.27 **Optical image [left] and size distribution [right] of EC-TPP (3.30±1.70 µm)**

Therefore, of the three crosslinkers, which all increased %ee >99%, TPP showed the most promise, as no coalescence was observed for the EC-TPP sample and also showed the least decrease in %ee after 20 heat freeze cycle.

3.3 Conclusion

In conclusion, PCM droplets were successfully dispersed in water, and stabilized with a mixture of PBA/CTS and Tween80, followed by successful crosslinking with TPP. Although the PCM dispersion could withstand heat-freeze cycles up to 20 with 5% encapsulation loss. Although crosslinking improves the phase change performance of the MEPCMs, it still could not satisfy the requirement for thermal storage applications as MEPCMs need to undergo hundreds of thermal cycles without PCM leakage and results indicate that there is PCM leakage upon 20 heat freeze cycles. Moreover, other problems associated with this approach were: 1) Interstices between the PBA/CTS still remain after crosslinking which leads to leakage due to incomplete coverage of the PCM droplet. 2) Moreover, the MEPCMs fractured and released PCM upon drying. 3) Solvent resistance of the MEPCMs were poor most probably due to interstices between the particles resulting in easy extraction of the PCM. In conclusion, this approach is still not quite satisfactory.

Chapter 4 Microencapsulation of Phase Change Materials through Coacervation Techniques

This chapter describes the development of the synthesis of MEPCMs through the coacervation method using chitosan-co-poly(methacrylic acid) (CTS-co-PMAA) polymer as the shell material for encapsulating the PCM of our interest, hexadecane.

The chapter begins by describing the synthesis and characterization of the amphoteric water-soluble polymer CTS-co-PMAA polymer. The CTS-co-PMAA was synthesized in two steps: 1) The chitosan was first modified with methacrylic acid (MAA) through an amidation reaction between the amine group of the chitosan and double bond of the MAA to form MAA-CTS, followed by 2) free radical polymerization of remaining MAA to generate the copolymer CTS-co-PMAA hydrogel. The shell material was further characterized with FTIR and NMR to determine the chemical composition, SEM for morphology and TGA to determine degradation profile.

The various effect studies to optimize the PCM encapsulation with CTS-co-PMAA are also described in this chapter. These effect studies include: initial pH of polymer solution, end pH of titration, CTS to PMAA ratios in the copolymer, CTS-co-PMAA crosslinking with glutaraldehyde (GLA) and addition of nucleating agent to reduce supercooling. The products were characterized with DSC to evaluate their

encapsulation efficiency and thermal profile. Their size distribution and morphology were also characterized with optical microscopy, DLS and SEM respectively.

Finally, the chapter describes the characterization of the optimized PCM encapsulates with FTIR for chemical composition, surface charge, SEM and TEM for morphology and DSC for phase change performance. Other studies include the phase change performance of the freeze dried optimized PCM encapsulates and PCM encapsulates synthesized in bulk based on the optimized recipe which were evaluated with DSC and temperature history test respectively.

4.1 Experimental

4.1.1 Materials

Methacrylic acid (MAA) monomer was purified via passing through a column packed with inhibitor remover. Chitosan (CTS) was obtained from AKBIO, (DDA 72.5% (calculated from elemental analysis)). Tert-butyl hydroperoxide (TBHP, 70 wt% solution in water), acetic acid (99%, glacial), Hexadecane (C16), KOH and glutaraldehyde (50 wt%) was obtained from Sigma Aldrich Co. and used as received. CNC was provided from NanoMalaysia and used as is. Deionized water (Milli-Q purified) was used as dispersion medium. Hexane (99%, Merck) was used for washing the PCM encapsulates.

4.1.2 Synthesis of chitosan-co-poly(methacrylic acid) copolymer

CTS was first dissolved in a 0.6% acetic acid solution (pH ≈ 3.3) completely, then mixed with MAA at room temperature (detailed recipe can be found in Table 4.1)

Table 4.1 Synthesis of CTS-co-PMAA with different chitosan to MAA ratio

Ingredient	**MAA to CTS Weight Ratio**				
	3 : 1	**2 : 1**	**1 : 1**	**1 : 2**	**1 : 3**
Chitosan (g)	0.5	0.67	1	1.33	1.5
Acetic acid (%)			0.60		

Methacrylic acid (g)	1.5	1.33	1	0.67	0.5
TBHP (100 mM)			1.0		
Water			96.4		
pH of final product	3.5	3.6	3.8	4.0	4.1

Solution pH of the mixtures were between pH 1.5 to 1.9 depending on the amounts of MAA added. The mixture was then stirred at 80 °C for 24 h under air, giving a transparent yellow liquid. The MAA conversion was between 60 and 71% as determined gravimetrically by drying the sample in an oven at 80 °C overnight. The MAA modified CTS was purged with nitrogen for 30 min to remove oxygen. A water-soluble initiator, *tert*-butyl hydroperoxide (TBHP) (1 mL, 100 mM) was added to the mixture to initiate the polymerization between MAA-modified chitosan and any unreacted MAA. The polymerization continues for 2 h at 80℃ under nitrogen with continuous stirring. The product is a slightly opaque gel and measured pH ranged from pH 3-4 depending on the amount of MAA used. Upon addition of glacial acetic acid (1-2 ml) the mixture gradually becomes a transparent yellow liquid.

4.1.3 Synthesis of CTS-co-PMAA/C16 microcapsules

4.1.3.1 Effect of different PMAA:CTS ratios in CTS-co-PMAA

Emulsification

CTS-co-PMAA polymer solution (pH 3-4, 2 wt%, 9 ml) is used. 1 ml of PCM (hexadecane) is added and an o/w emulsion is formed by homogenizing the two

components for 1 min under 10,000 rpm with IKA homogenizer T18. Followed by further breakdown of oil droplets with sonication probe (SONICS VC130) at 5W for 30min.

Coacervation

The formed emulsion is let alone for 30 min to cool to room temperature. pH is increased slowly up to pH 10 while stirring by addition of 0.1M KOH, drop by drop at a rate of 1 drop/4 sec.

Purification

To remove un-encapsulated or partially encapsulated PCM, the sample is washed with hexane in a separating funnel. The bottom part is then removed and purified with centrifugation remove excess CTS-co-PMAA. The MEPCMs are located on top of the supernatant as shown in Figure 4.1. The supernatant is drawn out with a long needled syringe and the MEPCM is re-dispersed and topped up to 10 ml with 0.01 M KOH. The centrifugation process is repeated twice. Total weight of product and solid content (wt%) is determined gravimetrically. The products were characterized with DSC and optical microscopy.

The process was repeated with CTS-co-PMAA polymer with PMAA:CTS = 3:1, PMAA:CTS = 2:1, PMAA:CTS = 1:2 and PMAA:CTS = 1:3.

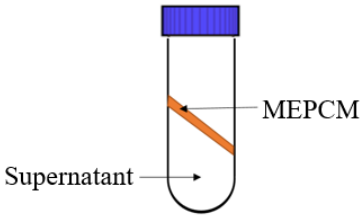


Figure 4.1 **Distribution of MEPCM after centrifugation**

4.1.3.2 Determination of the pH for highest solvation of CTS-co-PMAA

The pH of CTS-co-PMAA (PMAA:CTS = 1:1 w/w) solutions was adjusted with HCl (2 M) or NaOH (2 M) respectively to obtain pH from 1.5-7.5 followed by dilution to obtain concentrations of 0.5 wt%. The turbidity of the solutions was measured in: 1) Absorbance intensity (abs), the amount of light blocked and 2) Relative scattered light intensity (cps) amount of light scattered. Both measurements increase with the increase in insoluble moieties in the solution which would block and scatter light. The wavelength 690 nm was selected based on a UV/Vis scan indicating the sample does not absorb at this wavelength. (see Appendix) The two measurements were carried out using UV/Vis and fluorescence spectrophotometers (Horiba FluroMax-4) with detector angle located at 180 ^{o} and 90^{o} respectively.

4.1.3.3 Determination of optimal titration profiles

Emulsification

CTS-co-PMAA polymer solution (pH 1.4-1.7, 2 wt%, 9ml) is used. 1 ml of PCM (hexadecane) is added and an o/w emulsion is formed by homogenizing the two

components for 1 min with IKA homogenizer T18. This is followed by further breakdown of the oil droplets with sonication probe (SONICS VC130) at 5 W for 30min.

Coacervation

The emulsion is let alone for 30 min to cool to room temperature. pH is increased by addition of 0.1M KOH drop by drop (1 drop/4 sec) with slow stirring according to the titration profiles below:

Code	Titration profile
XCTS (pH 5.6)	Emulsion pH was titrated from initial pH 1.5 to 5.6;
XCTS (pH 10)	Emulsion pH was titrated from initial 1.5 to 10;
XCTS (10→5.6)	Emulsion pH was titrated from initial 1.5 to 10, followed by back titration from pH 10 to pH 5.6 (10→5.6).

Purification

To remove un-encapsulated or partially encapsulated PCM, the sample is washed with hexane in a separating funnel. The bottom part is removed and centrifuged twice to remove excess CTS-co-PMAA. To prevent pH change from affecting the MEPCMs, 0.01 M KOH was used as washing water during purification, dispersion medium after centrifugation.

4.1.3.4 Crosslinking with glutaraldehyde

Emulsification

CTS-co-PMAA (PMAA:CTS = 1:1 w/w) polymer solution (pH 1.4-1.7, 2 wt%, 9ml)

is used. 1 ml of PCM (hexadecane) is added and an o/w emulsion is formed by homogenizing the two components for 1 min under 10,000 rpm. Followed by further breakdown of oil droplets through sonication at 5W for 30min.

Coacervation

The emulsion is let alone for 30 min to cool to room temperature. As the emulsion is gently stirred, pH is increased up to pH 10 by addition of 0.1M KOH at rate of 1 drop/4 sec using a dropping funnel.

Crosslinking

The coacervate is diluted to 100 ml. The amount of GAL used was based on a ratio to CTS repeating units in CTS-co-PMAA. The average molecular weight of CTS repeating unit is calculated from the degree of deacetylation (DDA 72.5%). GAL:CTS+Chitin units ratios used were (5:1, 10:1, 15:1, 20:1). Suitable amount of the 50 wt% GAL solution is dissolved in DI water to obtain a 10 ml solution with GAL concentrations according to **Table 4.2**. The GAL solutions are added to the coacervates drop by drop (1 drop/4 sec) with gentle stirring. Stirring is continued for 24 h to allow completion of the crosslinking.

Table 4.2 **Recipe of XCTS-COA-C16**

Ingredient	**Weight (g)**			
GAL:CTS+Chitin ratio	5:1	10:1	15:1	20:1
Sample code	5X	10X	15X	20X
C16 (g)	0.776 (1 ml)			

2 wt% CTS-CO-PMAA (1:1) (g)		9.0		
10 ml GAL solution (wt%)	2.46%	4.92%	7.38%	9.84%

Purification

To remove un-encapsulated or partially encapsulated PCM, the sample is washed with hexane in a separating funnel. The bottom part is removed and centrifuged twice to remove excess CTS-co-PMAA or unreacted crosslinker. To prevent pH change from affecting the MEPCMs, 0.01 M KOH was used as washing water during purification, dispersion medium after centrifugation.

4.1.3.5 Incorporating nucleating agents into PCM cores

Emulsification

NA and PCM is heated at 60℃ for 30 min with gentle swirling to form a miscible solution. The various ingredients are listed in Table 4.3. CTS-co-PMAA (PMAA:CTS = 1:1 w/w) polymer solution (pH 1.4-1.7, 2 wt%, 9ml) is also heated to 60℃. 1 ml of the NA + PCM (hexadecane) mixture is added and an o/w emulsion is formed by sonication (SONICS VC130) of the two components at 5W for 30 min.

Table 4.3 **Recipe of XCTS-COA-EIC16**

Ingredient	**Weight (g)**

C16 (g)	0.776 (1 ml)
2 wt% CTS-CO-PMAA (1:1) (g)	9.0
GAL (g)	0.246
Eicosane (NA)	0.07

Coacervation

Five methods were tested to incorporate the nucleating agent into the MEPCM. The detailed procedures of each are as follows:

M1: The emulsion is let alone for 30 min to cool to room temperature. As the emulsion is gently stirred, pH is increased to pH 10 by addition of 0.1M KOH at rate of 1 drop/4 sec using a dropping funnel.

M2: The emulsion is placed in an ice bath. As the emulsion is gently stirred, pH is increased to pH 10 by addition of 0.1M KOH at rate of 1 drop/4 sec using a dropping funnel.

M3: The emulsion is placed in water bath at 40℃. As the emulsion is gently stirred, pH is increased up to pH 10 by addition of 0.1M KOH at rate of 1 drop/4 sec using a dropping funnel.

M4: The emulsion is placed in the refrigerator at 4℃ for 1 h. After that, the emulsion is gently stirred, pH is increased up to pH 10 by addition of 0.1M KOH at rate of 1 drop/4 sec using a dropping funnel.

M5: The emulsion is placed in the refrigerator at 4℃ for 1 h. After that, the emulsion is gently stirred, pH is increased up to pH 7 by addition of 0.1M KOH at rate of 1 drop/4 sec using a dropping funnel.

C*rosslinki*ng

10 ml of GAL (2.46 wt%) is added to the coacervates drop by drop (1 drop/4 sec) with a dropping funnel with gentle stirring. After addition of GAL, **M1-M4:** stirring is continued for 24 h to allow completion of the crosslinking; **M5:** stirring is continued for 1 h followed by pH increase to pH 10 by addition of 0.1M KOH at rate of 1 drop/4 sec using a dropping funnel. Stirring is continued for 24 h to allow completion of the crosslinking.

Purification

To remove un-encapsulated or partially encapsulated PCM, the sample is washed with hexane in a separating funnel. The bottom part is removed and centrifuged twice to remove excess CTS-co-PMAA or unreacted crosslinker. To prevent pH change from affecting the MEPCMs, 0.01 M KOH was used as washing water during purification, dispersion medium after centrifugation.

4.1.3.6 Effect of increasing amounts of nucleating agents

Refer to Section 4.1.3.5 for synthesis method M5. Recipe used for samples 3EI16, 6EI16 and 10EI16 are listed in the table below:

Table 4.4 **Recipe of MEPCMs with various amounts of NA**

Ingredient	Weight (g)		
	3EI16	**6EI16**	**10EI16**
PCM (g)	0.776	0.776	0.776
2 wt% CTS-co-PMAA (PMAA:CTS = 1:1 w/w) (g)	9.0	9.0	9.0
2.46 wt% GAL (g)	10	10	10
Eicosane (NA)	0.02	0.04	0.07

4.1.3.7 Effect of different nucleating agents

Refer to Section 4.1.3.5 for synthesis method M5. Recipe used for samples XCTS RTF 10CA16, XCTS RTF 10DA16 and XCTS RTF 10EI16.

Table 4.5 **Recipe of MEPCMs with different NA**

Ingredient	Weight (g)		
	XCTS RTF 10CA16	**XCTS RTF 10DA16**	**XCTS RTF 10EI16**
Nucleating agent (NA)	Cetyl alcohol	Decanoic acid	Eicosane
PCM (g)	0.706	0.706	0.706
2 wt% CTS-co-PMAA (PMAA:CTS = 1:1 w/w) (g)	9.0	9.0	9.0
GAL (g)	0.246	0.246	0.246
NA	0.07	0.07	0.07

Coacervation

The emulsion is placed in the refrigerator at 4℃ for 1 h. After which the emulsion is gently stirred while pH is increased up to pH 7 by addition of 0.1M KOH at rate of 1 drop/4 sec using a dropping funnel.

Rigidization of shell

0.492 g of 50 wt% GAL is diluted in 10 ml of water and added drop by drop (1 drop/4 sec) with gentle stirring. Stirring is continued for 1h followed by pH increase up to pH10 by addition of 0.1M KOH at rate of 1 drop/4 sec using a dropping funnel. Stirring is continued for 24 h.

Purification

To remove un-encapsulated or partially encapsulated PCM, the sample is washed with hexane in a separating funnel. The bottom part is removed and centrifuged twice to remove excess CTS-co-PMAA or unreacted GAL. Ultrafiltration is carried out at 60 psi overnight with membrane of MWCO 150 kDa for further concentration. To prevent pH change from affecting the coacervates, diluent used to wash the coacervates is 0.01 M KOH.

4.1.3.8 Synthesis of freeze dried nanoencapsulated PCM

1 ml of 4 wt% MEPCM was frozen at -20℃ for 2 h in 1 ml eppendorf tube. It was then freeze dried (Lab Kits FD-12-MR) overnight under vacuum pressure of 1 Pa to remove the water. A spongelike structure was obtained. The apparent volume the tapping method is used. [193]

The tapping method involves first obtaining the apparent density (ρ_s, unit: g/ml) of previously desiccated NaCl salt crystals using a volumetric cylinder and an electronic mass balance precise to 5 decimal places. Then, the aerogel is weighed to obtain its mass (m_a) and placed in a volumetric cylinder where any space between the aerogel and volumetric cylinder is filled by slowly adding the NaCl salt crystals, the weight of the NaCl added (M_S) and the total volume of the NaCl and the aerogel (V_{sa}) is noted. The apparent density of the aerogel is calculated according to the equation below:

$$\textbf{Apparent density, } \rho_a = \frac{m_a}{V_{sa} - (m_s/\rho_s)} \quad \textbf{Equation 4.1}$$

4.1.3.9 Synthesis of bulk MEPCMs

The synthesis of MEPCM was increased by 20 fold (Sample code: MEPCM20X) using previously optimized procedure with the following changes, 1) during formation of emulsion, the sonication time and power was increased to 12 W for 3 h; 2) 5 wt% of

CTS-co-PMAA solution was used instead. The various ingredients used are listed in the table below:

Table 4.6 **Recipe of MEPCM20X**

Ingredient	Weight (g)
Hexadecane (C16)	14.12
5 wt% CTS-co-PMAA (PMAA:CTS = 1:1 w/w) (g)	72
50% Glutaraldehyde (GAL)	9.84
Eicosane (NA)	1.4

4.1.4 Measurement and Characterization

4.1.4.1 Fourier transform infrared spectroscopy (FTIR)

FTIR (Nicolet iS50 FT-IR) was used to examine to chemical structure of the nanoparticles in the mid-infrared (4000 cm^{-1} to 400 cm^{-1}) at 4 cm^{-1} resolution for 64 scans. Depending on the type of sample, one of two sample preparation methods are used: 1) Film forming sample: The sample is dried for 2 days at room temperature, washed with ethanol, and placed in a desiccator for two days to remove moisture or ethanol. IR spectra is taken with the Attenuated Total Reflectance (ATR) method which uses a ZnSe crystal 2) Powder form sample: Sample is frozen and freeze dried (LAB-KITS FD-12-MR) to remove water for 2 days at -60 ^{0}C at <10 Pa. 2) 1-part sample is mixed with 100 parts desiccated KBr salt in a mortar and grinded with pestle. The mixture is added to a die and placed in a level-screw press and pressed at around

12,000 psi for 1-2 min. The KBr recrystallizes to form a clear glassy disk which is analyzed with FTIR by transmission method.

4.1.4.2 Nuclear Magnetic Resonance (NMR)

Samples of CTS, MAA-CTS and CTS-co-PMAA were prepared for NMR spectroscopy. The samples are dissolved in water, dried in an oven to remove water and any unreacted monomer followed by re-dissolution in a 2 wt%-d-Acetic acid in D_2O with sonication. After, dissolution in the deuterated solvent, it is transferred to a 5 mm NMR tube, and spectra was recorded on a Bruker 400 MHz spectrometer. The 1H spectra were referenced internally to the residual proton resonance D_2O (4.79 ppm).

4.1.4.3 Particle size and size distribution

4.1.4.3.1 Dynamic Light Scattering

Size distribution of the CTS-co-PMAA was measured with Dynamic Light Scattering (DLS). The DLS measurements were performed with Zetasizer Nano (Malvern) using a photon correlation spectroscopy with electrophoretic dynamic light scattering (a two-laser diode light source with a wavelength of 632.8 nm at 4 mW) operating at a detector angle of 180°.

Samples of CTS-co-PMAA were diluted to 500 ppm with 0.1 M HCl (pH ~1.5), 60 runs were performed, and repeated three times to obtain the intensity size distribution, z-average (z-ave.) and polydispersity index (PDI).

Samples of MEPCMs were diluted to 500 ppm concentrations using either a 0.1 M citric acid – Na_2HPO_4 buffer at pH 5.6 or 0.1 M sodium carbonate – sodium bicarbonate buffer solution at pH 10. Each measurement comprised of 60 runs, repeated three times to obtain the intensity size distribution, z-average (z-ave.) and polydispersity index (PI).

4.1.4.3.2 Nanosight

Size distribution of samples could be measured with Nanosight (NS300) which uses Nanoparticle Tracking Analysis (NTA). NTA is a method of measuring particle size by analyzing the rate of movement of particles in the liquid (Brownian motion) and correlation to water using the (Stokes-Einstein equation). Illuminated by a laser (CW: 642 nm) particles act as point scatterers and its movement can be visualized via camera, video clips of the particles' motion are taken with a CCD camera. The video is analyzed using Nanosight NTA software, size of each particle is determined individually to obtain the particle size distribution profiles.

Sample were prepared with concentrations were around 100-500 ppm. The samples were loaded into the sample chamber (O-ring top-plate) with a disposable syringe. Camera level was adjusted to obtain a best image for video capture. Capture times were set at 60 sec.

4.1.4.4 zeta-potential

For *zeta*-potential measurements samples were diluted to 500 ppm in 1 mM NaCl and measured at room temperature with Delsa Nano C Particle Analyzer

(Beckman Coulter, Brea, CA, USA). The *zeta*-potential measurements were measured with a monochromatic laser beam at 658 nm. The size range for *zeta*- potential measurements is between 0.6 nm and 30 μm. Samples were freeze dried, re-dispersed in 1) 0.1 M HCl and 2) 0.1 M NaOH. For *zeta*- potential across a pH range, an auto-titrator accessory was used to adjust the pH of the samples from 1) pH 1.5 to 7 and 2) pH 10 to 7 with solutions of 0.1 M NaOH and 0.1 M HCl accordingly.

4.1.4.5 *Differential Scanning Calorimetry*

MEPCM samples were analyzed with Differential Scanning Calorimetry (DSC) if product yield (calculated gravimetrically) exceeded 40%. Temperature profile used in the DSC scan was from a freezing profile 25°C to -10°C and a heating profile -10°C to 25°C at a rate of 4°C min¬¹ which encompasses the temperature range of freezing and melting of our PCM of interest, hexadecane. The sample was first scanned at a rate of 10°C min¬¹ to ensure PCM emulsions are destabilized. A known weight of the sample (1-30 mg) is hermetically sealed in an aluminum pan and placed in the sample holder inside the DSC (Mettler Toledo, 822e). An empty Al pan is used as reference. During the DSC scan, nitrogen is passed through the sample chamber at 20 ml/min for protection. Indium was used to calibrate the temperature and latent heat. From the thermal profile of the MEPCM we can determine the: 1) Encapsulation efficiency (%ee); 2) Depression of freezing temperature; 3) %PCM in MEPCM; and 4) %ee of MEPCM after multiple phase change cycles.

4.1.4.5.1 Encapsulation efficiency (%ee)

Encapsulation efficiency of the MEPCM is the amount of PCM encapsulated divided by the amount of PCM added. The amount of PCM encapsulated is obtained by calculating the %PCM in the sample times the total weight of the sample. %PCM in the sample is obtained from the thermal profile of the MEPCM (An example is shown in Figure 4.2), the area under the freezing curve of the encapsulated PCM divided by latent heat of hexadecane which is 249.14 J/g.

$$\%ee = \frac{\%PCM \times \text{Total Weight}}{\text{initial PCM added}} \qquad \textbf{Equation 4.2}$$

$$\%PCM = \frac{\text{Latent heat of sample}}{249.14} \qquad \textbf{Equation 4.3}$$

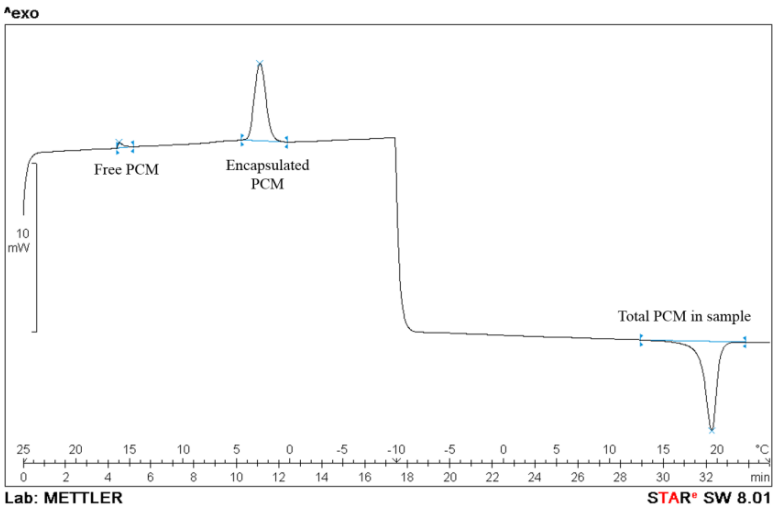


Figure 4.2 **DSC scan of microencapsulated hexadecane (from 25 °C to -10 °C and -10 °C to 25 °C at a rate of 4 °C min^{-1})**

4.1.4.5.2 Depression ***of freezing temperature***

Supercooling occurs in MEPCMs and is the depression of freezing temperature of unencapsulated or bulk PCM. Depression of freezing temperature (ΔT) is the difference between the onset freezing temperature of MEPCMs (T_{fo} [$MEPCM$]) and the PCM (T_{fo} [$C16$]:15.81 °C).

$$\boldsymbol{\Delta T = 15.81 - T_{fo}\,[MEPCM]} \qquad \textbf{Equation 4.4}$$

4.1.4.5.3 %PCM in MEPCM

The aqueous MEPCM is hermetically sealed in Al pan of known weight (ME27331) used in DSC (Mettler Toledo 822e). Holes are pricked in the cover of the Al pan, and then placed in a drybox together with dessicant for a week to ensure no moisture remains. The pan is weighed again to obtain the weight of the dried sample in the Al pan. The sample is then scanned in DSC from 25°C to -10°C and -10°C to 25°C at a rate of 4°C min¬ % PCM in microcapsules is the amount of PCM in MEPCMs per weight. It is calculated based on the LH_s of the dried MEPCM measured by DSC compared to the LHs of the PCM (249.14 J/g). The wt% of PCM in the MEPCM can be used to obtain PCM core:shell ratios of the MEPCM.

$$\textbf{\%PCM} = \frac{\boldsymbol{LH_{s\,(MEPCM)}}}{\boldsymbol{LH_{s\,(PCM)}}} \times \mathbf{100\%} \qquad \textbf{Equation 4.5}$$

4.1.4.5.4 Encapsulation efficiency of MEPCM after multiple phase change cycles

MEPCMs are used for thermal energy storage. They need to maintain their thermal storage capacity without PCM leakage over many cycles of storage/release of thermal energy. This means the MEPCM shell needs to withstand the volume change that the PCM undergoes during solidification and melting. To assess this ability, the MEPCMs are freeze and thawed over multiple cycles using DSC (Mettler Toledo, 822e) MEPCMs are cycled from 25°C to -10°C to -10°C to 25°C repeatedly at a rate of 20°C min¬ over either 20 (HF20), 50 (HF50) or 100 (HF100) cycles. The %ee before and after the multiple phase change cycles is compared to assess thermal capacity loss of the MEPCM or leakage of the PCM.

4.1.4.6 Surface tension

The surface tension was measured with the pendant drop method using an optical tensiometer (Theta lite, Attension) that was calibrated with a 4 mm metal ball. Calibration is deemed successful if surface tension measurements of deionized water is 72.8 dynes/cm, the reported value of surface tension of water in literature. Optical photographs of the pendant droplet are taken for 10 s at 12 fps. The silhouettes of the pendant droplet are repeatedly fitted to the Young-Laplace equation to calculate the surface tension. The measurements were repeated thrice with droplet volume between 12-14 μL.

4.1.4.7 Morphology

4.1.4.7.1 Optical microscope

Refer to Section 3.1.3.8.

4.1.4.7.2 Scanning electron microscopy

Samples for scanning electron microscopy (SEM) were prepared by dilution to 100 ppm concentrations approximately 10 µL was dropped onto a 3 mm diameter glass slide affixed to sample holder with conducting tape. The samples were either 1) air dried at room temperature and placed in a desiccator; 2) freeze dried to remove moisture. To increase conductivity, the samples were sputter coated with gold. SEM images were taken on JEOL SM-31010 with an accelerating voltage of 5 kV.

4.1.4.7.3 Transmission electron microscopy

Morphology of the sample was observed by transmission electron microscope (TEM) operating at an acceleration voltage of 120 kV (model: JEOL JEM-2011). Samples for TEM was prepared by pipetting 10 µL of the sample dispersion (sample concentration is from 20 to 100 ppm) on a carbon-coated copper grid, allowed to adsorb for 2 min and the surplus droplet was removed by wicking away with filter paper. The sample was then dried at ambient temperature overnight before being observed by TEM.

4.1.4.8 Thermal stability

Thermal decomposition was studied with thermogravimetric analysis (TGA) using TGA/DSC+ (Mettler Toledo). Known amounts of sample (1- 5 mg) was placed in the

aluminum oxide sample holder. Samples were heated under nitrogen atmosphere, flow rate of 20 ml/min. The heating profile used was 60-600℃ (ramp: 10℃/min). TGA graphs were plotted using Origin, the weight was normalized, and the first derivative was calculated with Saviztky-Golay smooth with a polynomial order of 2 and points of window as 20.

4.1.4.9 Turbidity

The turbidity was measured in terms of: 1) Absorbance intensity (abs), the amount of light blocked and 2) Relative scattered light intensity (cps) amount of light scattered. Both measurements increase with the increase in insoluble moieties in the solution which would block and scatter light. The wavelength 690 nm was selected based on a UV/Vis scan indicating the sample does not absorb at this wavelength. The two measurements were carried out using UV/Vis and fluorescence spectrophotometers (Horiba FluroMax-4) with detector angle located at 180^{o} and 90^{o} respectively.

4.1.4.10 Temperature History

The experimental setup shown in Figure 4.3 was used to measure temperature profile of bulk MEPCMs and bulk PCM, hexadecane (C16); 20g of the sample was loaded into the metal container. Temperature logger (LASCAR, EL-USB-1-PRO) was programmed to measure temperature at intervals of 20 sec with an initial delay of 8 h to allow samples to reach thermal equilibrium. As shown in Figure 4.3 the temperature logger (outer diameter 1.7 cm; length 11.4 cm) is placed at the center of a cylindrical metal container (outer diameter 2.3 cm wall thickness 0.1 cm and length 13 cm). It is then sealed with a stopper and paraffin film. The metal container is then placed in a sponge cutout with thickness around 1.5 cm on the sides and 5 cm on the top and bottom. This is to ensure that heat transfer rate enters from sides and is more or less the same. For cases of hexadecane, the stopper for the metal container is sealed loosely, if not the volume change during phase change causes the stopper to pop.

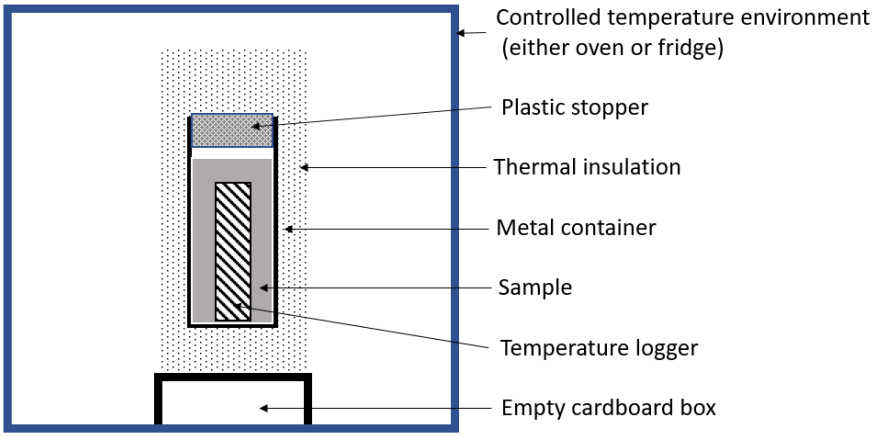


Figure 4.3 Experimental setup to measure temperature history of samples at ambient temperatures of 42-43 °C and 2-3 °C

The setup uses two controlled temperatures: room temperature (~23 °C). and refrigerator (~3 °C). Two temperature profiles are used to monitor: 1) PCM during solidification: The experimental setup is placed first at room temperature until thermal equilibrium, and then moved to the refrigerator, the temperature change in the MEPCM is monitored and logged with the temperature logger for periods of 12 h; and 2) PCM during melting: The experimental setup is placed in the refrigerator until thermal equilibrium, and then moved to room temperature, the temperature change in the MEPCM is monitored and logged with the temperature logger for periods of 12 h. The data is retrieved via USB hub in the temperature logger. Each sample is repeated thrice, and the results are averaged.

4.2 Results and Discussion

4.2.1 Synthesis of chitosan-co-poly(methacrylic acid) copolymer

The zwitterionic copolymer of chitosan-co-poly(methacrylic acid) (CTS-co-PMAA) was synthesized via a two-step reaction. The chitosan was first modified with methacrylic acid (MAA) through an amidation reaction between the amine group of the chitosan and the carboxylic acid group of the MAA (Figure 4.4). Chemical structure of the MAA-modified chitosan was identified by ^{1}H-NMR spectroscopy as shown in Figure 4.5. Comparing with spectrum of methacrylic acid (Figure 4.5a) , the modified chitosan possesses vinylic protons as observed at 5.916 and 5.538 ppm. The Ha peak slight shifted upfield from 6.003 to 5.916 pm, suggesting an amidation reaction between chitosan and the MAA. Furthermore, protons of methyl groups from both chitosan and MAA were found at 1.948 and 1.783 ppm, respectively (Figure 4.5b). Integration of the vinylic and methyl proton peaks gave almost the same value as of the original MAA. These results clearly indicated that the major reaction is between the amine and carboxylic acid groups under thermal treatment.

The resulting MAA modified chitosan and remaining MAA were subsequently subject to polymerization initiated by the *tert*-butyl hydroperoxide (TBHP) based on our previously established method [173]. The polymerization preceded through a redox reaction between TBHP and amine groups on the chitosan backbone to generate free radicals on the amine nitrogen atoms. The resultant radicals enabled polymerization of MAA monomer to generate CTS-co-PMAA copolymer. The radicals were also able to react with the double bond of the MAA-chitosan, forming crosslinked chitosan-PMAA

hydrogel. ^{1}H-NMR spectrum of the products shown in Figure 4.5c reveals that the both vinylic hydrogens and the Hc protons of methacrylic acid disappeared, and a new and broad peak appear between 0.7 and 1.5 ppm. The t-Bu-O· radical may also extract hydrogen from chitosan backbone to form a radical site because the peak area of the Hc protons of MAA-CTS (3.047 ppm) is reduced. All other characteristic peaks of chitosan remain unchanged. Various PMAA:CTS ratios were used to synthesize the CTS-co-PMAA, and in almost all cases MAA monomer conversion was above 90%.

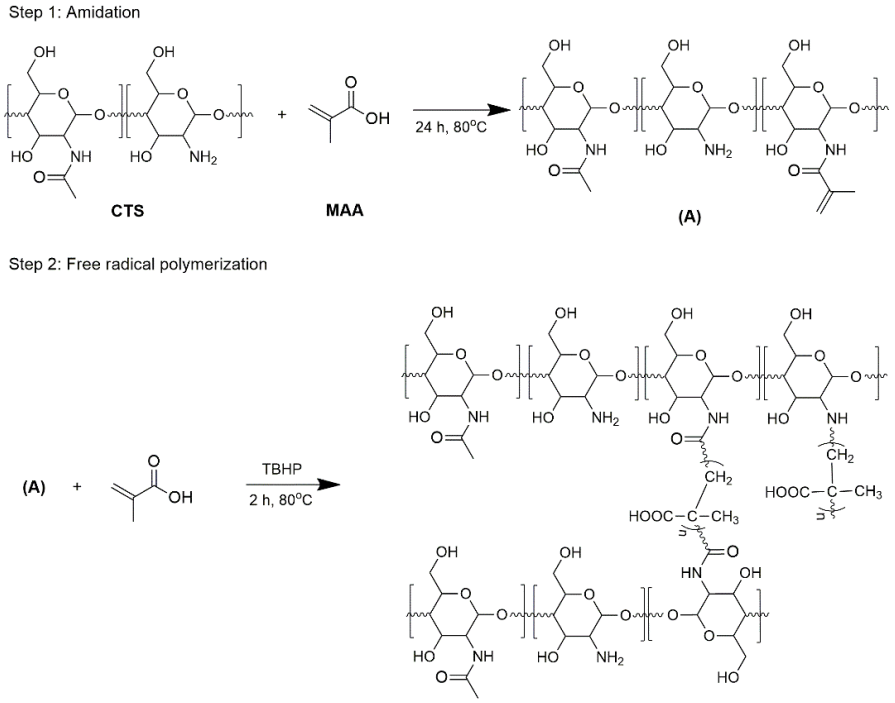


Figure 4.4 **Synthesis of zwitterionic copolymer of CTS-co-PMAA via the two-step reaction: Step 1. Amidation reaction; 2) Polymerization**

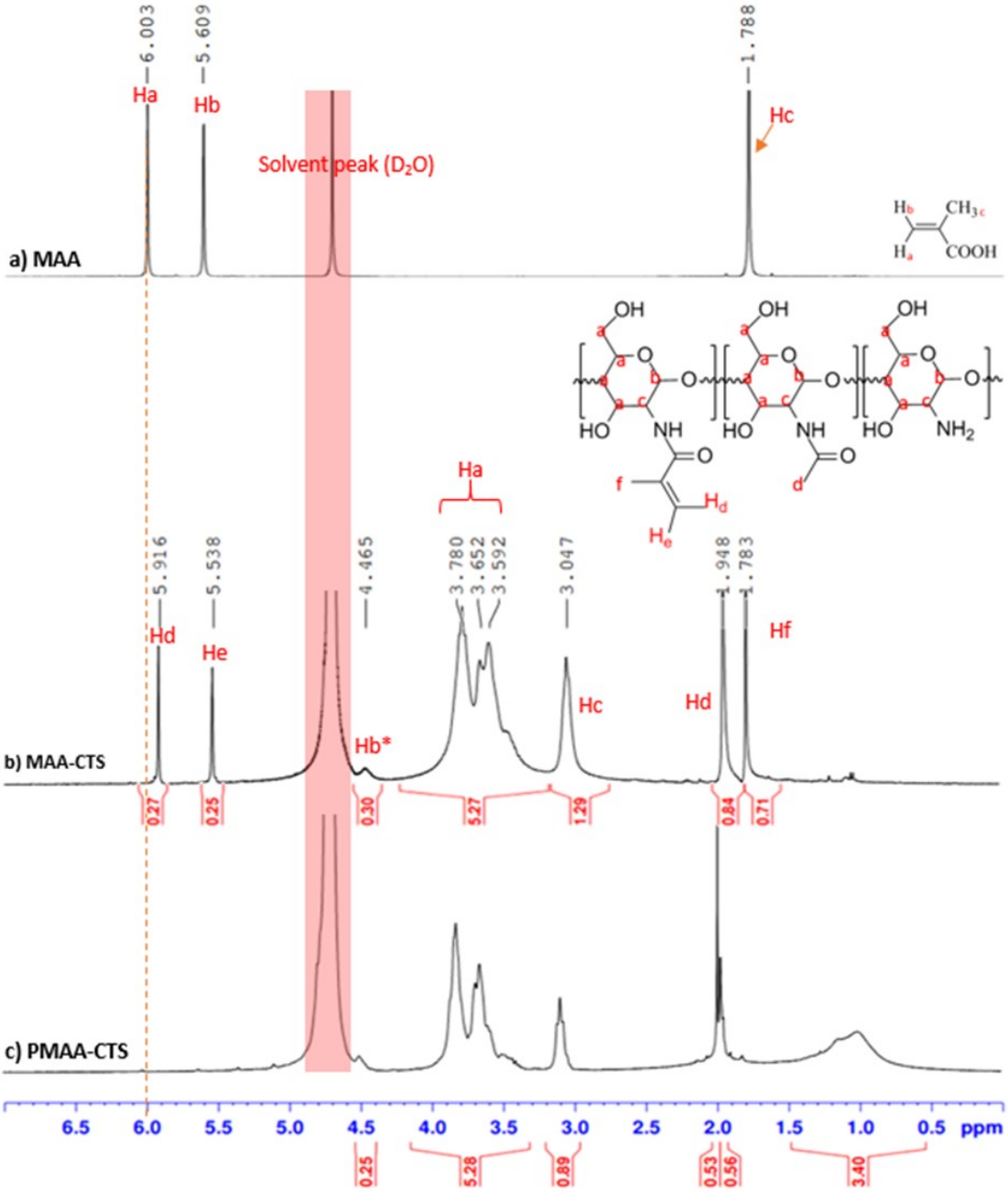


Figure 4.5 **^{1}H-NMR spectra in 2 wt%-d-Acetic acid in D_2O of MAA monomer, CTS, MAA-CTS and CTS-co-PMAA (*H1 peak is overlapped by solvent peak in the CTS spectra**

Figure 4.6 shows FTIR spectra of the chitosan, MAA modified chitosan (MAA-CTS) and CTS-co-PMAA. Comparing to the chitosan spectrum, the MAA-CTS

spectrum shows all characteristic bands of the chitosan (OH stretching at 3256 cm^{-1}, amide stretching band and saccharide structure at 1552 cm^{-1} and C-O stretching at 1068 and 1019 cm^{-1}) together with increasing peak intensity in the carbonyl stretching band of amide at about 1647 cm^{-1} and C-N stretching band at 1065 cm^{-1}. Furthermore, a small peak at 2133 cm^{-1} corresponding to the C=C stretching is also detected. The FTIR spectrum of the MAA-CTS confirms the proposed intermediate product. The spectrum of the CTS-co-PMAA shows typical peaks of carboxylic acid group (a very broad O-H stretching band between 3600 and 2500 cm^{-1}, C=O stretching at about 1698 cm^{-1}, C-O stretching at 1968 cm^{-1}), Two strong absorption bands at 1698 and 1627 cm^{-1} are assigned to carbonyl group of carboxylic acid and amide, respectively. The intensity of C-N stretching peak at 1152 cm^{-1} has increased, indicating the formation of increasing C-N bonding. Furthermore, intensity of the C=O stretching of the amide group at 1627 cm^{-1} was also enhanced, suggesting the increase of amide formation.

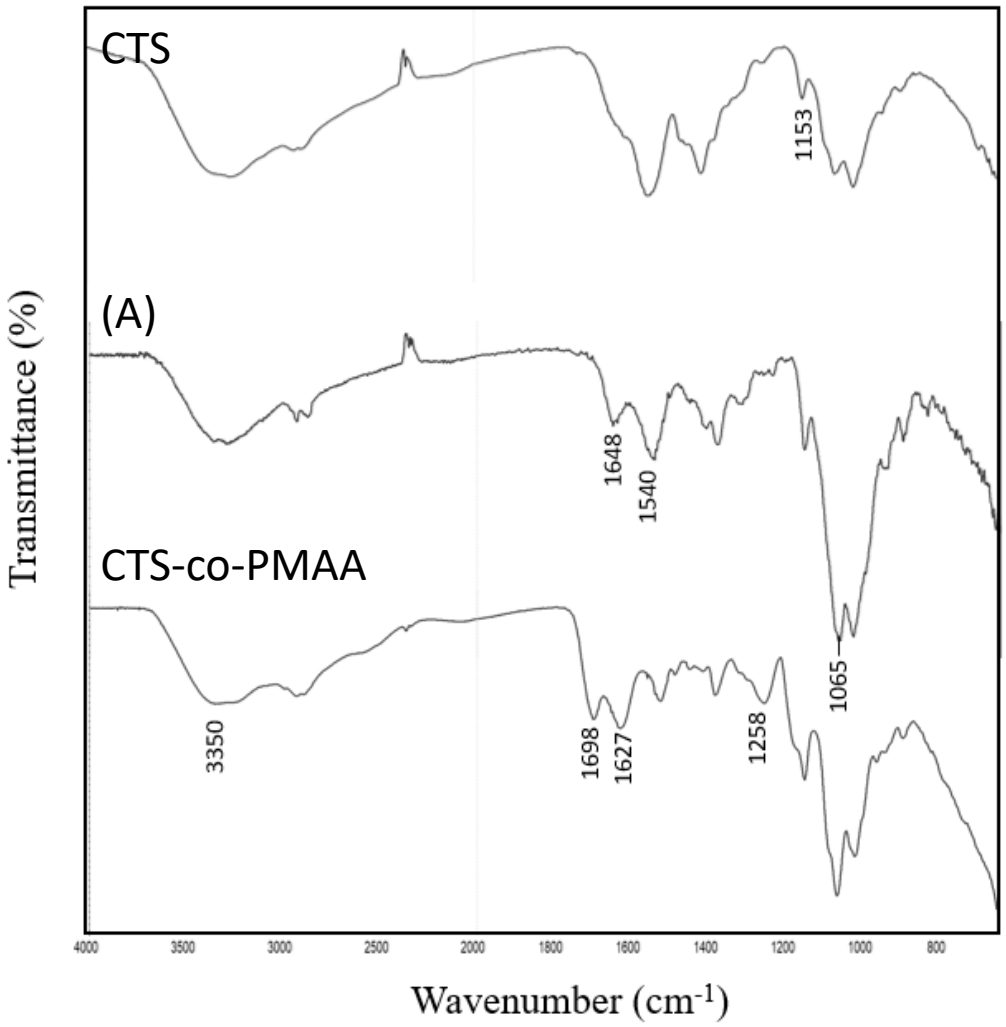


Figure 4.6 **FTIR spectra of chitosan, MAA modified chitosan and CTS-co-PMAA (synthesized with 1:1 w/w).**

4.2.1.1 zeta-potential

The *zeta*-potential as a function of pH of the CTS-co-PMAA (PMAA:CTS = 1:1 w/w) is shown in Figure 4.7. At acidic pHs, the polymer has a positive surface charge around 40 mV. It decreases rapidly at pH 4 which coincides with the pKa value of

carboxylic acids on PMAA moiety. The isoelectric point (IEP) of the resultant polymer was around pH 5.6. The CTS-co-PMAA reached maximum negative surface charge (-35 mV) around pH 8.

The *zeta*-potential as a function of pH of the CTS-co-PMAA (PMAA:CTS = 1:2 w/w) shown in Figure 4.7 indicates that the isoelectric point was at pH 7.05. The maximum positive surface charge was around +40 mV and maximum negative charge was around -10 mV. Higher chitosan content requires more negative charges to neutralize the amino groups, however, PMAA content in the copolymer is lower. Thus, the IEP is at a higher pH compared to PMAA:CTS = 1:1

The zeta-potential as a function of pH of the CTS-co-PMAA (PMAA:CTS = 2:1 w/w) shown in Figure 4.7 indicates that the isoelectric point was at pH 7.7. The maximum positive surface charge was around +40 mV and maximum negative charge was around -30 mV. The IEP is close to the IEP of CTS-co-PMAA (2:1) even though the ratios between the PMAA and CTS moiety is not the same. It has been reported that pKa of CTS is affected by solubility and hydrogen bonding.[194] Therefore, the high IEP may be due to the high PMAA content which increases solubility of the CTS. As a result, the pKa of CTS moiety in the copolymer shift to higher pH.

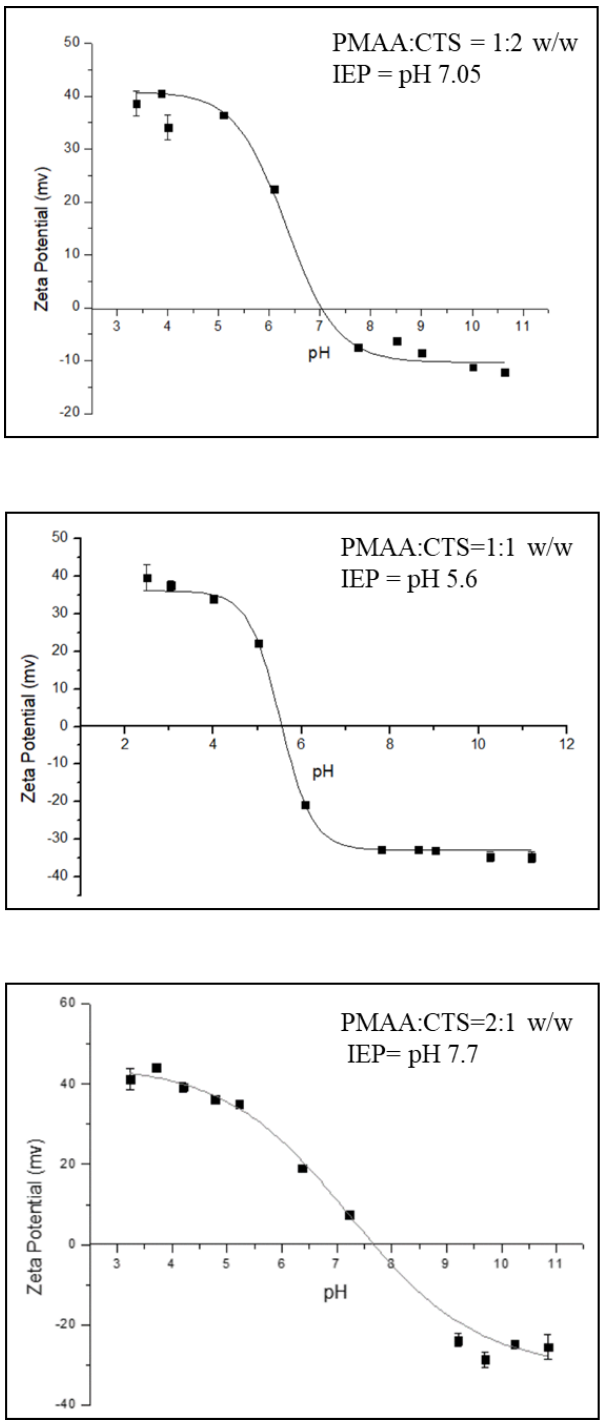


Figure 4.7 ***zeta*-Potential curves of CTS-co-PMAA (PMAA:CTS=1:2 w/w), CTS-co-PMAA (PMAA:CTS=1:1 w/w) and CTS-co-PMAA (PMAA:CTS=2:1 w/w)**

4.2.1.2 Morphology

Figure 4.8 shows sample of CTS-co-PMAA copolymer (PMAA:CTS = 1:1 w/w) which was freeze dried and imaged with SEM. The SEM images show that the CTS-co-PMAA copolymer exists as fibers in solution with diameter distribution ranging from 115 to 300 nm after freeze-drying.

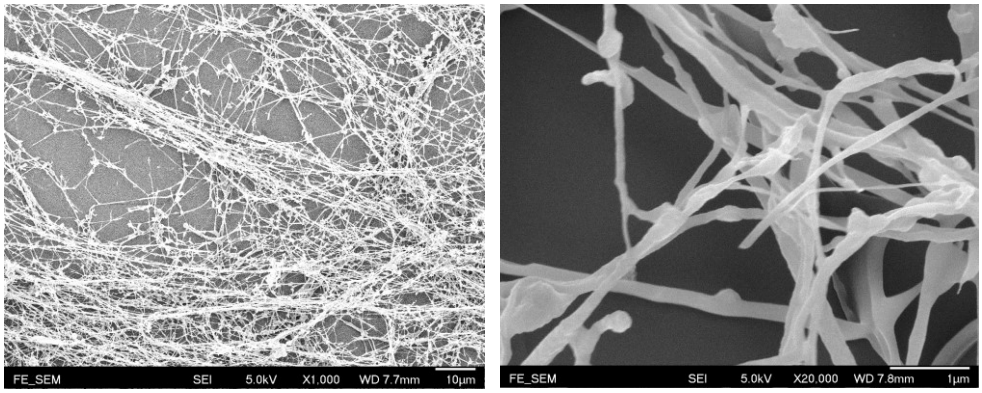


Figure 4.8 **SEM image of CTS-co-PMAA (1:1) (Freeze dried) a) X1000; b) X20,000 magnification**

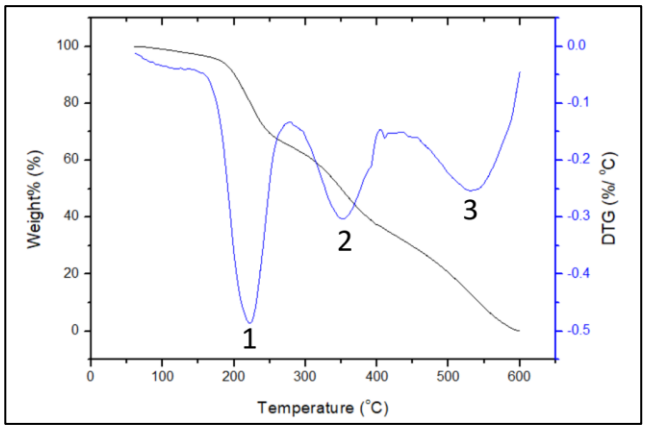
4.2.1.3 Thermal stability

Figure 4.9 shows the thermogravimetric (TGA) curve of CTS-co-PMAA (PMAA:CTS=1:1 w/w). Since the degradation peaks are broad and tend to overlap, the %weight loss is calculated based on peak area of differentiated thermogravimetric (DTG) graph through peak fitting.

The degradation peak at 218 ^{o}C is attributed to degradation of CTS units.(Figure 4.9**).** Figure 4.10 shows the TGA and DTG curve of CTS prior to modification which has a higher degradation peak at 293 ^{o}C. This could indicate that the CTS was successful

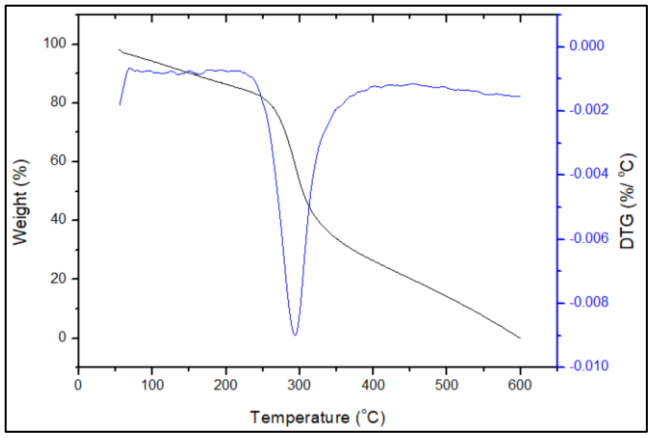
grafted with PMAA. Also, part of this peak could be attributed to loss of water from the formation of anhydride between carboxylic acid groups in the repeating units of PMAA.[195] The final degradation peak at 532 °C is attributed to the PMAA homopolymer, which coincides with Schild's data[196]. Therefore, the degradation peak occurs at 350 ℃ could be the degradation of the graft copolymer CTS-co-PMAA.

In conclusion, the degradation profile of CTS-co-PMAA shows the presence of grafted copolymer with a thermal degradation onset of 157 °C. From the DTG graph, we estimate that the CTS-co-PMAA graft copolymer is around 27 wt%.



Peak	Weight loss (%)	Degradation temperature (℃)		
		Onset	Peak	Endset
1	32%	157	218	268
2	27%	268	350	393
3	35%	393	532	593

Figure 4.9 **TGA curve of CTS-co-PMAA (1:1)**



Peak	Weight loss (%)	Degradation temperature (℃)		
		Onset	Peak	Endset
1	100%	220	293	415

Figure 4.10 **TGA curve of CTS prior to PMAA modification**

4.2.2 Optimization of encapsulation of hexadecane through coacervation using CTS-co-PMAA as shell material

4.2.2.1 Stabilization and encapsulation abilities of the CTS-co-PMAA

The emulsifying property of the CTS-co-PMAA was evaluated with a surface tension study. Figure 4.11 shows that the surface tension of water at room temperature is 72 mN/cm. Addition of various surfactants such as T80, CTAB and SDS reduces surface tension by -20 mN/cm. This is achieved by the surfactant's orientation at the water/air interface (see Figure 4.12), where the hydrophobic part orienting towards the air and the

hydrophilic part orienting towards the water. However, surface tension of the CTS-co-PMAA solution shows a reduced surface tension of -6 mN/cm. Furthermore, hexadecane emulsions cannot be formed readily with CTS-co-PMAA through methods of mixing. Therefore, CTS-co-PMAA does not possess hydrophobic and hydrophilic regions at room temperature and cannot act as a surfactant.

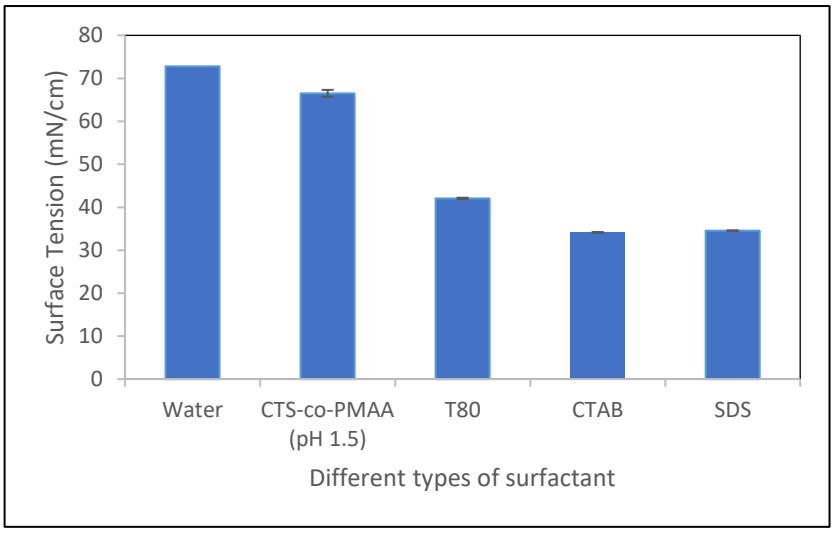


Figure 4.11 **Surface tension of CTS-co-PMAA (pH 1.5) compared to conventional surfactants**

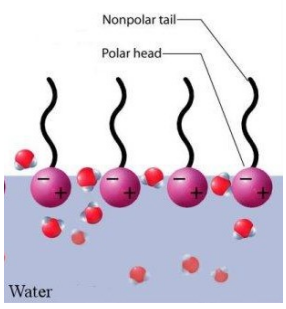


Figure 4.12 **Surfactant molecules oriented at the air-water interface**

However, when the hexadecane was dispersed in the CTS-co-PMAA polymer solution under sonication, highly stable emulsion was formed. There was no phase separation even after storage for a year, asides from creaming which could be easily re-dispersed through agitation. It was also found that decreasing the temperature below T_f of the PCM showed no precipitation of solid PCMs or phase separation. The emulsion was still very stable upon increase of temperatures back above T_m. These phenomena indicate that CTS-co-PMAA is able to stabilize the PCM droplets in water.

The CTS-co-PMAA was a clear solution at room temperature (see Figure 4.13), but became cloudy with increasing solution temperature up to 70ºC. Figure 4.14 shows the turbidity measurements of the CTS-co-PMAA as a function of temperature. There si a sharp phase change ~72 ºC indicating hydrophobic phase transition.

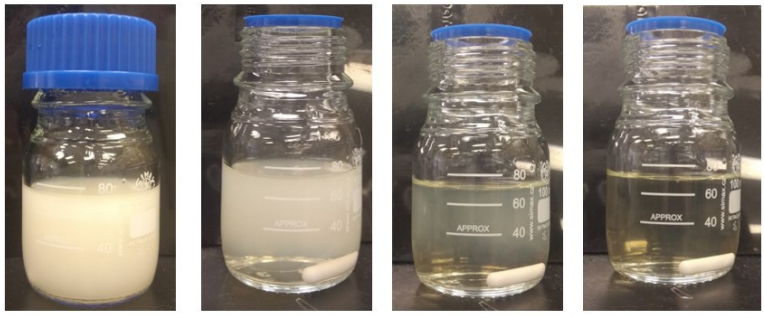


Figure 4.13 **CTS-co-PMAA (1:1) at 80ºC (left) cooled to room temperature (right)**

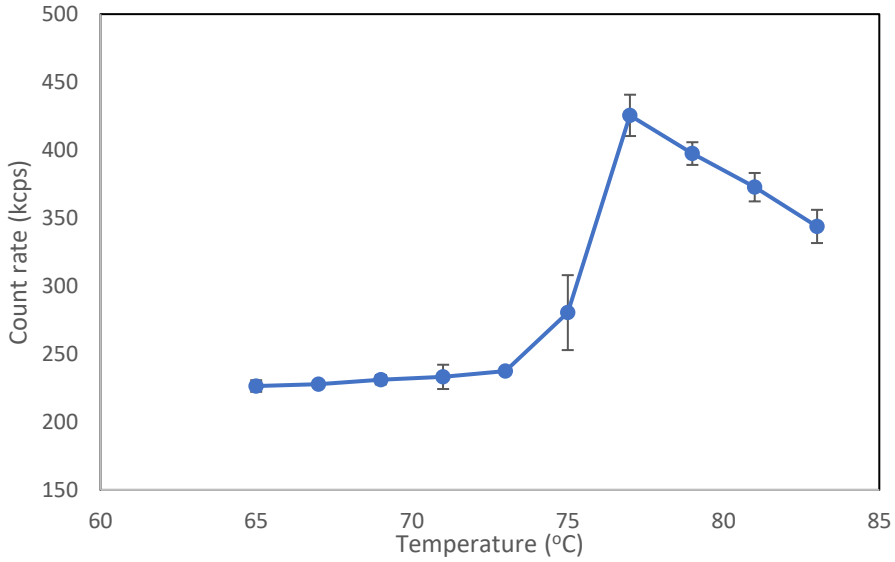


Figure 4.14 Turbidity of CTS-co-PMAA vs temperature, measured with 633 nm laser at 173°

We theorize that during formation of the emulsion, sonication process generates high localized temperatures in the solution, resulting in weakening of the hydrogen bonds between CTS-co-PMAA and water. Thus, intra or interpolymer hydrogen bonding between carboxylic acid groups and amide groups of the CTS-co-PMAA may be established (Figure 4.15). The increased hydrophobicity of the CTS-co-PMAA is capable of emulsifying the oil droplets in water. Based on these results, we propose the structure of CTS-co-PMAA on the emulsified PCM droplet as shown in Figure 4.16. The hydrophobic part of the CTS-co-PMAA dissolves in the PCM droplets, while the hydrophilic part remains in water which leads to replacement of the o/w interface thus forming a stable emulsion.

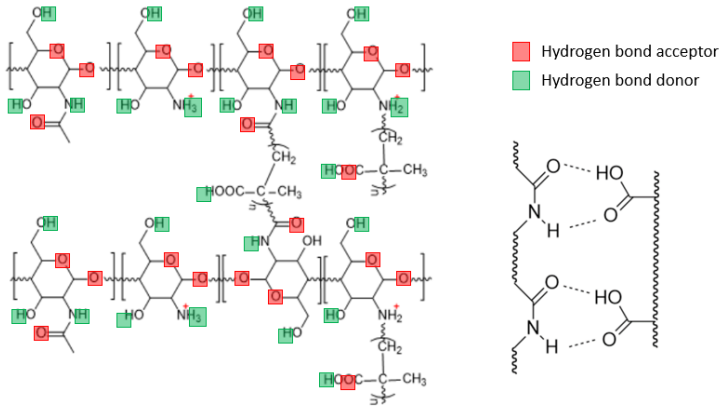


Figure 4.15 **Hydrogen bonding between PMAA and CTS moiety in CTS-co-PMAA**

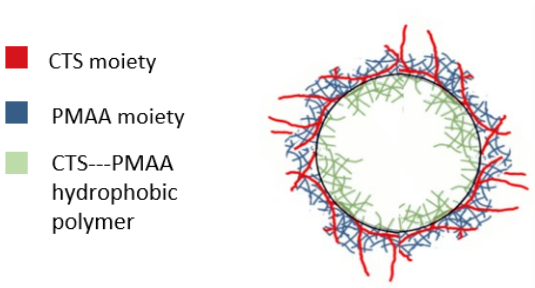


Figure 4.16 **Structure of CTS-co-PMAA stabilized emulsion droplet**

4.2.2.2 Effect of different PMAA:CTS ratios in CTS-co-PMAA

Phase change performance

Thermal properties of the MEPCMs dispersed in water synthesized with different PMAA:CTS ratios are summarized in Table 4.7. The results show that encapsulation efficiency of PCM (%ee) is the highest for PMAA:CTS =1:1 (61%) compared to PMAA:CTS=2:1 and PMAA:CTS=1:2.

Table 4.7 **DSC summary of aqueous CTS-CO-PMAA /C16 coacervates synthesized various PMAA:CTS ratios**

Sample	Freezing curve				ΔT_f (°C)	Heating curve				%ee
	LH_f (J/g)	T_{fo} (°C)	T_{fp} (°C)	T_{fe} (°C)		LH_m (J/g)	T_{mo} (°C)	T_{mp} (°C)	T_{me} (°C)	
CTS-CO-PMAA (2:1) /C16	1.64 8.08	10.0 2.9	7.0 1.7	4.5 0	5.8 7.4	- 11.7	17.4	18.7	20	39%
CTS-CO-PMAA (1:1) /C16	1.16 7.36	10.3 2.6	7.2 1.2	5.0 -0.9	5.5 13.2	- 9.93	16.5	18.7	20.0	61%
CTS-CO-PMAA (1:2) /C16	8.05	2.7	1.5	-0.3	13.1	- 9.00	16.8	18.3	19.5	48%

The three MEPCMs synthesized were also assessed for their encapsulation efficiency after multiple phase change cycles. The samples were subjected to 100 phase change cycles. For all three samples, the loss of encapsulation efficiency was <1% after 100 phase change cycles. At the same time, the structure of the freezing peak remained the same which means that the MEPCM structure remains unchanged after 100 phase change cycles.

After drying the CTS-co-PMAA encapsulated PCM under air at room temperature, it was found that the freezing peak shifted from < 10°C to 16°C as shown in Figure 4.17. This left shift of the freezing peak to the freezing temperature (T_f) of bulk C16 means that the PCM is no longer encapsulated and has leaked out during the freeze-drying process.

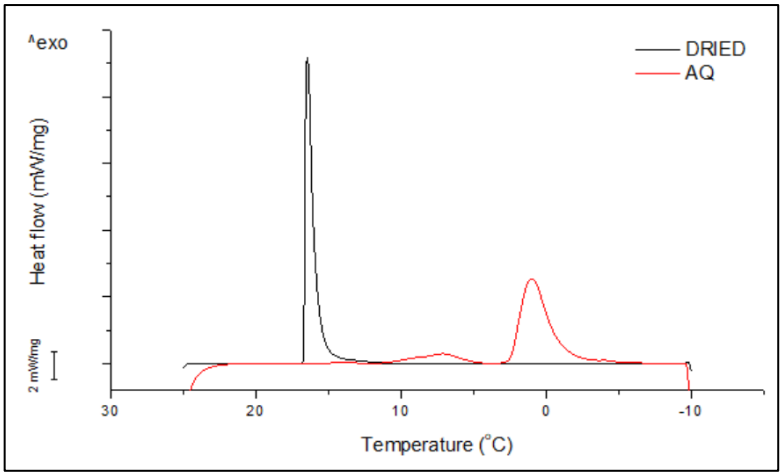


Figure 4.17 **DSC of aqueous CTS-co-PMAA/C16 coacervates (PMAA:CTS ratio = 1:1) before and after drying**

To conclude, the CTS-co-PMAA copolymer (PMAA:CTS = 1:1 wt ratio) has the highest %ee and is selected for further study. However, further studies are needed to increase both the %ee and rigidity of shell in order to prevent collapse of MEPCM upon drying.

4.2.2.3 Determination of the pH for highest solvation of CTS-co-PMAA

In the previous section, the highest measured %ee of of the MEPCM was 61% which still needs to be improved. The %ee may be increased by optimizing the coacervation technique. Since the encapsulation via coacervation involves the gradual dissolution of a polymer from the solution which is the driving force for its shell formation around the hydrophobic cores, it is important to ensure that the polymer is completely dissolved in the medium prior to coacervation process.

Since the CTS-co-PMAA containing both amine and carboxylic acid groups, their degree of protonation is significantly affected by the solution pH. When electrostatic interaction between amine and COO- groups, complexed nanoparticles may form with increasing solution turbidity. Therefore, turbidity changes of CTS-co-PMAA copolymer at different solution pH were monitored to determine the lowest turbidity, which means the highest polymer solvation.

Figure 4.18 shows the turbidity measurements of the CTS-co-PMAA at different pHs with both absorbance (abs) and scattered light intensity (cps). There are no significant changes in turbidity below pH 3.5. Turbidity increased markedly from pH 3.5, indicating the deprotonation of COOH groups to form complexed particles.

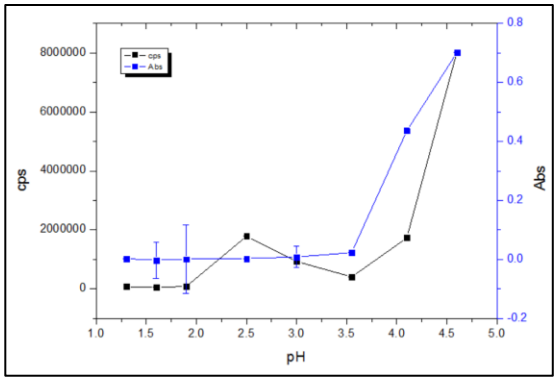


Figure 4.18 **Turbidity of CTS-co-PMAA as a function of pH.**
Blue: Absorbance intensity (abs) at 690 nm; and Black: Relative scattered light intensity (cps) at 90º with laser at 690 nm

Figure 4.19 shows the appearance of the CTS-co-PMAA solution from pH 1.3 to 7.5. The CTS-co-PMAA solutions at pHs between 1.3-2.0 have the highest solvation because they are clear solutions. The solutions show obviously turbidity at pH 4.1 and 4.6. When the pHs are higher than 5.0, the copolymer forms precipitates and settle down.

Therefore, CTS-co-PMAA solution with pH in the range of 1.3 to 2.0 were used to form the MEPAM via the coacervation approach.

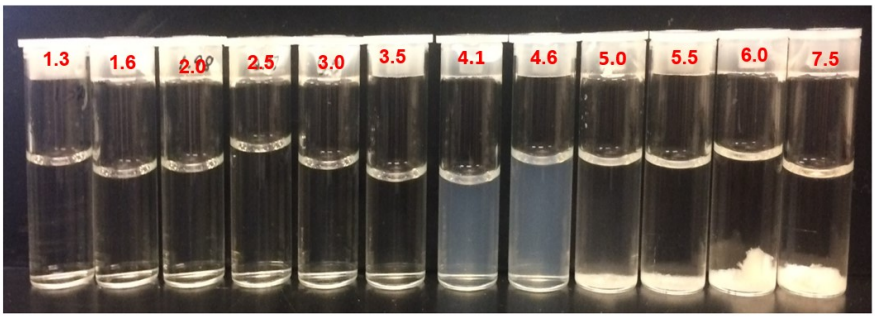


Figure 4.19 **CTS-CO-PMAA (0.5 wt%) at various pHs (From left to right: 1.3, 1.6, 1.9, 2.5, 3.0, 3.5, 4.1, 4.6, 5.0, 5.5, 6.0, 7.5)**

4.2.2.4 Determination of optimal titration profiles

The coating of CTS-co-PMAA into a continuous shell around the PCM droplets is driven by gradually decreasing solubility of CTS-co-PMAA polymer through the increase of pH. The increase of pH decreases the polymers' solubility due to the following two reasons : 1) increased electrostatic interaction between the PMAA and CTS moieties via formation of complexes which is maximized at the pH 5.6 (IEP); or 2) increased hydrophobic interaction of the CTS moiety which is maximized at pH 10. In order to optimize titration profiles for higher %ee, MEPCMs were synthesized using different titration profiles and evaluated based on their phase change performance and morphology. The titration profiles selected were

1) XCTS (pH 5.6): pH from initial 1.5 to 5.6;

2) XCTS (pH 10): pH from initial 1.5 to 10 directly;

3) XCTS (10→5.6): pH from initial 1.5 to 10, followed by back titration from pH 10 to pH 5.6.

4.2.2.4.1 Phase change performance

The phase change performance results are summarized in the Table 4.8**.** XCTS (pH 5.6) and XCTS (10→5.6) have the highest %ee at 67% and 66% respectively. The samples were subjected to multiple phase change cycles according to procedure in Section 4.1.4.1. All samples showed no decrease in percentage encapsulation after 100 cycles of freezing and melting. These results show that the CTS-co-PMAA polymer shell can prevent the C16 core from leakage or coalescence during multiple melting/freezing cycles. %PCM in MEPCMs was not evaluated, as all dried MEPCM samples had product yield <40%.

Table 4.8 **Effect on end titration pH of coacervates on encapsulation percentage before and after 100 phase change cycles**

Code	Percentage encapsulation of HD (%)	Drop in %ee after 100 phase change cycles
XCTS (pH 10)	60	0%
XCTS (pH 5.6)	67	0%
XCTS (10→5.6)	66	0% (HF50)

Figure 4.20 shows the thermal profile of the MEPCMs after multiple phase change (HF) cycles. MEPCM (XCTS pH 5.6) and MEPCM (XCTS pH 10) showed very little change even up to 100 HF cycles. However, for sample XCTS (10→5.6), the PCM cores merge together over HF cycles to form larger confinements of PCM as exhibited by the growth of freezing peaks at higher freezing temperatures at the expense of reduced area of freezing peaks at lower freezing temperatures. This indicates that back titration of the MEPCMs from pH 10 to pH 5.6 may cause some of the CTS-co-PMAA shell to redissolve into the water leading incomplete encapsulation which is not strong enough to withstand the volume change of the PCM during phase change.

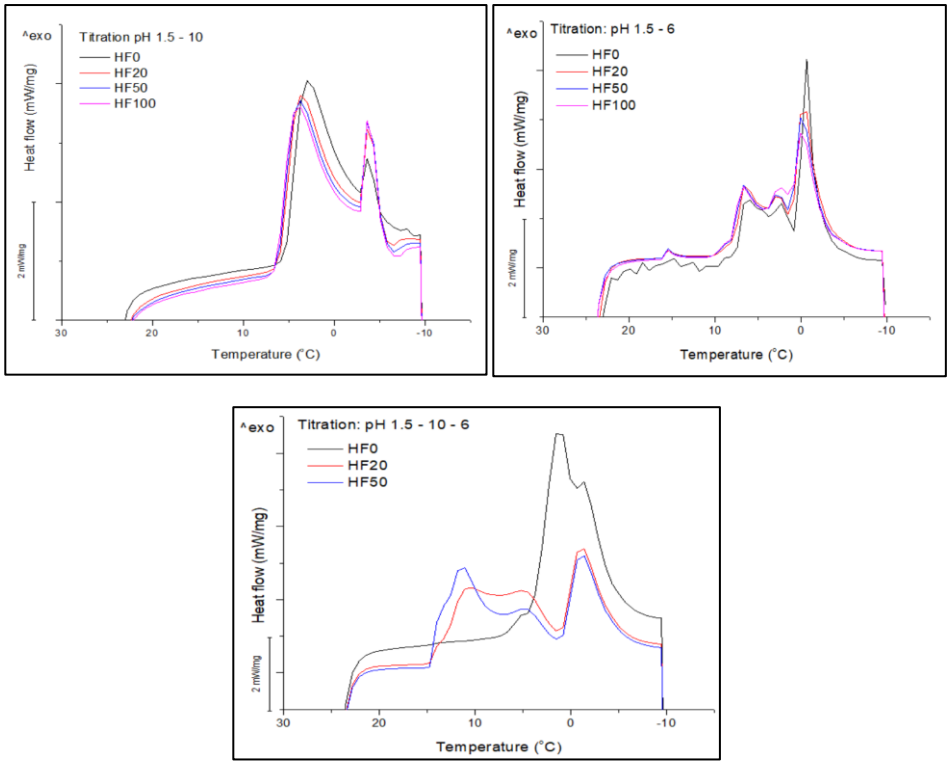


Figure 4.20 **DSC freezing profiles of CTS-co-PMAA/C16 coacervates synthesized with different titration profiles**

4.2.2.4.2 Morphology

Figure 4.21 shows optical images of the three MEPCMs: XCTS (pH 10), XCTS (pH 5.6), and XCTS (10→5.6). For XCTS (pH 10), the microcapsules were well-dispersed spherical particles with an average size of 1.99±0.35µm. XCTS (pH 5.6), and XCTS (10→5.6) microcapsules showed signs of aggregation (red circles) due to neutralization of the polymer charges. XCTS (10→5.6) shows smaller size compared to XCTS (pH 5.6) and XCTS (pH 10), possibly the back titration with acid causes some of the CTS-co-PMAA copolymer shell re-dissolve into water and detach from MEPCM.

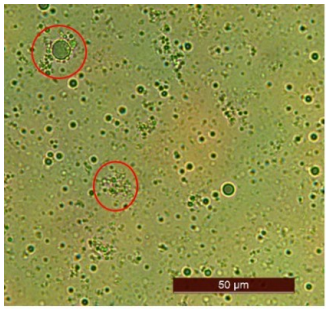
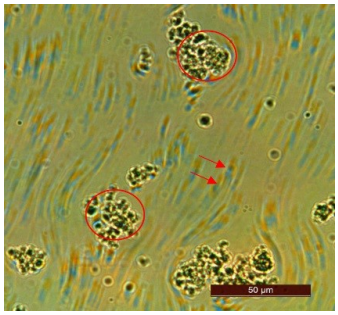
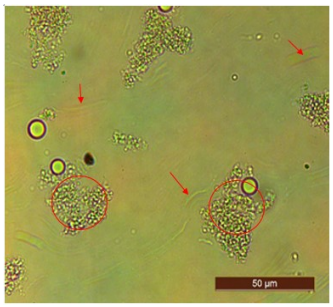
		
XCTS (pH 10)	XCTS **(pH 5.6)**	**XCTS (10→5.6)**
1.91 ±0.24 µm,	1.99 ±0.35 µm	1.10 ±0.30 µm,

Figure 4.21 **Morphologies and particle sizes of encapsulated HD particles (CTS-co-PMAA-C16) observed with an optical microscopy. (Red Circles): Aggregation has occurred. (Red Arrows): Relatively fast flowing non-aggregated particles that couldn't be captured.**

The size distribution of the MEPCMs synthesized with different titration profiles are shown in Table 4.9. The z-ave. for XCTS (pH 5.6) and XCTS (10→5.6) are higher than XCTS (pH 10) which may be attributed to the aggregation as shown in the optical images. The z-ave for XCTS (pH 10) is similar to the size distribution measured in the optical images (Figure 4.25).

Table 4.9 **z-Ave. of MEPCMs prepared with different titration profiles**

Sample code	pH during measurement	z.ave (µm)
XCTS (pH 10)	**pH 10**	**1.4 (PDI 0.39)**
XCTS (pH 5.6)	**pH 5.6**	**6.1 (PDI 0.32)**
XCTS (10→5.6)	**pH 5.6**	**2.8 (PDI 0.84)**

Morphologies of samples: 1) XCTS (pH 10); 2) XCTS (pH 5.6); 3) XCTS (10→5.6) have been examined with a scanning electron microscopy (Figure 4.22). SEM images reveal that during drying, the MEPCMs aggregate to form a network structure, causing rupture of the MEPCMs and releasing the hexadecane. SEM shows that XCTS (pH 10) has a broken bubble structure probably due to increased rigidity of the CTS shell at higher pH.

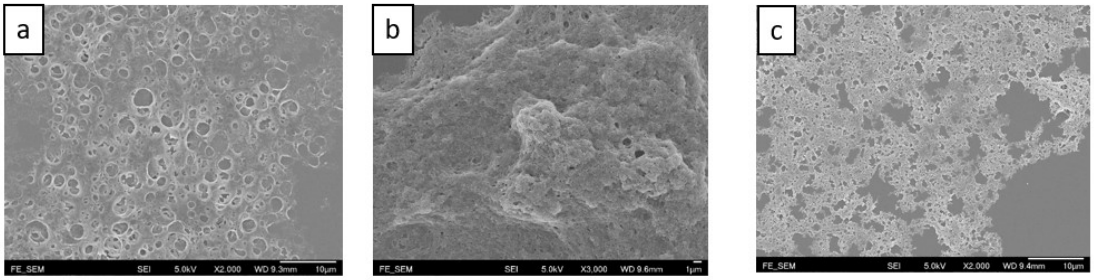


Figure 4.22 **SEM image of dried CTS-co-PMAA/C16 coacervates synthesized with different titration profiles: a) XCTS (pH 10); b XCTS (pH 5.6) and c) XCTS(10→5.6)**

In conclusion, MEPCMs were formed via the three titration profiles XCTS (10→5.6), XCTS (pH 5.6) and XCTS (pH 10). These approaches gave similar PCM encapsulation efficiency (60-67%). However, phase change cycling ability for XCTS (10→5.6) was poor and XCTS (pH 5.6) showed aggregation. Therefore, the optimal titration profile selected for further study is titration from pH 1.5 to 10.

4.2.2.5 Crosslinking with glutaraldehyde

4.2.2.5.1 Synthesis and morphology

Glutaraldehyde (GAL) was used as a crosslinking agent for CTS-co-PMAA copolymer to increase rigidity of the MEPCM shell, thus the integrity of the MEPCM structure can be preserved after drying. The reaction between CTS and GAL has been well established with numerous publications.[197-200] The amine group on CTS reacts with the aldehyde to form a Schiff base (imine group adjacent to an ethylene bond) or possibly a Michael addition.[181](Figure 4.23) Various amounts of GAL was added for crosslinking based on GAL:CTS mol ratios of 5:1, 10:1, 15:1 and 20:1. The sample code for the MEPCMs were 5X, 10X, 15X and 20X respectively. Excess or unreacted GAL was removed by dilution of the MEPCMs with DI H_2O.

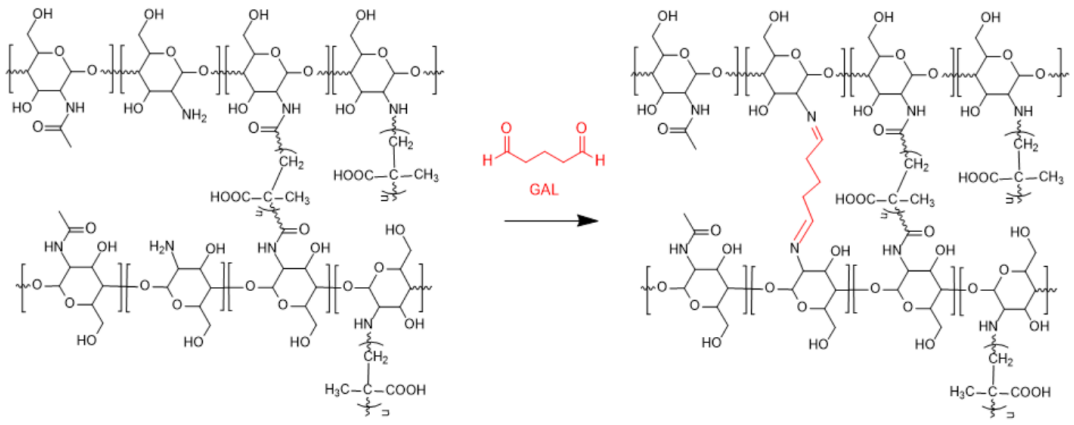


Figure 4.23 **Chemical reaction of GAL and CTS-co-PMAA**

Figure 4.24 shows FTIR spectra of C16, CTS-co-PMAA and dried CTS-co-PMAA/C16 microcapsules crosslinked with GAL. Characteristic C-H stretching peaks of C16 with high intensity (1464 cm^{-1}, 2852 cm^{-1} to 2956 cm^{-1}) are identified for the GAL-

crosslinked CTS-co-PMAA/C16 sample, indicating successful encapsulation of the PCM after drying. The crosslinking of chitosan with glutaraldehyde shows a new absorption at 1548 cm^{-1} due to imine bonds (C=N) formed between the amine residues of chitosan and the aldehyde terminals of the GAL. The FTIR spectra confirm that the microcapsules have been successfully crosslinked with GAL via the Schiff base. The presence of the hexadecane also indicates that the GAL crosslinking was able to increase strength of the CTS-co-PMAA shell to prevent MEPCMs from releasing C16 upon drying.

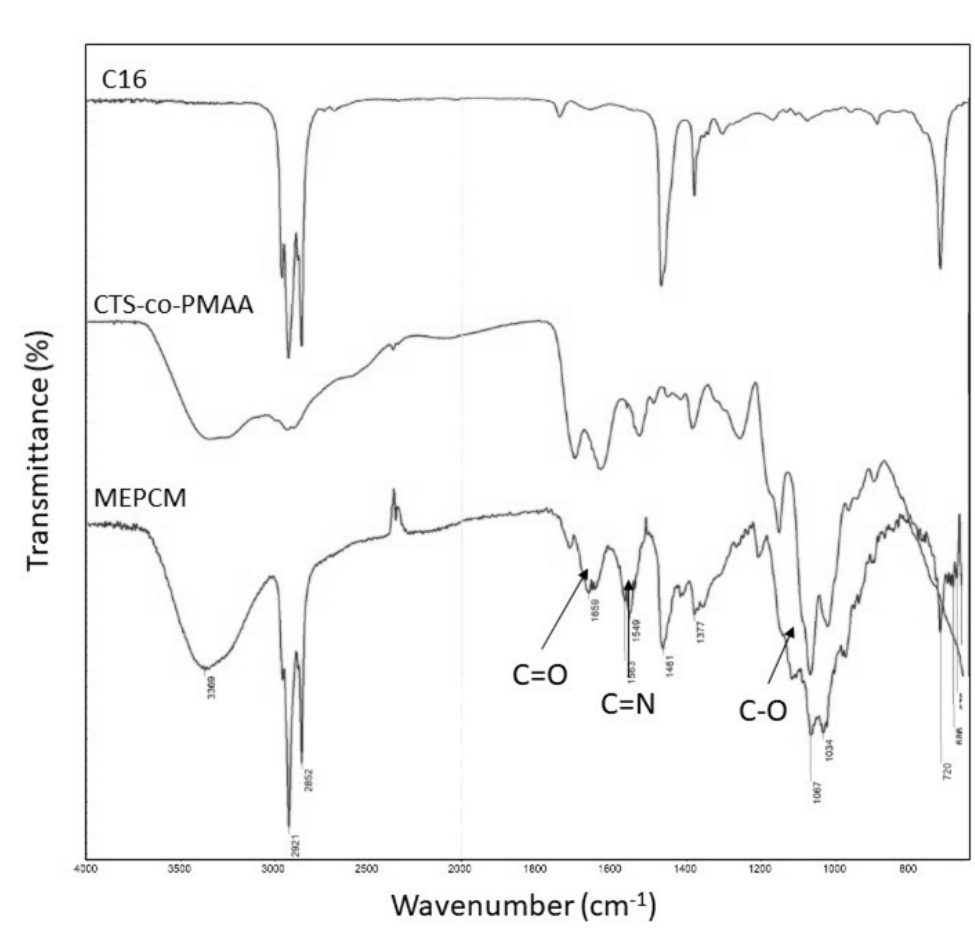


Figure 4.24 **FTIR spectra of C16, CTS-co-PMAA and dried CTS-co-PMAA/C16 microcapsules crosslinked with GAL**

Figure 4.25 shows SEM images of the MEPCMs synthesized with GAL crosslinking. Samples 5X and 10X are similar in morphology, capsule-like structures are scattered in a network which is possibly polymerized glutaraldehyde. However, 15X and 20X shows formation of a porous film upon drying, which could also be polymerized glutaraldehyde. In all cases, GAL seems to be in excess.

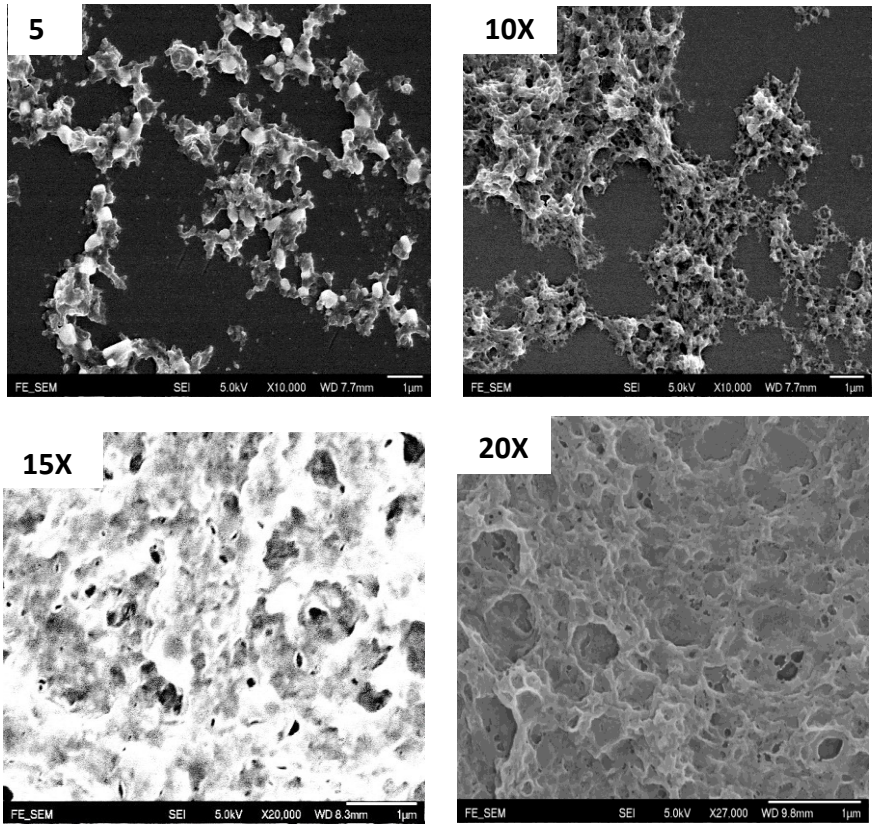


Figure 4.25 **SEM image of CTS-co-PMAA/C16 GAL:CTS ratio a) 5:1 (5X) b) 10:1 (10X) c) 15:1 (15X) and d) 20:1 (20X) (clockwise from top left)**

Phase change performance

Thermal profile of the MEPCMs was evaluated and summarized in Table 4.10. The DSC curves are shown in the Figure 30. All samples have varying degrees of PCM leakage upon drying as exhibited by the sharp peak around 16℃. However, compared to previous samples without GAL crosslinking which shows complete PCM leakage, this is a significant improvement. The %ee is highest for samples 5X and 10X. Therefore, GAL concentration of monomeric ratio of 5 GAL to 1 CTS unit is sufficient for crosslinking.

Therefore, GAL crosslinking of the CTS-co-PMAA with GAL:CTS = 5:1 successfully increases the rigidity of the microcapsules, which allows drying of the coacervates. The %ee of dried MEPCMs was 77%. However, %ee of the dried MEPCMs is similar to MEPCMs dispersed in water prior to the crosslinking. This indicates that crosslinking does not improve PCM encapsulation efficiency.

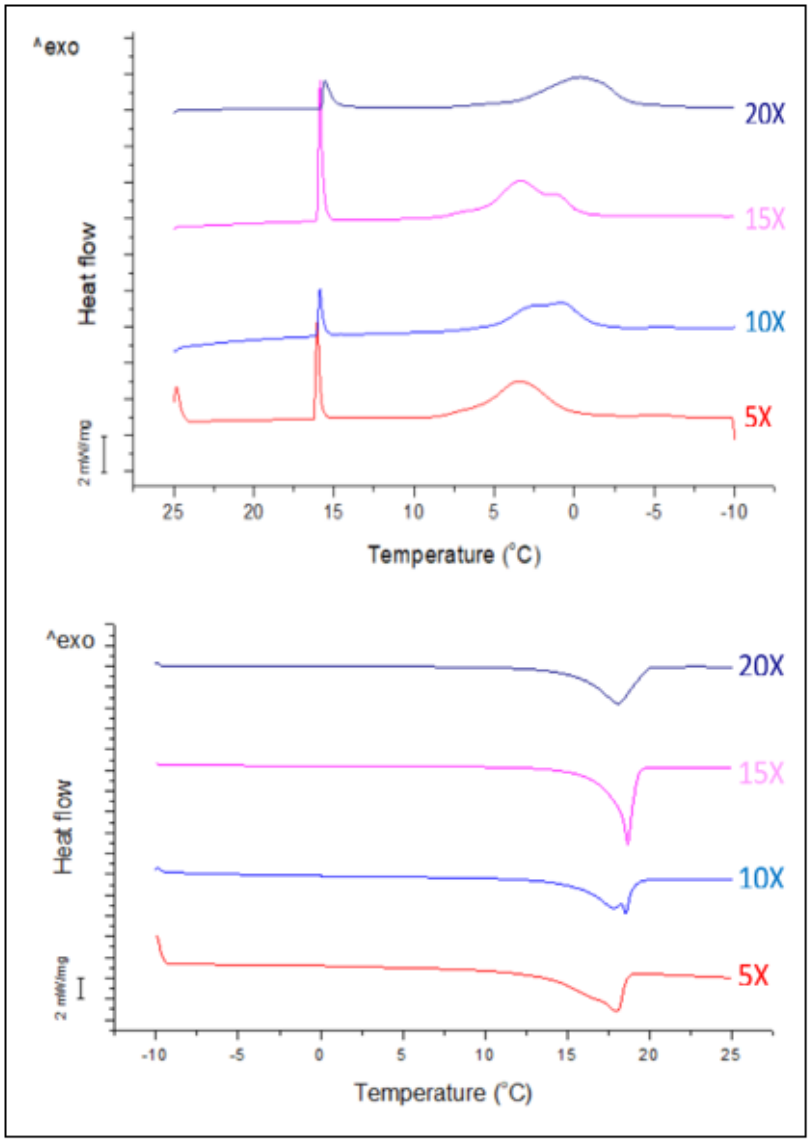


Figure 4.26 **DSC curves (TOP: cooling) and (BOTTOM: heating) of CTS-co-PMAA-C16-GAL coacervates crosslinked with various amounts of GAL**

Table 4.10 **Summary of DSC data for CTS-co-PMAA C16 pH10 GAL crosslinked coacervates (LH_m for some samples is N/A as the peak for leaked PCM overlaps with the encapsulated PCM)**

Sample	Freezing				ΔT_f[1] (°C)	Melting				%ee[3]	%PCM
	LH_f (J/g)	T_{fo} (°C)	T_{fp} (°C)	T_{fe} (°C)		LH_m [2] (J/g)	T_{mo} (°C)	T_{mp} (°C)	T_{me} (°C)		
5X	94.4	6.48	3.50	0.17	14.8	N/A	27.06	18.37	19.0	74%	38%
10X	94.3	5.16	0.83	-1.23	17.6	N/A	15.7	18.47	19.1	77%	38%
15X	129.4	5.91	3.38	0.13	15.1	N/A	17.4	18.45	19.3	57%	52%
20X	131.9	4.21	-0.27	-3.58	18.3	N/A	15.5	17.99	19.8	55%	53%

[1]Freezing temperature depression calculated from difference between and T_{mp}

[2]Latent heat of melting is not available because free PCM peak overlaps with encapsulated PCM.

[3]Dried sample

4.2.2.6 Incorporating nucleating agents into PCM cores

4.2.2.6.1 Synthesis and morphology

The previous results of phase changes in MEPAM show supercooling problem. Depression of the freezing temperature of PCM means lower temperatures are required to re-solidify the PCM and this requires higher cooling power. Therefore, MEPCMs with freezing temperature similar to the melting temperature of the PCM is more useful. To overcome supercooling, nucleating agents (NAs) to serve as nucleation sites for solidification have been investigated.

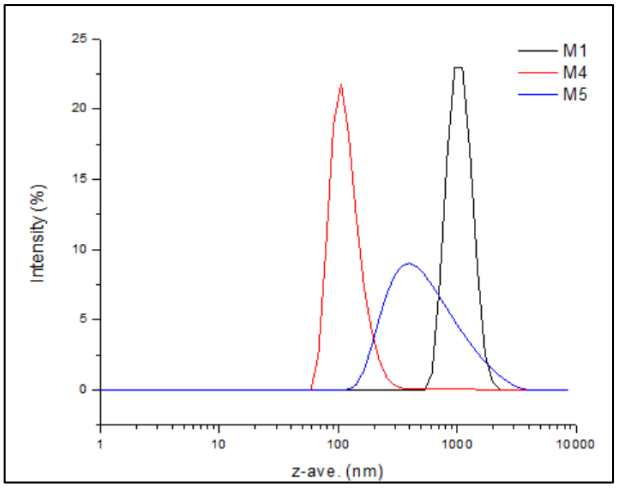
The incorporation of nucleating agents into MEPCM met with complications since the eicosane (Ei) is a solid at room temperature, and need to be melted before it could be mixed with the hexadecane (PCM). The Ei+PCM mixture was added to CTS-co-PMAA polymer solution which was also preheated to 60 ℃ followed by sonication to form an emulsion. During titration of the emulsion, Ei phase separated from the PCM. (Sample code: M1).

To prevent the eicosane from separating from the PCM during titration, the emulsion have been treated with the following three approaches: M2: Formed emulsion is immersed in an ice bath during titration (Sample code: M2) to solidify the Ei and PCM together; M3) Formed emulsion is immersed in a hot water bath of 40 ℃ (Sample code: M3) to maintain the molten state of Ei in the PCM. However, both M2 and M3 also exhibited phase

separation of Ei. For M2 and M3, it is likely that the agitation introduced during titration displaced the Ei from the PCM.

The next method, M4: The formed Ei+PCM emulsion was diluted to ten volume times, followed by placing in the refrigerator at 4℃ for 1 h (Sample code: M4) prior to titration. The last method used, M5, was the same as M4 only that GAL crosslinking was carried out at pH 7 for 1 followed by base titration to pH 10. M4 and M5 showed no phase separation during titration of the emulsion.

Figure 4.27 shows the size distribution of M1, M4 and M5. The M4 and M5 have smaller z-ave. compared to M1. This is due to the solidification of the PCM droplets prior to titration. This probably prevented PCM droplets from coalescing during titration. The higher z-ave of M5 is possibly due to increased GAL crosslinking efficacy at pH 7 compared to pH 10 leading to thicker MEPCM shells.



Sample	Dh **(nm)**
M1	1210 (PDI 0.3)
M4	113 (PDI 0.24)
M5	438 (PDI 0.25)

Figure 4.27 Size distribution (DLS) of the MEPCMs sample synthesized with method M1, M4 and M5. Figure 4.28 shows the SEM images of dried MEPCMs, M1, M4 and M5. Both samples of M1 and M4 show formation of a broken bubble structure. This is due to the deformation of the MEPCMs during evaporation of water, leading to coalescence of the MEPCMs and subsequent breakage of the shell releasing the core material.

M5 shows MEPCMs which are spherical with diameters 220 ± 82 nm, approximately half of the hydrodynamic diameter as measured by DLS. Although, the MEPCMs in sample M5 have aggregated and are closely adjacent to each other, however

are better able to maintain their spherical structure, signifying higher shell rigidity compared to samples M1 and M4.

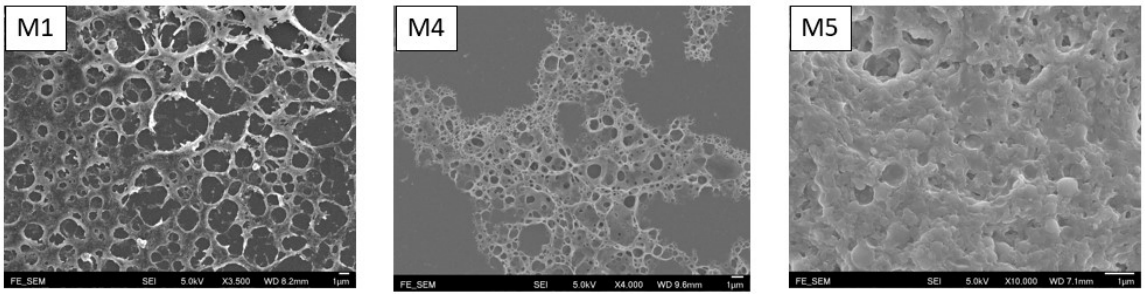


Figure 4.28 **SEM images of M1, M4 and M5**

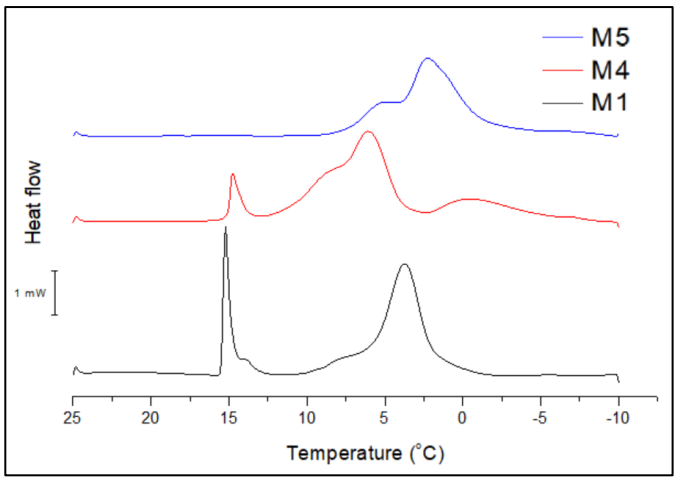
4.2.2.6.2 Phase change performance

The DSC results are summarized in Figure 4.29. DSC of M1 sample shows that majority of the sample had a freezing temperature peak of 2-3℃. This result suggests that the nucleating agent have not been encapsulated together with the PCM during coacervation. Samples prepared by M2 and M3 approaches showed significant phase separation during coacervation and thus was not evaluated with DSC.

DSC scan of sample prepared by M4 and M5 method shows decreased supercooling which means that the nucleating agent has been incorporated into the MEPCM. The T_{fo} (Onset temperature of freezing peak) is close to 11℃. But the freezing temperature range is very broad and most of the freezing peaks' area are located at 2-3℃. However, M5 has %ee of 94% compared to M4 which has only 55%ee. This suggests that the GAL crosslinking efficacy is increased at pH 7 and forms a complete crosslinked CTS-

co-PMAA shell around the PCM droplet which could be more impermeable to solvent extraction during the MEPCM purification.

To summarize, precipitation of nucleating agent during titration can be prevented through freezing the PCM at 4℃. GAL crosslinking at pH 7 increases the encapsulation efficiency up to 94%. Although the addition of the nucleating agent does reduce supercooling to T_{fo} around 10℃, the freezing temperature range is broad and majority of PCM still solidifies at 2-3℃.



Sample	Freezing					%ee[1]	%PCM in MEPCM (wt%)
	LH_f (J/g)	T_{fo} (°C)	T_{fp} (°C)	T_{fe} (°C)	ΔT_f (°C)		
M1	170.11	9.8	2.99	-0.32	-6.0	66%	68%
M2	N/A (phase separation during titration)						
M3							
M4	170.7	12.3	6.15	-9.9	-3.5	55%	69%
M5	140.2	10	2.3	-7.8	-5.8	94%	56%

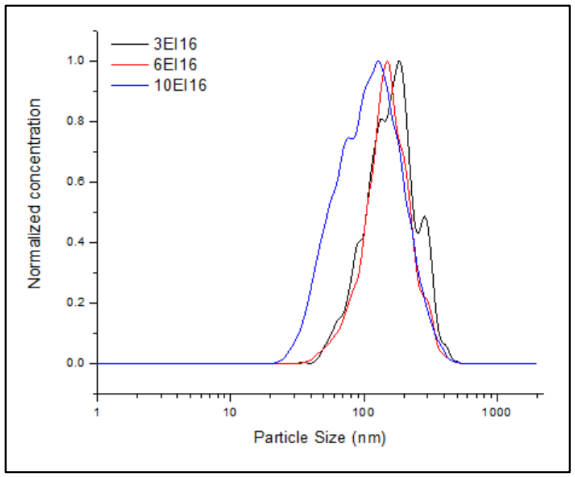
[1]dried sample

Figure 4.29 **Summary of DSC results for M1, M4 and M5**

4.2.2.7 Effect of increasing amounts of nucleating agents

4.2.2.7.1 Synthesis and morphology

MEPCMs with increased amount of eicosane in the PCM was synthesized in an effort to decrease supercooling. The eicosane in PCM synthesized was 3 wt%, 6 wt% and 10 wt% (Sample codes were 3EI16, 6EI16 and 10EI16). The size distributions of all three MEPCMs measured with Nanosight are shown in **Figure 4.30**. We observe that increased amount of nucleating agent decrease size of the MEPCMs in water.



Sample	Diameter (Mean ± Stdev)
3EI16	206 ± 80
6EI16	183 ± 70
10EI16	163 ± 80

Figure 4.30 **Size distribution of MEPCMs with different amounts of nucleating agent measured with the Nanosight**

SEM images of 3EI16, 6EI16 and 10EI16 are shown in Figure 4.31 to Figure 4.33. It shows that morphologies of the dried MEPCMs are spheres embedded in a network structure. The size of the MEPCMs, 3EI16, 6EI16 and 10EI16 are around 200-300 nm. The increased content of nucleating agent does not affect morphology of the MEPCM.

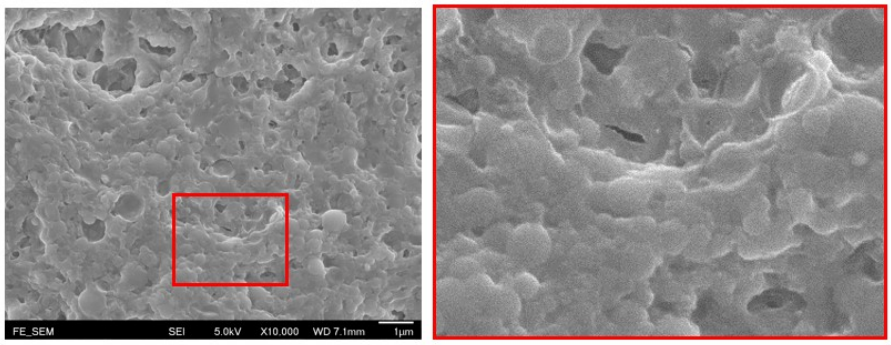


Figure 4.31 **SEM image of sample 3EI16 (Diameter: 220 ± 82 nm)**

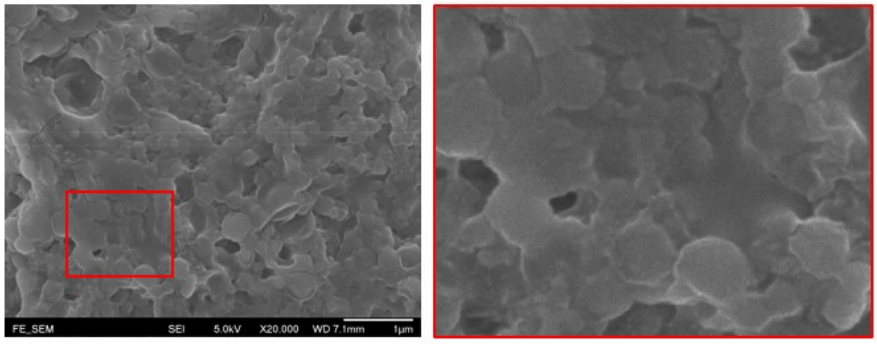


Figure 4.32 **SEM images of 6EI16 (Diameter: 254±109 nm)**

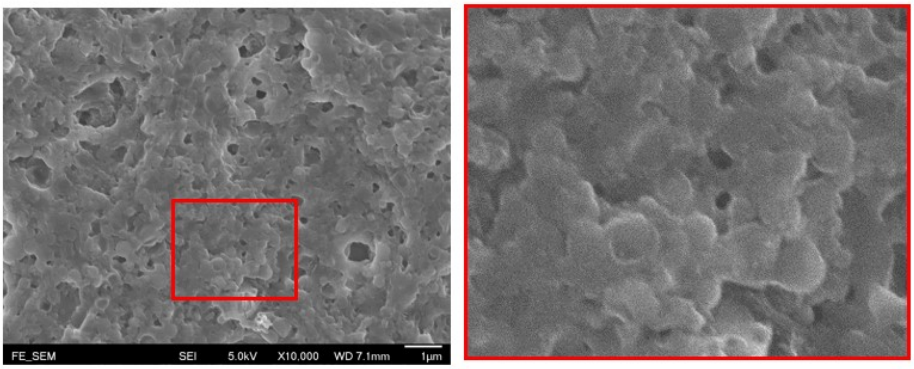
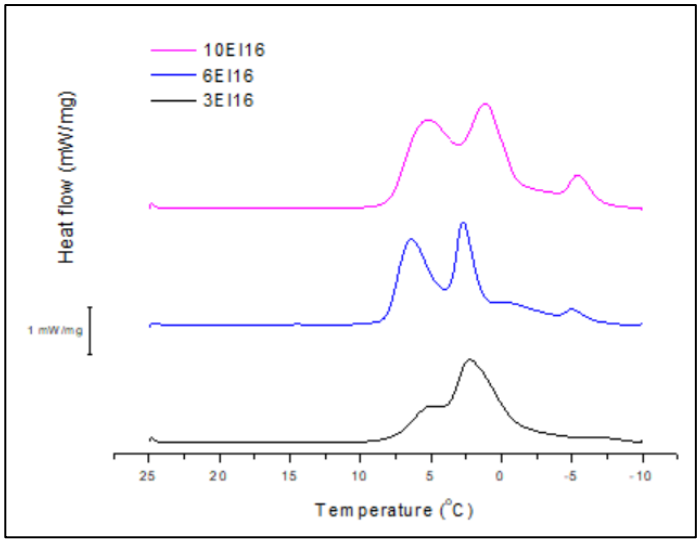


Figure 4.33 **SEM image of 10EI16 (Diameter: 243 ± 69 nm)**

4.2.2.7.2 Phase change performance

Summary of the DSC results can be found in Figure 4.34. PCM encapsulation efficiency (%ee) exceeded 90% for all samples. However, the MEPCMs had a freezing temperature onset (T_{fo}) ~ 9 ℃. The MEPCMs' freezing temperature depression (ΔT_f) compared to bulk PCM was depressed by~6-8 ℃. Further addition of nucleating agent to 10 wt% of PCM shows no significant increase of the T_{fo}. On the other hand, the freezing peaks for 6EI16 and 10EI16 show more PCM solidifies at higher temperatures compared to 3EI16. Increased addition of NA above 10wt% of PCM (10EI16) was not attempted, because 1) low concentrations of NA should be adequate to reduce supercooling [201-204]; 2) NA > 10 wt% of PCM would significantly decrease the MEPCMs thermal storage capacity as NA does not contribute to the latent heat.



Sample name	LH_s (J/g)	Freezing				%ee*	%PCM
		T_{fo} (°C)	T_{fp} (°C)	T_{fe} (°C)	ΔT_f (°C)		
C16	249.14	15.81	16.39	14.53	-	-	-
3EI16	140.2	8.3	2.3	-7.8	-7.5	94%	56%
6EI16	140	9.3	6.2	-8.7	-6.5	92%	56%
10EI16	165	9.4	5.4	-8.7	-6.4	94%	66%

*Dried sample

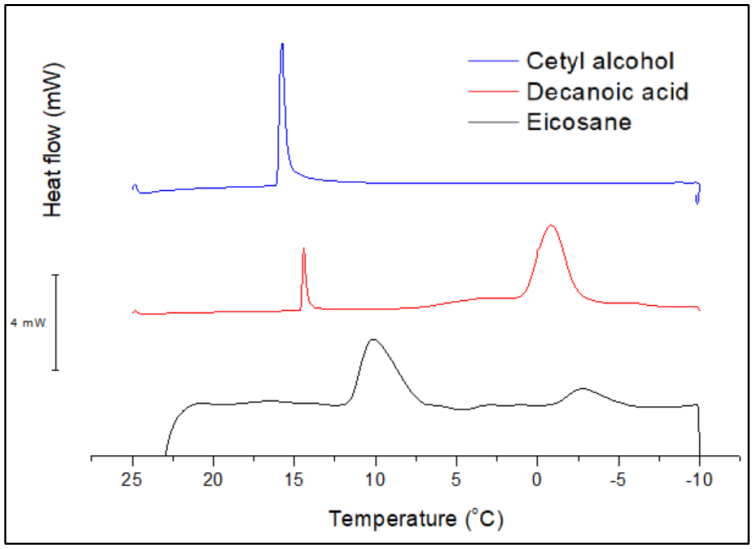
Figure 4.34 **DSC scan of MEPCMs synthesized with different amounts of nucleating agent**

4.2.2.8 Effect of different nucleating agents

Previous study used eicosane as the nucleating agent, which still had ΔT_f of -5℃ with freezing peak at 5℃. Different types of nucleating agent were used to examine if ΔT_f could be further reduced. Three MEPCMs were synthesized with cetyl alcohol (CA16), decanoic acid (DA16) and eicosane (EI16), followed by evaluation of their respective freezing profiles.

4.2.2.8.1 Phase change performance

DSC curves of XCTS/C16 coacervates with different nucleating agents are shown in Figure 4.35. MEPCMs synthesized with cetyl alcohol (CA16) as nucleating agent causes failure of GAL to crosslink which leads to PCM leaking upon drying, thus the freezing peak temperature is very close to bulk PCM. The PCM leakage could be observed by the presence of oil droplets in the sample CA16 after drying. The DSC curve with decanoic acid as nucleating agent (DA16) shows supercooling of -15℃ which indicates that either the decanoic acid does not solidify in the MEPCM to act as a nucleating agent or decanoic acid solidified but is not crystalline enough to act as a nucleating agent. Therefore, the only suitable nucleating agent is the eicosane which can increase the freezing temperature without affecting the properties of the coacervate.



Sample name	Nucleating agent used	Freezing			
		LH_f (J/g)	T_{fo} (°C)	T_{fp} (°C)	ΔT_f (°C)
Hexadecane (bulk)	-	15.81	16.39	14.53	0
XCTS RTF 10CA16	Cetyl alcohol	N/A (PCM has leaked)			
XCTS RTF 10DA16	Decanoic	0.9	-0.7	-2.5	-14.9
XCTS RTF 10EI16	Eicosane	11.8	10.3	7.1	-4.1

Figure 4.35 **DSC freezing curves of XCTS/C16 with different nucleating agents**

A schematic diagram concluding the optimized parameters for the synthesis of MEPCMS via coacervation of the amphoteric copolymer CTS-co-PMAA is shown in Figure 4.36. CTS-co-PMAA polymer solution has a PMAA:CTS ratio = 1:1 at pH ~1.5 for maximum initial solvation. Both the CTS-co-PMAA solution and the Ei+PCM mixture needs to be heated to 60 ℃ to prevent phase separation upon addition of the aqueous phase into oil phase. This is followed by gradual decrease of the temperature by placing in a refrigerator with temperature around 4 ℃ to solidify the Ei+PCM core to prevent phase separation of the Ei and PCM, due to solidification of Ei at room temperature. Following refrigeration, the optimal titration profile is a slow base titration up to pH 10, as the COO- groups provide electrostatic stabilization while the CTS serves as a rigid shell. However, titration is paused for 1 h at pH 7 for GAL crosslinking, to form a more densely networked MEPCM shell which enables the MEPCMs' structure to remain intact upon drying. Lastly, supercooling of the MEPCMs was successfully reduced from ΔT_f = -10 ℃ to ΔT_f = -4 ℃ by addition of nucleating agent at 10 wt% Ei in PCM. Other nucleating agents, decanoic acid and cetyl alcohol, were used but unable to decrease supercooling. Further characterization of the optimized MEPCMs is elaborated in the next Section.

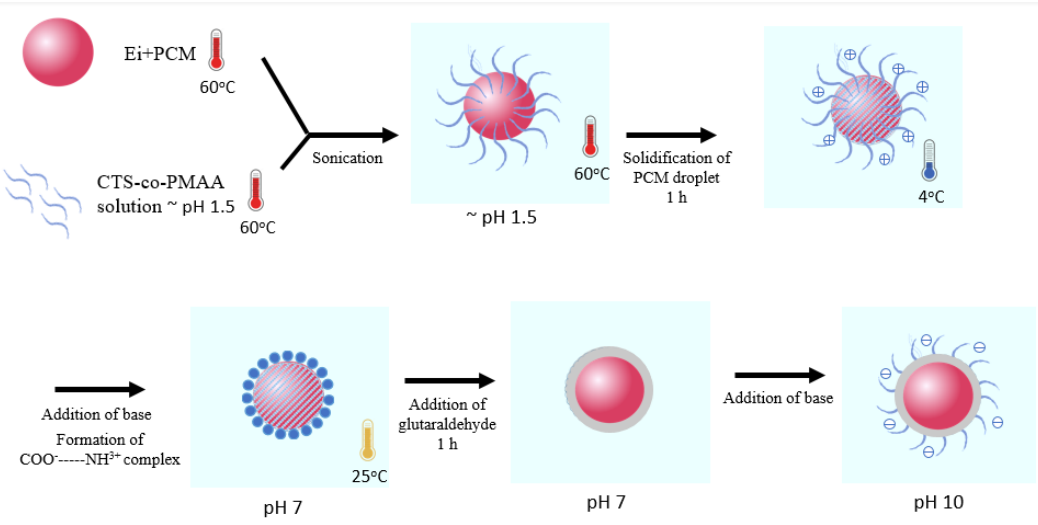


Figure 4.36 **Schematic diagram of optimized synthesis of MEPCMs via coacervation of CTS-co-PMAA**

4.2.3 Characterization of CTS-co-PMAA/C16 Nanocapsules

4.2.3.1 Appearance

The optimized CTS-co-PMAA/C16 encapsulates were dried under air at room temperature for 3-5 days, and then ground to become a powder. Figure 4.37 shows appearance of the NEPCM samples in water dispersion and powder form. Their light yellow color is due to glutaraldehyde crosslinking of the CTS moiety which produces a chromophore group, imine (-C=N-) on the NEPCM shell via the Schiff base reaction.[205]

a)  b) 

Figure 4.37 **Appearance of NEPCM a) dispersed in water ; b) dried powder**

4.2.3.2 Size distribution and morphology

The optimized encapsulation of PCM via coacervation of CTS-co-PMAA was able to synthesize nanocapsules which have diameters in the range of 10 – 1000 nm. The Nanoencapsulated PCM (NEPCM) has a hydrodynamic diameter 438 nm with PDI 0.22 (size distribution shown in Figure 4.38. Dried NEPCMs were imaged with SEM, and their sizes are in the range of 243 ± 69 nm (Figure 4.39) which is approximately half the hydrodynamic diameter. This size shrinkage is due to collapse of the extended PMAA moiety located on the NEPCM shell upon removal water. TEM images of the NEPCM (Figure 4.40) show spherical particles with a distinct core-shell structure. However, it is unclear if the NEPCMs possess a core-shell structure or a matrix structure. In both cases, the shell is likely the GAL crosslinked CTS-co-PMAA. Their particle diameters are in the range of 90-140 nm with shell thickness of 6-20 nm.

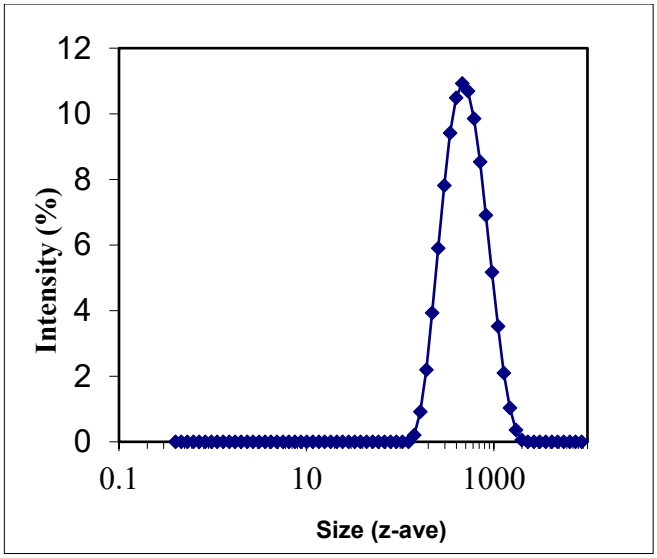


Figure 4.38 **Size distribution of NEPCM measured by DLS**

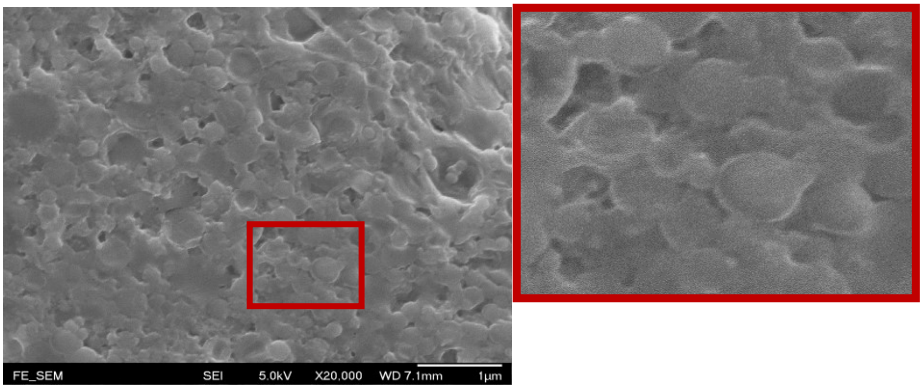


Figure 4.39 **SEM images of NEPCM (Diameter: 243 ± 69 nm)**

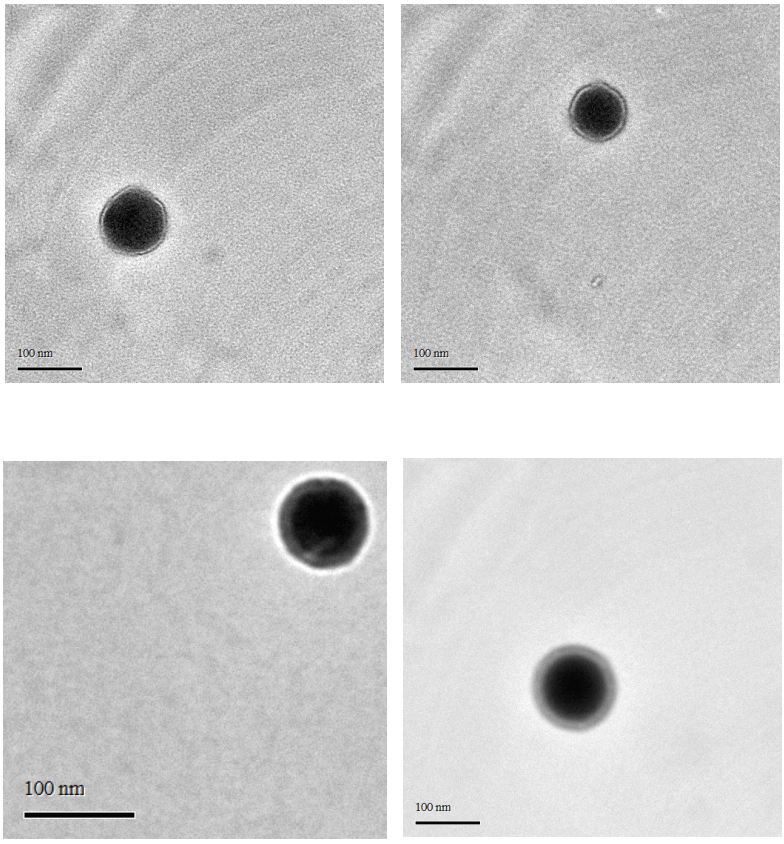


Figure 4.40 **TEM images of NEPCM (Diameters between 90 and140 nm with shell thickness of 6-20 nm)**

4.2.3.3 Chemical composition

FTIR spectra of the PCM encapsulates (red) and hexadecane (blue) is shown in Figure 4.41. The imine bond (C=N) is identified at 1548 cm^{-1}, while a broad peak at 1656 cm^{-1} indicates the presence of left shifted C=O stretching of carboxylic acid and amide groups due to glutaraldehyde crosslinking. Characteristic peaks of hexadecane located at 1464 cm^{-1}, 2852 cm^{-1} and 2956 cm^{-1} are found which represent to -CH bending, $–CH_2$, and

-CH_3 stretching in the NEPCM sample. These results indicate successful encapsulation of the PCM and retention of the PCM after drying.

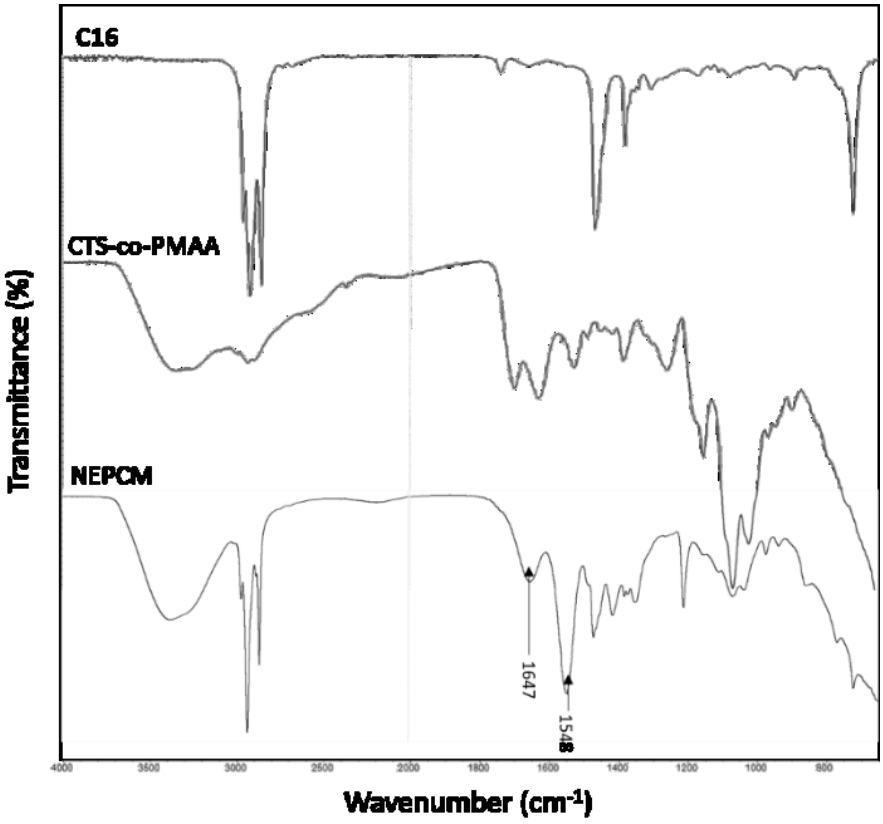


Figure 4.41 FTIR spectrum of C16 (Blue) and NEPCM (Red)

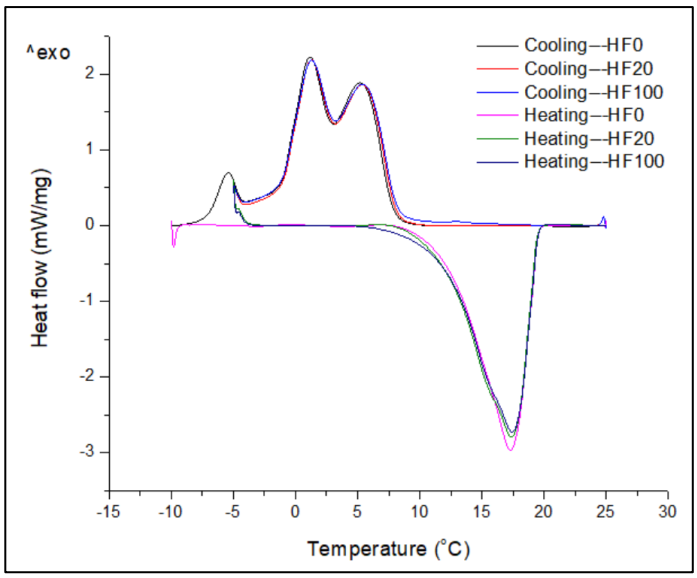
4.2.3.4 zeta-Potential

zeta-Potential of the NEPCMs was -50.4±7.9 mV at pH 10. The high negative *zeta*- potential is due to deprotonated carboxylic acid groups (COO-) located on the shell of the NEPCM. This means the shell of the NEPCM is composed of PMAA moiety from

the CTS-co-PMAA used to encapsulate the PCM. This also explains the high stability of NEPCMs in aqueous dispersions over a long period of time.

4.2.3.5 Phase change performance

Figure **4.42** shows the phase change properties of the NEPCMs. A broad exothermic peak with multiple peaks from 9 to -7.9 ℃ and a broad endothermic peak at 8.4 - 19.5 ℃ were detected. Compared to the pure PCM, hexadecane, the NEPCM has a decreased freezing temperature (supercooling) due to the nano-confinement of the PCM. Literature has reported that supercooling increase as confinements of the PCM decreased.[206] To reduce the supercooling effect, 10 wt% eicosane (nucleating agent) was added in PCM core. Althrough the presence of eicosane could reduce supercooling, itcaused peak broadening. The exothermic peak and the endothermic peak are a result of the PCM core transitioning from the liquid to solid phase and back to the liquid phase.This represents one phase change cycle of the NEPCMs. NEPCMs were subjected to multiple phase change cycles from 0, 20 up to 100. The number of phase change cycles is denoted as HF0, HF20 and HF100 respectively. From Figure 4.42, no change in the structure of the exothermic peak and the endothermic peak is observed, signifying no change in the NEPCM structure after 100 phase change cycles and no decrease in the thermal storage capacity.



Sample	Freezing curve				ΔT_f (°C)	Heating curve				%PCM
	LH_f (J/g)	T_{fo} (°C)	T_{fp} (°C)	T_{fe} (°C)		LH_m (J/g)	T_{mo} (°C)	T_{mp} (°C)	T_{me} (°C)	
C16	267	15.8	16.4	14.5	-2.7	261	17.4	19.1	20.4	-
NEPCM HF0	165	9.0	1.2	-7.9	-8.4	169	8.4	17.6	19.6	67%
NEPCM HF20	165	9.0	1.2	-7.9	-8.4	169	8.4	17.6	19.6	67%
NEPCM HF100	165	9.0	1.2	-7.9	-8.4	163	8.4	17.6	19.6	65%

Figure 4.42 **DSC curves and thermal characteristics of optimized NEPCMs (air dried) over 100 phase change cycles**

4.2.3.6 Proposed encapsulation mechanism

Figure 4.43 shows the proposed encapsulation mechanism of CTS-co-PMAA/C16 to form nanocapsules. The hexadecane droplets are trapped in the hydrophobic polymer (refer to the temperature-sensitive property of the CTS-co-PMAA)formed at high temperatures at localized areas during sonication (refer to Section 4.2.2.1).

By lowering the temperature below the T_f of hexadecane, the hexadecane droplets are solidified, thus coalescence cannot take place during titration. As a result, nanosized capsule can be formed. Indeed, in cases where emulsion temperatures were gradually reduced to 4^{o}C, encapsulation efficiency increased by ~30%. This is because lowering temperatures to 4^{o}C solidifies the dispersed PCM droplets, resulting in arresting the movement of the hydrophobic polymer in the PCM, thus reducing droplet coalescence

The second part of the coacervation is increasing pH by slowly titrating with base, allowing carboxylic groups in PMAA to become negatively charged ($COOH \rightarrow COO^-$) (pKa 4.5-4.75) [207]. The COO^- groups can complex with NH^{3+} of CTS to form a shell. A coarsening of the emulsion occurs and particles can be observed with the naked eye around pH 5.6-5.8.

Upon further increase of the pH >> 5.6, the emulsion became fine again. CTS became increasingly insoluble ($NH^{3+} \rightarrow NH_2$ pKa 6.5)[208] and could form a shell around the droplet, and stabilize with negatively charged COO- groups on the PMAA moiety.

The electrostatic repulsion and steric hindrance were able to stabilize the coacervates. No additional stabilizing agents are necessary.

After, deposition of polymer onto PCM droplet to form a shell, rigidization of the shell was carried out by adding the chemical crosslinker, glutaraldehyde which reacts with amine groups to form a Schiff base. Crosslinking of the CTS-co-PMAA/C16 coacervates rigidized the shell, thus preventing the shell rupture during conditions such as drying, ultrafiltration and even freeze drying. The coacervate remains stable over prolonged periods of time without emulsifiers.

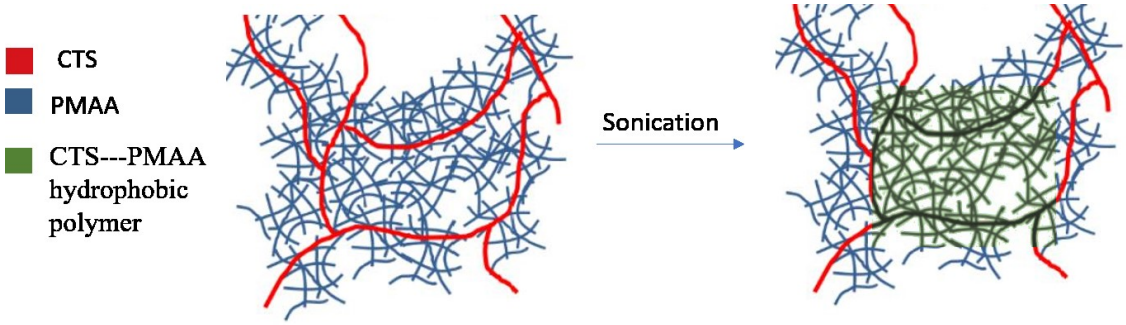
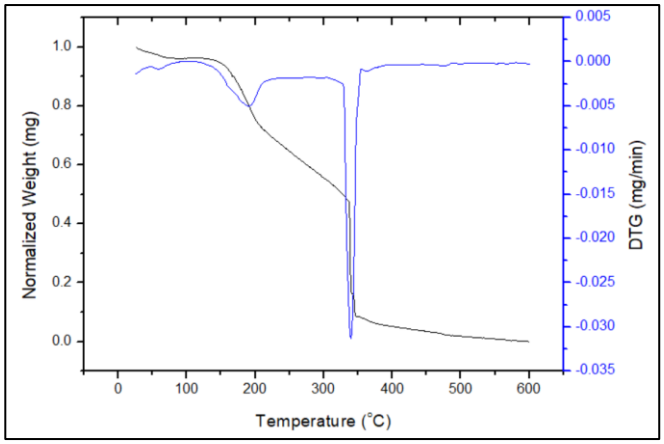


Figure 4.43 **Proposed encapsulation mechanism of CTS-co-PMAA/C16 nanocapsules**

4.2.3.7 Thermal stability

Thermogravimetric curves of NEPCMs were carried out to assess their thermal stability and PCM content. Thermal analysis was from 60-600 °C at a rate of 10°C/min

under nitrogen atmosphere. According to literature, hexadecane, the PCM core in the NEPCMs, evaporates around 200 °C [209] and GC/MS analysis by Ford showed that decomposition of hexadecane takes place from 330-370°C[210]. Thermogravimetric analysis of the NEPCMs (Figure 4.44) shows that both evaporation and decomposition of hexadecane takes place. The first peak with maxima at 189 °C is the degradation of the CTS homopolymer and the evaporation of the PCM. Due to encapsulation, the PCM does not vaporize immediately, instead evaporates at a steady rate until 340 °C where thermal decomposition takes place. A small shoulder peak at 340 °C is observed and might be the degradation peak from decomposition of PMAA homopolymer in the CTS-co-PMAA. The degradation temperature is significantly decreased compared to results in probably due to the thermal decomposition of the PCM which could increase the combustibility of the PMAA homopolymer. Due to the overlap between the thermal decomposition temperatures of CTS-co-PMAA and the evaporation and thermal decomposition temperatures of the PCM, hexadecane, it is not possible to accurately estimate the PCM content from TGA. In conclusion, the TGA curve shows successful PCM encapsulation and can withstand temperatures up to 127 °C. The CTS-co-PMAA shell also shows ability to prevent PCM evaporation.



Peak	Peak area (%weight loss)	Degradation temperature (℃)		
		Onset	Peak	Endset
1	17%	142	189	228
Plateau	32%	228	-	311
2	39%	311	340	353

Figure 4.44 **TGA curve of CTS-co-PMAA/C16 NEPCMs**

4.2.4 Characterization of freeze-dried CTS-co-PMAA/C16 nanocapsules

4.2.4.1 Synthesis and morphology

Optimized NEPCMs were freeze dried to give a yellowish white sponge that was easily broken (Figure 4.45). Calculations showed that the freeze dried NEPCMs had an apparent density of 0.03 g/ml which is lighter than the NEPCM powder (apparent density of 0.61 g/ml).



Figure 4.45 **Appearance of freeze-dried NEPCMs**

SEM images of the NEPCM and the freeze dried NEPCMs are shown in Figure 4.46. The NEPCM dried at room temperature shows spheres embedded in a network. Freeze dried NEPCM shows deflated spheres connected in a porous network. The deflation of the NEPCMs could be due to the sublimation of part of the PCM core during freeze drying. This correlates with DSC results which show a 37 wt% loss of encapsulated PCM after NEPCM were freeze dried.

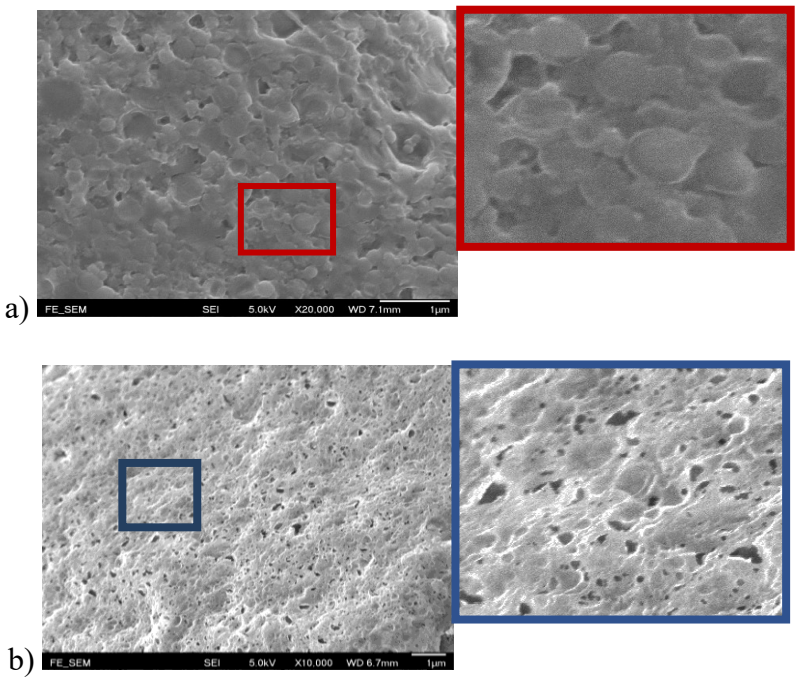
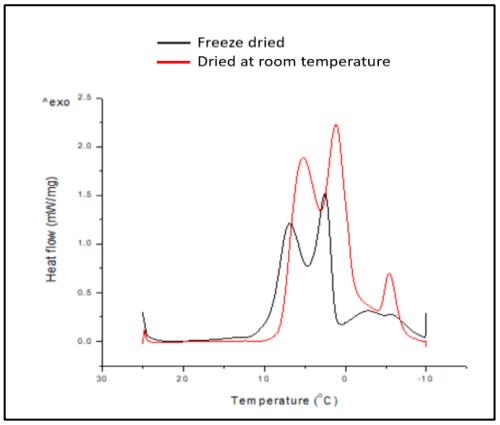


Figure 4.46 **SEM images of a) NEPCM (Diameter: 243 ± 69 nm) ; b) freeze dried NEPCM**

4.2.4.2 Phase change performance

Freeze-dried NEPCMs were characterized with DSC. Figure 4.47 shows the freezing curve of the NEPCMs dried via 1) freeze drying compared with 2) air dried at room temperature. Freeze-dry process removes encapsulated PCM in the sample as shown by loss of ~40% LH_f compared to NEPCMs dried at room temperature.

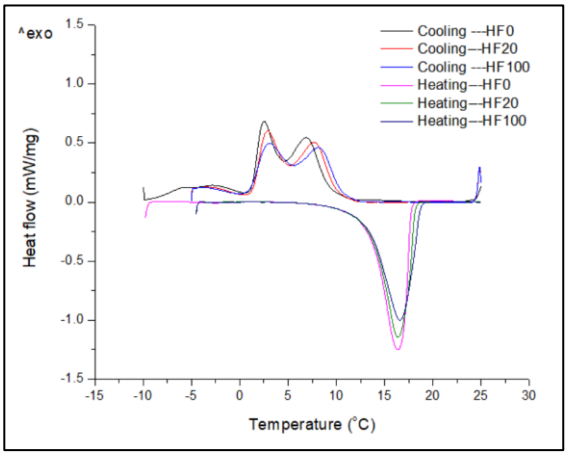


Sample	Freezing curve					%PCM
10EI16 RTF	**LH_f (J/g)**	**T_{fo} (°C)**	**T_{fp} (°C)**	**T_{fe} (°C)**	**ΔT_f (°C)**	
Freeze dried	105	11.7	2.5	0.7	-5.7	42%
		0.53	-2.7	-9.4		
Dried at room temperature	165	9.0	1.2	-7.9	-8.4	67%

Figure 4.47 **Freezing curve of freeze dried NEPCMs and NEPCMs dried at room temperature**

Encapsulation efficiency after multiple phase change cycles

Freeze-dried NEPCMs was also tested with multiple phase change cycles using DSC. Figure 4.48 shows the thermal profile of the freeze-dried NEPCMs over 100 phase change cycles. There is a 10% decrease of thermal storage capacity after 100 phase change cycles.



Phase change cycles	Freezing curve					Heating curve				%PCM
	LH_f (J/g)	T_{fo} (°C)	T_{fp} (°C)	T_{fe} (°C)	ΔT_f (°C)	LH_m (J/g)	T_{mo} (°C)	T_{mp} (°C)	T_{me} (°C)	
0	105	11.7 0.53	2.5 -2.7	0.7 -9.4	-5.7	102	11.4	16.5	19.3	42%
20	96	-	-	-	-	95	-	-	-	39%
100	94	-	-	-	-	92	-	-	-	38%

Figure 4.48 **DSC summary of optimized NEPCMs (freeze dried) over 100 heat-freeze cycles**

4.2.5 Bulk synthesis and characterization of CTS-co-PMAA/C16 microcapsules

4.2.5.1 Synthesis and morphology

Figure 4.49 shows the MEPCMs which were synthesized based on the optimized recipe with scaling up 20 times (MEPCM 20X). The light brown hue is attributed to glutaraldehyde crosslinking of the CTS moiety which produces a chromophore group, imine (-C=N-) on the MEPCM shell via Schiff base reaction.[205] After drying at room temperature under air for several days, approximately 20 g of MEPCM 20X was obtained.



Figure 4.49 **Appearance of C16/CTS-co-PMAA MEPCMs synthesized via bulk procedure**

Size distribution of MEPCM 20X obtained from DLS is shown in Figure 4.50. The hydrodynamic diameter of the MEPCM 20X were much larger compared to the previous synthesis which was ~400 nm. This is expected as volume of the emulsion has increased by 10 fold, and the amount of PCM dispersed increased 20 fold. The sonication power was likewise increased for the larger emulsion volume from 5 W to 13 W and time was

lengthened from 0.5 h to 2 h. Statistical analysis of optical images reveal that the size distribution (1.89±0.27 µm) is similar to that obtained from DLS (Figure 4.50**B**). Furthermore, the MEPCM20X shows some aggregation which might be due to the high pressure during MEPCM purification via ultrafiltration.

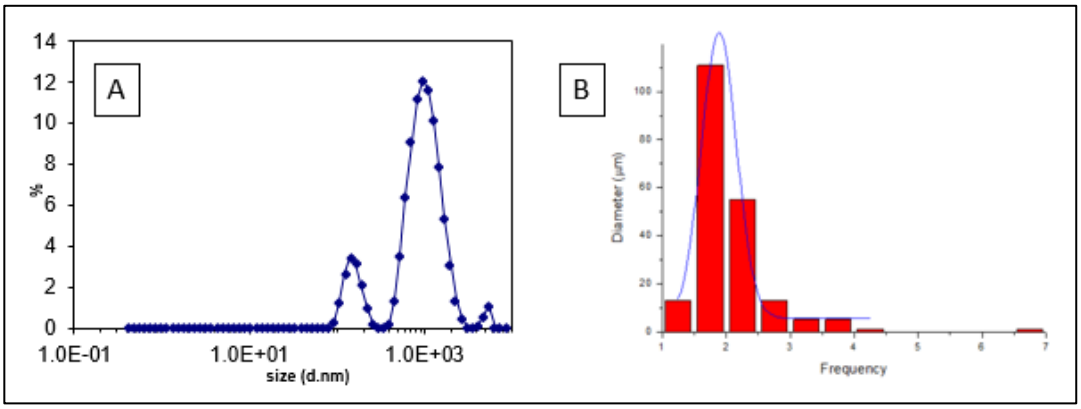
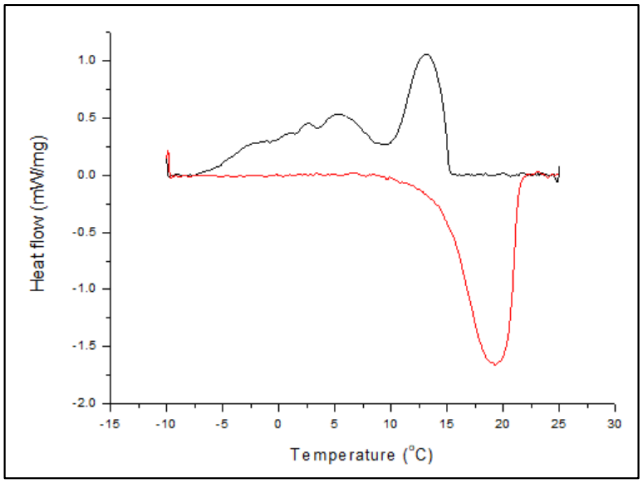


Figure 4.50 **(A) DLS of size intensity distribution of C16/CTS-co-PMAA microcapsules via bulk synthesis , (B) Optical images of MEPCM20X (Size distribution: 1.89±0.27 µm)**

4.2.5.2 Phase change performance

Thermal properties of MEPCM20X are summarized in Figure 4.51. The exothermic peak is broad and spans from -7.4 to 15.2 ℃. The freezing temperature depression (ΔT_f) is much lower due to the increased size of the MEPCMs. However, %ee of the PCM is only 57%. The encapsulation efficiency is low in comparison to the optimal recipe which attains >90% easily. The decrease could be attributed to the increase of time needed to complete the titration (5 times longer).



Sample	Freezing curve					Heating curve					%PCM
	LH_f (J/g)	T_{fo} (°C)	T_{fp} (°C)	T_{fe} (°C)	ΔT_f (°C)	LH_m (J/g)	T_{mo} (°C)	T_{mp} (°C)	T_{me} (°C)	%ee ^	
Hexadecane (C16)	267	15.8	16.4	14.5	-2.7	261	17.4	19.1	20.4	-	-
B-10EI16	137	15.2	13.4	-7.4	-1.6	-124	14.6	19.1	21.3	57%	50%

^Dried sample

Figure 4.51 **DSC of PCM encapsulated by CTS-co-PMAA using bulk synthesis method (Sample: MEPCM20X)**

Previously, the heat storage/release was observed with DSC using small quantities of MEPCM (<5 mg). We desire to evaluate the heat storage/release of the MEPCM in larger quantities. Figure 4.52 shows temperature profiles of MEPCM20X compared to temperature profiles of hexadecane with the same weight which were equilibrated at ~3 °C and then placed in environment temperature of 23 °C. The temperature of the MEPCM20X microcapsules increases at a similar rate to C16. At ~15 °C, a plateau is

observed which is the latent heat released from the sample. The plateaus coincides with the DSC results shown in Figure 4.52. The temperature profile curve continues to increase until it is in equilibrium with the ambient temperature. The length of time for MEPCM to reach equilibrium was 6.6 h while C16 was 11 h. However, it has to be taken into account that the amount of PCM in the MEPCM was around 50%. Therefore the thermoregulatory property of the MEPCM is directly comparable to the bulk PCM in terms of PCM content.

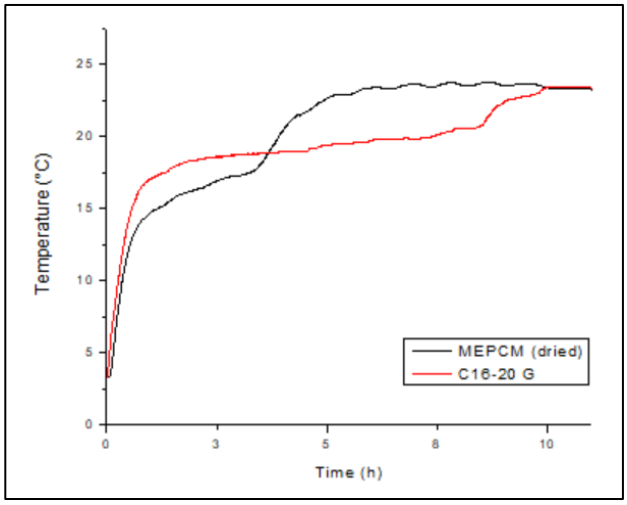


Figure 4.52 **Temperature profile of hexadecane (C16) and MEPCM20X equilibrated at ~3 °C placed in ambient temperature of ~23 °C**

Figure 4.53 shows the temperature history of the samples previously equilibrated at ~23 °C and then placed in environment temperature of 3 °C. For the MEPCMs, two plateaus are observed at ~16 °C and ~9 °C which are the latent heat released from the sample. The temperature profile curve continues to decrease until it is in equilibrium with the environment temperature. Both the MEPCM and C16 samples reached thermal equilibrium at approximately the same time, this is due to the supercooling phenomena

for MEPCMs, solidificiation takes place at much lower temperatures as indicated by a plateau at ~8 ℃ and continues even below 3 ℃.

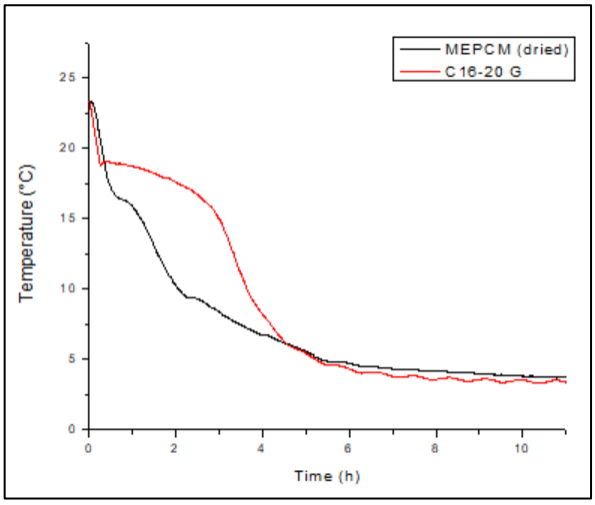


Figure 4.53 **Temperature profiles of hexadecane (C16) and MEPCM20X equilibrated at ~23 °C placed in controlled environment temperature of ~3 °C**

4.3 Conclusion

In conclusion, CTS-co-PMAA amphoteric copolymer have been synthesized with high monomer conversion close to 100%. The synthesis of proceeded via two steps: 1) The chitosan was first modified with methacrylic acid (MAA) through an amidation reaction between the amine group of the chitosan and carboxylic acid group of the MAA to form MAA-CTS, followed by 2) free radical polymerization of remaining MAA to generate the copolymer CTS-co-PMAA hydrogel.

The CTS-co-PMAA is able to form highly stable PCM emulsions through stabilization of the PCM droplets through the formation of hydrophobic CTS—PMAA polymer during sonication which is able to entrap the similarly hydrophobic PCM. The CTS-co-PMAA/PCM oil droplets were further stabilized through adjusting the solution pH to 10. The hydrophilic PMAA of the copolymer dissolves in the aqueous phase, capable of providing both electrostatic repulsion and steric hindrance against coalescence.

The preparation of the highly stable CTS-co-PMA/C16 emulsions is followed by coacervation via pH titration to form encapsulated PCMs. Based on our studies, an optimal recipe for the encapsulation of PCM with CTS-co-PMAA via coacervation has been concluded as follows: The encapsulation efficiency was the highest for PMAA:CTS = 1:1 wt ratio in the CTS-co-PMAA copolymer; the highest dissolution of the CTS-co-PMAA copolymer occurred at pH < 2; The highest point of solvation for the CTS-co-PMAA copolymer coincides with the pH for CTS-co-PMAA solutions with lowest surface

tension. The precipitation of nucleating agent, eicosane, during titration can be prevented by freezing the PCM at ~4℃. The optimal titration profile for coacervation was from pH 1.5 to 7 followed by GAL crosslinking for 1h and alkaline titration to pH 10. However, decrease of supercooling via addition of nucleating agents could only reduce freezing temperature depression from ~ -10 ℃ to ~ -5 ℃.

The optimized PCM nanoencapsulates showed encapsulation efficiency could increase up to 94% with high thermal storage capacity (LH_s 165 J/g / LH_m 169 J/g), high stability in water without addition of surfactants, resistance to solvent extraction, no leakage upon drying. The optimized recipe yielded successful synthesis of PCM nano-capsules (NEPCM) with an average diameter of 243 ± 69 nm and possess distinct core-shell structure. The NEPCMs were stable over 100 phase change cycles and showed no decrease in the thermal storage capacity. In addition, the NEPCMs showed increased thermal stability of PCM after encapsulation and protected ~60%PCM from evaporation under freeze-dry conditions.

Chapter 5
Conclusion and Recommendations for Future Study

5.1 Conclusions

In conclusion, this study has successfully developed a method for synthesizing nanoencapsulated phase change material (NEPCM) with high encapsulation efficiency and thermal capacity through a coacervation approach.

The initial method for synthesizing MEPCMs in water was a Pickering emulsion-based template using PBA/CTS particles as shell material. However, the MEPCMs proved unstable during thermal cycling and upon drying. Results showed that the PCM had leaked from the MEPCMs.

A method for synthesizing NEPCMs in water was prepared using CTS-co-PMAA as the shell material via coacervation techniques. The variables studied to optimize the encapsulation efficiency and thermal cycling were: composition of PMAA:CTS ratios in CTS-co-PMAA, pH and wt% of CTS-co-PMAA solution with lowest surface tension and various titration profiles. Other factors to increase the rigidity of the NEPCMs to prevent collapse during drying include addition of cellulose nanocrystals (CNC) and crosslinking with glutaraldehyde (GAL). In an effort to decrease supercooling phenomena which was

fairly severe due to the small dimensions of the NEPCMs, various amounts and types of nucleating agents were studied.

An optimal recipe was concluded based on the studies: CTS-co-PMAA with PMAA:CTS ratio = 1:1 and initial pH 1.5-2.0, glutaraldehyde crosslinking and addition of 10 wt% eicosane per PCM to decrease supercooling. The NEPCMs obtained had encapsulation efficiency >90% and thermal capacity of 165 J/g. PCM accounted for 66wt% of the MEPCMs and diameters were ~200 nm revealed by SEM which classifies them as nano-encapsulated PCMs. However, decrease of supercooling via addition of nucleating agents could only reduce freezing temperature depression to ~ -5 °C. Thermal analysis of the NEPCMs showed that they could withstand up to 100 thermal cycles with no decrease in thermal capacity.

5.2 Recommendations for Future Study

5.2.1 Investigation of NEPCMs in water as heat transfer fluid

In recent years, PCM slurries have gained much attention as heat transfer fluids due to their efficient heat transfer medium - water, improved heat storage capacity which in turn reduces the size of the heat exchanger, pipeline for transferring the fluid and energy consumption during transport.[78, 85, 211, 212] However, the two large categories of PCM slurries which are: MEPCMs dispersed in water or PCMs stabilized with emulsifiers in

water have increased viscosity which for simple water pumps, where the fluid is passes through the internal bearings causes pump failure. However, by substituting the simple water pumps for dry runner pumps, this issue can be resolved. Still, compared to simple water pumps, dry runner pumps consume more energy for transporting the same amount as fluid.[82, 213, 214] Due to NEPCMs smaller dimensions, a NEPCM slurry could potentially have lower overall viscosity compared to an MEPCM slurry.[215] The NEPCMs synthesized in this study have high thermal storage capacity and high stability and dispersibility in water. It would be interesting to measure the performance of our NEPCMs as a heat transfer fluid.

5.2.2 Encapsulation of fragrances or other volatile materials

Fragrance oils are present in components of essential oils with unique odors. They are present in cosmetics, toiletries, detergents and production of scented products. These fragrances are synthesized or extracted from natural sources for scenting products in various industries. However, many of these fragrance molecules have functional groups such as aldehyde, ketone and terpenes which are prone to reaction with the environment leading to degradation of the fragrance but more importantly formation of allergenics.[216]

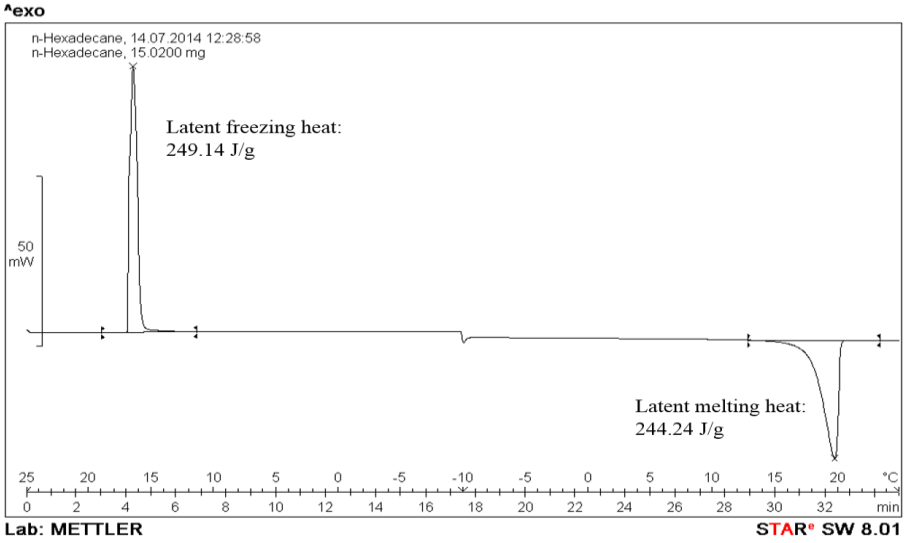
To prolong the shelf life and quality of scented products, encapsulation of fragrances is key to 1) isolation from the environment, 2) reduce vaporization through controlled release of the encapsulated molecules, 3) ease of handling; 4) reduced

flammability and 5) oil-based fragrances can be easily dispersed in water via water dispersible encapsulates. It will be quite interesting to modify the coacervation technique developed to encapsulate fragrances with CTS-co-PMAA, as our current approach to synthesize MEPCMs shows high encapsulation efficacy and reduced volatility in freeze drying conditions.

Chapter 6

Appendix

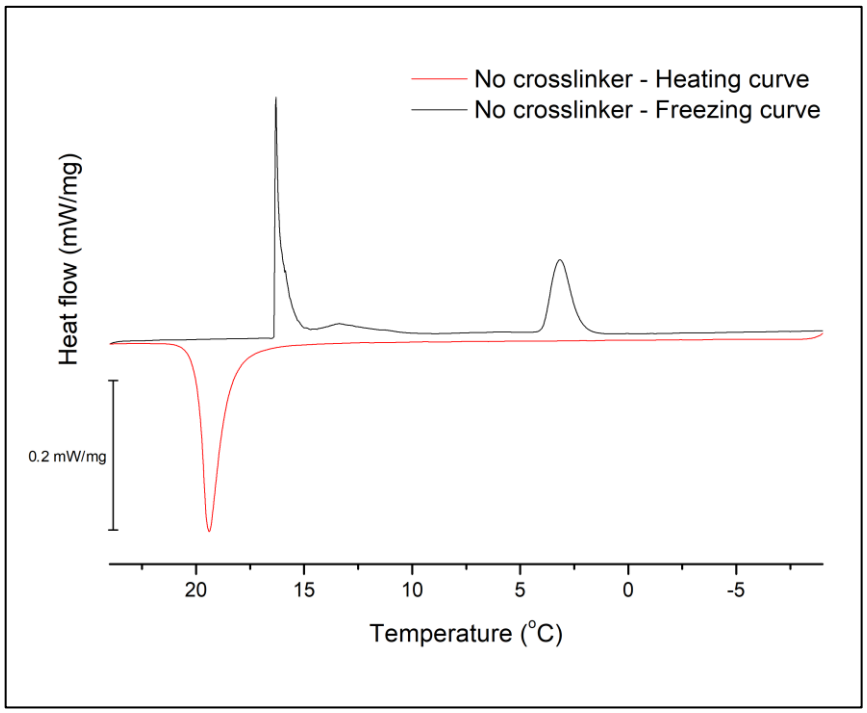
6.1 DSC scan of PCM, hexadecane



Sample	Freezing					Melting			
	LH_f (J/g)	T_{fo} (°C)	T_{fp} (°C)	T_{fe} (°C)	ΔT_f (°C)	Latent heat (J/g)	T_{mo} (°C)	T_{mp} (°C)	T_{me} (°C)
Hexadecane (C16)	249.15	15.81	16.39	14.53	2.69	244.24	17.44	19.08	20.39

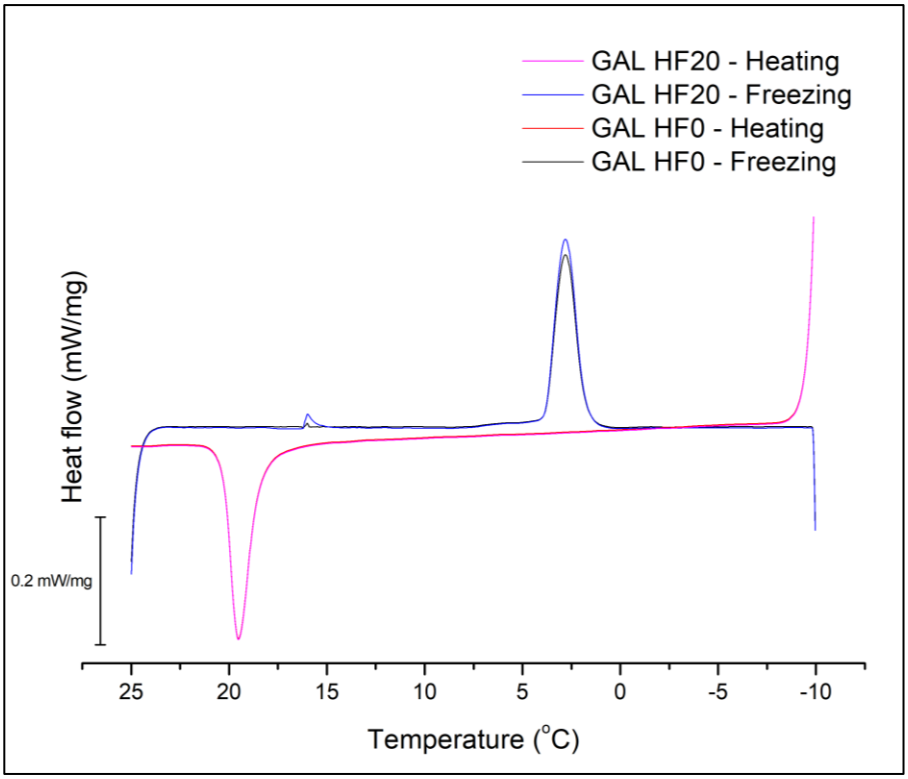
Figure 6.1 **DSC scan of hexadecane (from 25 °C to -10 °C and -10 °C to 25 °C at a rate of 4 °C min^{-1})**

6.2 Thermal profiles of MEPCMs synthesized via crosslinking of C16-PBA/CTS emulsions



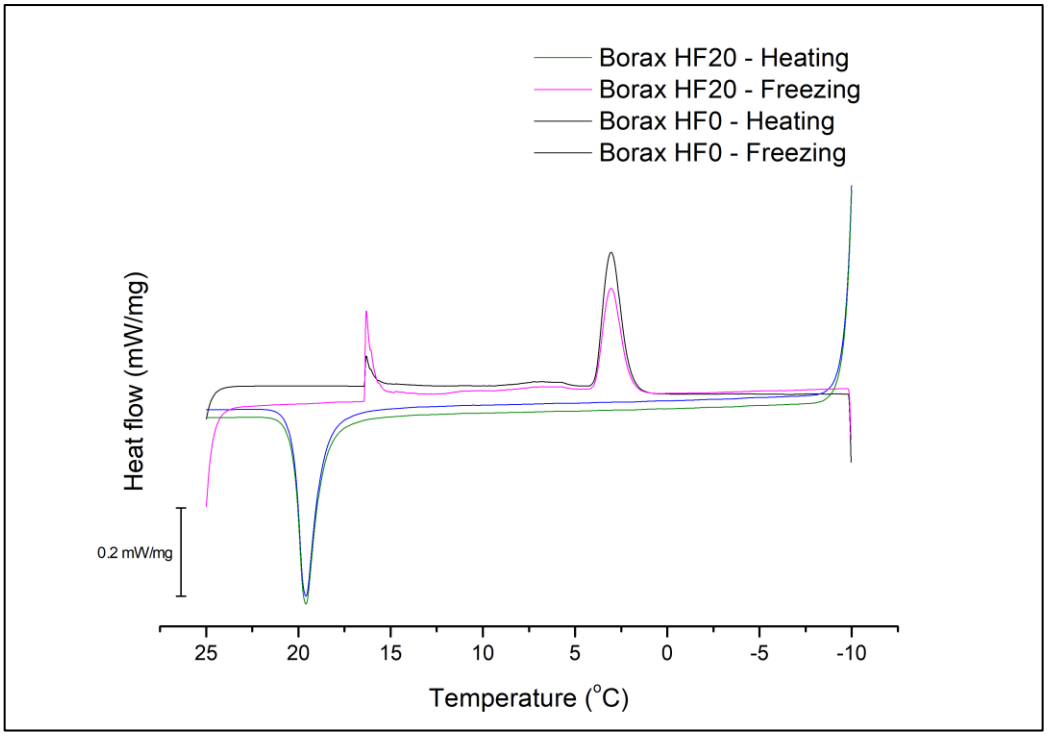
Sample	Freezing curve					Heating curve			
	LH_f (J/g)	T_{fo} (°C)	T_{fp} (°C)	T_{fe} (°C)	ΔT_f (°C)	LH_m (J/g)	T_{mo} (°C)	T_{mp} (°C)	T_{me} (°C)
Hexadecane (C16)	267	15.8	16.4	14.5	-2.7	261	17.4	19.1	20.4
No crosslinker HF0	7.52 1.24	16.5 10.7	16.8 8.3	15.9 6.1	+0.7 -5.8	-10.7	18.3	19.3	20.1

Figure 6.2 **Thermal profile C16-PBA/CTS emulsions with no crosslinker added**



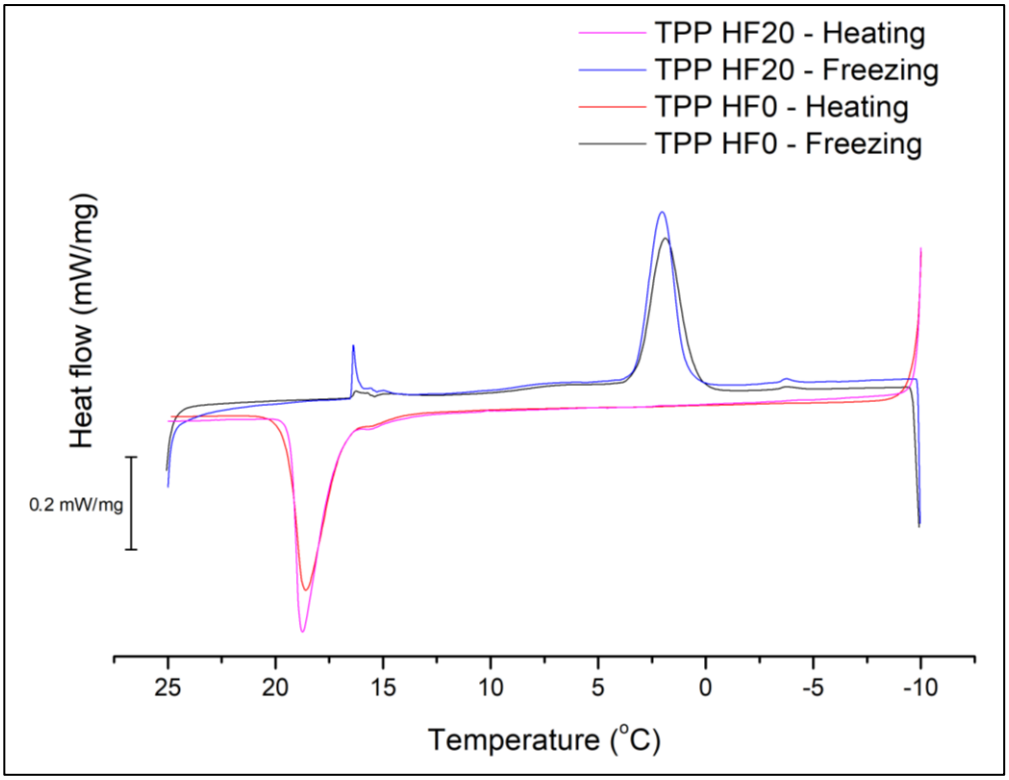
Sample	Freezing curve					Heating curve			
	LH_f (J/g)	T_{fo} (°C)	T_{fp} (°C)	T_{fe} (°C)	ΔT_f (°C)	LH_m (J/g)	T_{mo} (°C)	T_{mp} (°C)	T_{me} (°C)
C16	267	15.8	16.4	14.5	-2.7	261	17.4	19.1	20.4
GAL HF0	5.3	3.9	3.0	1.9	-11.9	-6.5	18.3	19.3	20.2
GAL HF20	5.0	3.9	3.0	1.9	-11.9	-6.5	18.3	19.3	20.2
	0.2	16.4	16.1	15.6					

Figure 6.3 **Thermal profile C16-PBA/CTS emulsions crosslinked with GAL (EC-GAL)**



Sample	Freezing curve					Heating curve			
	LH_s (J/g)	T_{so} (°C)	T_{sp} (°C)	T_{se} (°C)	ΔT_f (°C)	LH_m (J/g)	T_{mo} (°C)	T_{mp} (°C)	T_{me} (°C)
C16	267	15.8	16.4	14.5	-2.7	261	17.4	19.1	20.4
Borax HF0	0.2	16.6	16.5	15.9	-11.8	-8.7	18.4	19.3	20.1
	5.5	4.0	3.2	2.2					
Borax HF20	1.6	16.6	16.5	15.9	-11.8	-8.7	18.4	19.3	20.1
	4.1	4.0	3.2	2.2					

Figure 6.4 **Thermal profile C16-PBA/CTS emulsions crosslinked with Borax (EC-Borax)**



Sample	Freezing curve					Heating curve			
	LH_s (J/g)	T_{so} (°C)	T_{sp} (°C)	T_{se} (°C)	ΔT_f (°C)	LH_m (J/g)	T_{mo} (°C)	T_{mp} (°C)	T_{me} (°C)
C16	267	15.8	16.4	14.5	-2.7	261	17.4	19.1	20.4
TPP HF0	0.32	16.6	16.3	16.1	-12.6	-10.9	16.7	18.6	19.5
	8.21	3.2	1.9	0.5					
TPP HF20	0.8	16.6	16.5	16.1	-12.5	-10.8	17.0	18.6	19.2
	8.1	3.3	2.2	1.1					

Figure 6.5 **Thermal profile C16-PBA/CTS emulsions crosslinked with TPP (EC-TPP)**

References

1. Cohen, J.E., *Human population: the next half century.* science, 2003. **302**(5648): p. 1172-1175.
2. Petroleum, B., *BP Statistical Review of World Energy 2017*. 2017, British Petroleum Co.: London.
3. *Global Energy Statistical Yearbook 2017*. 15/8/2017]; Available from: https://yearbook.enerdata.net/total-energy/world-consumption-statistics.html.
4. Shafiee, S. and E. Topal, *When will fossil fuel reserves be diminished?* Energy Policy, 2009. **37**(1): p. 181-189.
5. Guimaraes, K.B.R.D., *Renewable Infrastructure Investment Handbook :A Guide for Institutional Investors*. 2016, World Economic Forum.
6. Schlenker, W. and M.J. Roberts, *Nonlinear temperature effects indicate severe damages to US crop yields under climate change.* Proceedings of the National Academy of sciences, 2009. **106**(37): p. 15594-15598.
7. Kucharik, C.J. and S.P. Serbin, *Impacts of recent climate change on Wisconsin corn and soybean yield trends.* Environmental Research Letters, 2008. **3**(3): p. 034003.
8. Peng, S., et al., *Rice yields decline with higher night temperature from global warming.* Proceedings of the National academy of Sciences of the United States of America, 2004. **101**(27): p. 9971-9975.
9. Yagi, J. and T. Akiyama, *Storage of thermal energy for effective use of waste heat from industries.* Journal of Materials Processing Technology, 1995. **48**(1): p. 793-804.
10. Dincer, I. and M. Rosen, *Thermal energy storage: systems and applications*. 2002: John Wiley & Sons.
11. Katter, L. and D. Peterson, *Applications of thermal energy storage to process heat and waste heat recovery in the iron and steel industry.* 1978.
12. *Estimating the Cost and Energy Efficiency of a Solar Water Heater*. Available from: https://energy.gov/energysaver/estimating-cost-and-energy-efficiency-solar-water-heater.
13. Hasnain, S.M., *Review on sustainable thermal energy storage technologies, Part I: heat storage materials and techniques.* Energy Conversion and Management, 1998. **39**(11): p. 1127-1138.

14. Mehling, H. and L.F. Cabeza, *Basic thermodynamics of thermal energy storage.* Heat and cold storage with PCM, 2008: p. 1-10.

15. Williams, P.N., et al., *Package having phase change materials and method of use in transport of temperature sensitive payload*. 2011, Google Patents.

16. Ohkawara, H., et al. *A newly developed container for safe, easy, and cost-effective overnight transportation of tissues and organs by electrically keeping tissue or organ temperature at 3 to 6 C*. in *Transplantation proceedings*. 2012. Elsevier.

17. Purdum, H.E., *Phase change system for temperature control*. 1999, Google Patents.

18. Gin, B. and M.M. Farid, *The use of PCM panels to improve storage condition of frozen food.* Journal of Food Engineering, 2010. **100**(2): p. 372-376.

19. Hoang, H., et al., *Heat transfer study of submicro-encapsulated PCM plate for food packaging application.* International Journal of Refrigeration, 2015. **52**: p. 151-160.

20. Ahmed, M., O. Meade, and M.A. Medina, *Reducing heat transfer across the insulated walls of refrigerated truck trailers by the application of phase change materials.* Energy Conversion and Management, 2010. **51**(3): p. 383-392.

21. Oró, E., et al., *Thermal analysis of a low temperature storage unit using phase change materials without refrigeration system.* International Journal of Refrigeration, 2012. **35**(6): p. 1709-1714.

22. Ryms, M., et al., *The use of lightweight aggregate saturated with PCM as a temperature stabilizing material for road surfaces.* Applied Thermal Engineering, 2015. **81**: p. 313-324.

23. Nelson, K.M. and G.A. Butler, *Controlling Temperature in Exothermic Reactions with a Phase Change Material*. 2012, Google Patents.

24. Li, K., et al., *A yolk/shell strategy for designing hybrid phase change materials for heat management in catalytic reactions.* Journal of Materials Chemistry A, 2017. **5**(46): p. 24232-24246.

25. Omer, S.A., S.B. Riffat, and X. Ma, *Experimental investigation of a thermoelectric refrigeration system employing a phase change material integrated with thermal diode (thermosiphons).* Appl. Therm. Eng., 2001. **21**(12): p. 1265-1271.

26. Riffat, S.B., S.A. Omer, and X. Ma, *A novel thermoelectric refrigeration system employing heat pipes and a phase change material: An experimental investigation.* Renewable Energy, 2001. **23**(2): p. 313-323.

27. Trelles, J.P. and J.J. Dufly, *Numerical simulation of porous latent heat thermal energy storage for thermoelectric cooling.* Appl. Therm. Eng., 2003. **23**(13): p. 1647-1664.

28. Huang, M.J., P.C. Eames, and B. Norton, *Thermal regulation of building-integrated photovoltaics using phase change materials.* Int. J. Heat Mass Transfer, 2004. **47**(12-13): p. 2715-2733.

29. Nomura, T., N. Okinaka, and T. Akiyama, *Waste heat transportation system, using phase change material (PCM) from steelworks to chemical plant.* Resources, Conservation and Recycling, 2010. **54**(11): p. 1000-1006.

30. Maruoka, N., et al., *Development of PCM for recovering high temperature waste heat and utilization for producing hydrogen by reforming reaction of methane.* ISIJ International, 2002. **42**(2): p. 215-219.

31. Kaizawa, A., et al., *Thermophysical and heat transfer properties of phase change material candidate for waste heat transportation system.* Heat and Mass Transfer, 2008. **44**(7): p. 763-769.

32. *Key world energy statistics*. Available from: https://www.iea.org/publications/freepublications/publication/KeyWorld2017.pdf.

33. Zhang, M., M.A. Medina, and J.B. King, *Development of a thermally enhanced frame wall with phase-change materials for on-peak air conditioning demand reduction and energy savings in residential buildings.* International Journal of Energy Research, 2005. **29**(9): p. 795-809.

34. Castell, A., et al., *Life Cycle Assessment of alveolar brick construction system incorporating phase change materials (PCMs).* Applied energy, 2013. **101**: p. 600-608.

35. Ismail, K.A.R. and A.B. de Jesus, *Parametric study of solidification of PCM around a cylinder for ice-bank applications.* Int. J. Refrig., 2001. **24**(8): p. 809-822.

36. Lorsch, H.G., K.W. Kauffman, and J.C. Denton, *Thermal energy storage for solar heating and off-peak air conditioning.* Energy Convers., 1975. **15**(1-2): p. 1-8.

37. Farid, M.M. and R.M. Husian, *An electrical storage heater using the phase-change method of heat storage.* Energy Convers. Manage., 1990. **30**(3): p. 219-30.

38. Mehling, H., et al., *PCM-module to improve hot water heat stores with stratification.* Renewable Energy, 2002. **28**(5): p. 699-711.

39. Cabeza, L.F., et al., *Heat transfer enhancement in water when used as PCM in thermal energy storage.* Appl. Therm. Eng., 2002. **22**(10): p. 1141-1151.

40. Canbazoğlu, S., et al., *Enhancement of solar thermal energy storage performance using sodium thiosulfate pentahydrate of a conventional solar water-heating system.* Energy and Buildings, 2005. **37**(3): p. 235-242.

41. Shukla, A., D. Buddhi, and R.L. Sawhney, *Solar water heaters with phase change material thermal energy storage medium: A review.* Renewable and Sustainable Energy Reviews, 2009. **13**(8): p. 2119-2125.

42. Prakash, J., H.P. Garg, and G. Datta, *A solar water heater with a built-in latent heat storage.* Energy Conversion and Management, 1985. **25**(1): p. 51-56.

43. Najjar, A. and A. Hasan, *Modeling of greenhouse with PCM energy storage.* Energy Conversion and Management, 2008. **49**(11): p. 3338-3342.

44. Öztürk, H.H., *Experimental evaluation of energy and exergy efficiency of a seasonal latent heat storage system for greenhouse heating.* Energy Conversion and Management, 2005. **46**(9): p. 1523-1542.

45. Boulard, T., et al., *Performance of a greenhouse heating system with a phase change material.* Agricultural and Forest Meteorology, 1990. **52**(3): p. 303-318.

46. Kabeel, A.E. and M. Abdelgaied, *Improving the performance of solar still by using PCM as a thermal storage medium under Egyptian conditions.* Desalination, 2016. **383**: p. 22-28.

47. Kandasamy, R., X.-Q. Wang, and A.S. Mujumdar, *Transient cooling of electronics using phase change material (PCM)-based heat sinks.* Applied Thermal Engineering, 2008. **28**(8-9): p. 1047-1057.

48. Tan, F. and C. Tso, *Cooling of mobile electronic devices using phase change materials.* Applied thermal engineering, 2004. **24**(2-3): p. 159-169.

49. Ramanathan, N., *A new weighting system for mean surface temperature of the human body.* Journal of applied physiology, 1964. **19**(3): p. 531-533.

50. *MACROENCAPSULATION - CSM: PCM in aluminum case*. 2018; Available from: https://www.rubitherm.eu/en/index.php/productcategory/makroverkaspelung-csm.

51. *Consumers Could Benefit from Demand Programs, but Challenges Remain*, in *ELECTRICITY MARKETS*. 2004, United States Government Accountability Office.

52. Costa, M., D. Buddhi, and A. Oliva, *Numerical simulation of a latent heat thermal energy storage system with enhanced heat conduction.* Energy Convers. Manage., 1997. **39**(3/4): p. 319-330.

53. Hasnain, S.M., *Review on sustainable thermal energy storage technologies, part II: cool thermal storage.* Energy Convers. Manage., 1998. **39**(11): p. 1139-1153.

54. Enibe, S., *Performance of a natural circulation solar air heating system with phase change material energy storage.* Renewable Energy, 2002. **27**(1): p. 69-86.

55. Esakkimuthu, S., et al., *Experimental investigation on phase change material based thermal storage system for solar air heating applications.* Solar Energy, 2013. **88**: p. 144-153.

56. Brown, R.C., J.D. Rasberry, and S.P. Overmann, *Microencapsulated phase-change materials as heat transfer media in gas-fluidized beds.* Powder Technol., 1998. **98**(3): p. 217-222.

57. Izquierdo-Barrientos, M.A., C. Sobrino, and J.A. Almendros-Ibáñez, *Thermal energy storage in a fluidized bed of PCM.* Chemical engineering journal, 2013. **230**: p. 573-583.

58. Hatfield, J.C., *Encapsulation of phase change materials*. 1987, Google Patents.

59. Nomura, T., et al., *Microencapsulation of metal-based phase change material for high-temperature thermal energy storage.* Scientific reports, 2015. **5**: p. 9117.

60. Abe, Y., et al., *Charge and discharge characteristics of a direct contact latent thermal energy storage unit using form-stable high-density polyethylene.* Journal of solar energy engineering, 1984. **106**(4): p. 465-474.

61. Khudhair, A.M. and M.M. Farid, *A review on energy conservation in building applications with thermal storage by latent heat using phase change materials.* Energy Conversion and Management, 2004. **45**(2): p. 263-275.

62. Castellón, C., et al., *Effect of microencapsulated phase change material in sandwich panels.* Renewable Energy, 2010. **35**(10): p. 2370-2374.

63. Navarro, L., et al., *Thermal energy storage in building integrated thermal systems: A review. Part 2. Integration as passive system.* Renewable Energy, 2016. **85**: p. 1334-1356.

64. Shang, J., Q. Li, and Z. Wang, *Preparation and thermal performance tests of microencapsulated gypsum-based phase change building material.* Taiyangneng Xuebao/Acta Energiae Solaris Sinica, 2012. **33**(12): p. 2140-2144.

65. Ma, S., et al., *UV irradiation-initiated MMA polymerization to prepare microcapsules containing phase change paraffin.* Solar Energy Materials and Solar Cells, 2010. **94**(10): p. 1643-1647.

66. Cabeza, L.F., et al., *Use of microencapsulated PCM in concrete walls for energy savings.* Energy and Buildings, 2007. **39**(2): p. 113-119.

67. Park, S.-K., et al., *Development of anti-fungal mortar and concrete using Zeolite and Zeocarbon microcapsules.* Cement and Concrete Composites, 2009. **31**(7): p. 447-453.

68. Hunger, M., et al., *The behavior of self-compacting concrete containing micro-encapsulated phase change materials.* Cement and Concrete Composites, 2009. **31**(10): p. 731-743.

69. Fenollera, M., et al., *The Influence of Phase Change Materials on the Properties of Self-Compacting Concrete.* Materials, 2013. **6**(8): p. 3530.

70. Kuznik, F. and J. Virgone, *Experimental assessment of a phase change material for wall building use.* Applied Energy, 2009. **86**(10): p. 2038-2046.

71. Sanchez, P., et al., *Development of thermo-regulating textiles using paraffin wax microcapsules.* Thermochimica Acta. **498**(1-2): p. 16-21.

72. Alay, S., F. Göde, and C. Alkan, *Synthesis and thermal properties of poly(n-butyl acrylate)/n-hexadecane microcapsules using different cross-linkers and their application to textile fabrics.* Journal of Applied Polymer Science, 2011. **120**(5): p. 2821-2829.

73. Wang, S.X., et al., *Effect of phase-change material on energy consumption of intelligent thermal-protective clothing.* Polymer Testing, 2006. **25**(5): p. 580-587.

74. Nelson, G., *Application of microencapsulation in textiles.* International Journal of Pharmaceutics, 2002. **242**(1â€“2): p. 55-62.

75. Inaba, H., *New challenge in advanced thermal energy transportation using functionally thermal fluids.* International Journal of Thermal Sciences, 2000. **39**(9): p. 991-1003.

76. Lu, W. and S.A. Tassou, *Experimental study of the thermal characteristics of phase change slurries for active cooling.* Applied Energy, 2012. **91**(1): p. 366-374.

77. Kaizawa, A., et al., *Thermal and flow behaviors in heat transportation container using phase change material.* Energy Conversion and Management, 2008. **49**(4): p. 698-706.

78. Buttitta, G., G. Serale, and Y. Cascone, *Enthalpy-temperature Evaluation of Slurry Phase Change Materials with T-history Method.* Energy Procedia, 2015. **78**: p. 1877-1882.

79. Mulligan, J.C., D.P. Colvin, and Y.G. Bryant, *Microencapsulated phase-change material suspensions for heat transfer in spacecraft thermal systems.* Journal of Spacecraft and Rockets, 1996. **33**(2): p. 278-284.

80. Velraj, R., et al., *Heat transfer enhancement in a latent heat storage system.* Sol. Energy, 1999. **65**(3): p. 171-180.

81. Shibutani, S. *PCM micro-capsule slurry thermal storage system for cooling in narita airport*. in *3rd Workshop of the IEA ECES IA Annex*. 2002.

82. Griffiths, P.W. and P.C. Eames, *Performance of chilled ceiling panels using phase change material slurries as the heat transport medium.* Appl. Therm. Eng., 2007. **27**(10): p. 1756-1760.

83. Yamagishi, Y., et al., *An evaluation of microencapsulated PCM for use in cold energy transportation medium.* Proc. Intersoc. Energy Convers. Eng. Conf., 1996. **31st**: p. 2077-2083.

84. Yamagishi, Y., et al., *Characteristics of microencapsulated PCM slurry as a heat - transfer fluid.* AIChE Journal, 1999. **45**(4): p. 696-707.

85. Chen, Z. and G. Fang, *Preparation and heat transfer characteristics of microencapsulated phase change material slurry: A review.* Renewable and Sustainable Energy Reviews, 2011. **15**(9): p. 4624-4632.

86. Delgado, M., et al., *Experimental analysis of a microencapsulated PCM slurry as thermal storage system and as heat transfer fluid in laminar flow.* Applied Thermal Engineering, 2012. **36**: p. 370-377.

87. Özonur, Y., et al., *Microencapsulation of coco fatty acid mixture for thermal energy storage with phase change material.* International Journal of Energy Research, 2006. **30**(10): p. 741-749.

88. Himran, S., A. Suwono, and G.A. Mansoori, *Characterization of alkanes and paraffin waxes for application as phase change energy storage medium.* Energy Sources, 1994. **16**(1): p. 117-28.

89. Zhao, C.Y. and G.H. Zhang, *Review on microencapsulated phase change materials (MEPCMs): Fabrication, characterization and applications.* Renewable and Sustainable Energy Reviews. **15**(8): p. 3813-3832.

90. Alkan, C., A. Sarı, and A. Karaipekli, *Preparation, thermal properties and thermal reliability of microencapsulated n-eicosane as novel phase change material for thermal energy storage.* Energy Conversion and Management, 2011. **52**(1): p. 687-692.

91. Sharma, A., et al., *Review on thermal energy storage with phase change materials and applications.* Renewable and Sustainable Energy Reviews, 2009. **13**(2): p. 318-345.

92. Farid, M.M., et al., *A review on phase change energy storage: materials and applications.* Energy Conversion and Management, 2004. **45**(9): p. 1597-1615.

93. Mondal, S., *Phase change materials for smart textiles ： An overview.* Applied Thermal Engineering, 2008. **28**(11 （12）): p. 1536-1550.

94. Yuan, Y., et al., *Fatty acids as phase change materials: A review.* Renewable and Sustainable Energy Reviews, 2014. **29**: p. 482-498.

95. Sarı, A., *Eutectic mixtures of some fatty acids for low temperature solar heating applications: Thermal properties and thermal reliability.* Applied Thermal Engineering, 2005. **25**(14-15): p. 2100-2107.

96. Herrmann, U. and D. Kearney, *Survey of Thermal Energy Storage for Parabolic Trough Power Plants.* Journal of Solar Energy Engineering, 2002. **124**(2): p. 145-152.

97. Fabien, S., *The Manufacture of Microencapsulated Thermal Energy Storage Compounds Suitablefor Smart Textile*, in *Developments in Heat Transfer*, D.M. Aurelio, Editor. 2011, InTech.

98. Harini, K., A. Leena, and V.R.G. Dev, *Microencapsulation and its application.* Synth. Fibres, 2007. **36**(1): p. 21-28.

99. Huang, H.J., X.D. Chen, and W.K. Yuan, *Microencapsulation based on emulsification for producing pharmaceutical products: A literature review.* Developments in Chemical Engineering and Mineral Processing, 2006. **14**(3-4): p. 515-544.

100. Jamekhorshid, A., S.M. Sadrameli, and M. Farid, *A review of microencapsulation methods of phase change materials (PCMs) as a thermal energy storage (TES) medium.* Renewable and Sustainable Energy Reviews, 2014. **31**: p. 531-542.

101. Jyothi, N.V., et al., *Microencapsulation techniques, factors influencing encapsulation efficiency.* J Microencapsul, 2010. **27**(3): p. 187-97.

102. Borreguero, A.M., et al., *Synthesis and characterization of microcapsules containing Rubitherm®RT27 obtained by spray drying.* Chemical Engineering Journal. **166**(1): p. 384-390.

103. Rosenberg, M., I.J. Kopelman, and Y. Talmon, *Factors affecting retention in spray-drying microencapsulation of volatile materials.* Journal of Agricultural and Food Chemistry, 1990. **38**(5): p. 1288-1294.

104. Hawlader, M.N.A., M.S. Uddin, and M.M. Khin, *Microencapsulated PCM thermal-energy storage system.* Applied Energy, 2003. **74**(1): p. 195-202.

105. Pielichowska, K. and K. Pielichowski, *Biodegradable PEO/cellulose-based solid–solid phase change materials.* Polymers for Advanced Technologies, 2011. **22**(12): p. 1633-1641.

106. Liang, X.-H., et al., *Crystalline-amorphous phase transition of poly (ethylene glycol)/cellulose blend.* Macromolecules, 1995. **28**(19): p. 6551-6555.

107. Alkan, C., A. Sari, and O. Uzun, *Poly(ethylene glycol)/acrylic polymer blends for latent heat thermal energy storage.* AIChE Journal, 2006. **52**(9): p. 3310-3314.

108. Borreguero, A.M., et al., *Synthesis and characterization of microcapsules containing Rubitherm®RT27 obtained by spray drying.* Chemical Engineering Journal, 2011. **166**(1): p. 384-390.

109. Wurster, D.E., *Granulating and coating process for uniform granules*. 1963, Google Patents.

110. Wurster, D.E., *Means for applying coatings to tablets or the like*. 1957, Google Patents.

111. Wurster, D.E. and J.A. Lindlof, *Particle coating apparatus*. 1966, Google Patents.

112. Chavarri, M., I. Maranon, and M. Carmen, *Encapsulation Technology to Protect Probiotic Bacteria.* 2012.

113. Chen, J.C. and J.L. Eichelberger, *Method for preparing encapsulated phase change materials*. 1985, Google Patents.

114. Cho, J.-S., A. Kwon, and C.-G. Cho, *Microencapsulation of octadecane as a phase-change material by interfacial polymerization in an emulsion system.* Colloid Polym. Sci., 2002. **280**(3): p. 260-266.

115. Wei, J., et al., *Preparation and characterization of novel polyamide paraffin MEPCM by interfacial polymerization technique.* Journal of Applied Polymer Science, 2013. **127**(6): p. 4588-4593.

116. Lone, S., et al., *Facile and highly efficient microencapsulation of a phase change material using tubular microfluidics.* Colloids and Surfaces A: Physicochemical and Engineering Aspects, 2013. **422**: p. 61-67.

117. Zhang, H. and X. Wang, *Fabrication and performances of microencapsulated phase change materials based on n-octadecane core and resorcinol-modified melamine–formaldehyde shell.* Colloids and Surfaces A: Physicochemical and Engineering Aspects, 2009. **332**(2-3): p. 129-138.

118. Fang, G., et al., *Preparation and characterization of nano-encapsulated n-tetradecane as phase change material for thermal energy storage.* Chem. Eng. J. (Amsterdam, Neth.), 2009. **153**(1-3): p. 217-221.

119. Sarier, N. and E. Onder, *The manufacture of microencapsulated phase change materials suitable for the design of thermally enhanced fabrics.* Thermochimica Acta, 2007. **452**(2): p. 149-160.

120. Suzuki, T., T. Mizowaki, and M. Okubo, *Versatile synthesis of high performance, crosslinked polymer microcapsules with encapsulated n-hexadecane as heat storage materials by utilizing microsuspension controlled/living radical polymerization (ms CLRP) of ethylene glycol dimethacrylate with the SaPSeP method.* Polymer, 2016. **106**(Supplement C): p. 182-188.

121. Chaiyasat, P., et al., *Innovative synthesis of high performance poly(methyl methacrylate) microcapsules with encapsulated heat storage material by microsuspension iodine transfer polymerization (ms ITP).* Solar Energy Materials and Solar Cells, 2016. **157**: p. 996-1003.

122. Ma, Y., et al., *Preparation and thermal reliabilities of microencapsulated phase change materials with binary cores and acrylate-based polymer shells.* Thermochimica Acta, 2014. **588**: p. 38-46.

123. Alkan, C., A. Sari, and A. Karaipekli, *Preparation, thermal properties and thermal reliability of microencapsulated n-eicosane as novel phase change material for thermal energy storage.* Energy Convers. Manage., 2010. **52**(1): p. 687-692.

124. Yin, D., et al., *Pickering emulsion: A novel template for microencapsulated phase change materials with polymerâ€“silica hybrid shell.* Energy. **64**(0): p. 575-581.

125. Janssen, L.J.J.M. and K. te Nijenhuis, *Encapsulation by interfacial polycondensation. II. The membrane wall structure and the rate of the wall growth.* Journal of Membrane Science, 1992. **65**(1): p. 69-75.

126. Saihi, D., et al., *Microencapsulation of ammonium phosphate with a polyurethane shell. Part II. Interfacial polymerization technique.* Reactive and Functional Polymers, 2006. **66**(10): p. 1118-1125.

127. Yadav, S.K., A.K. Suresh, and K.C. Khilar, *Microencapsulation in polyurea shell by interfacial polycondensation.* AIChE Journal, 1990. **36**(3): p. 431-438.

128. Cho, J.-S., A. Kwon, and C.-G. Cho, *Microencapsulation of octadecane as a phase-change material by interfacial polymerization in an emulsion system.* Colloid and Polymer Science, 2002. **280**(3): p. 260-266.

129. Su, J., L. Wang, and L. Ren, *Fabrication and thermal properties of microPCMs: used melamine-formaldehyde resin as shell material.* J. Appl. Polym. Sci., 2006. **101**(3): p. 1522-1528.

130. Zhang, X.X., et al., *Expansion space and thermal stability of microencapsulated n-octadecane.* Journal of Applied Polymer Science, 2005. **97**(1): p. 390-396.

131. Salaün, F., et al., *Influence of process parameters on microcapsules loaded with n-hexadecane prepared by in situ polymerization.* Chemical Engineering Journal, 2009. **155**(1-2): p. 457-465.

132. Choi, J.-k., et al., *Preparation of microcapsules containing phase change materials as heat transfer media by in-situ polymerization.* J. Ind. Eng. Chem. (Seoul, Repub. Korea), 2001. **7**(6): p. 358-362.

133. Sanchez-Silva, L., J.F. Rodriguez, and P. Sanchez, *Influence of different suspension stabilizers on the preparation of Rubitherm RT31 microcapsules.* Colloids and Surfaces A: Physicochemical and Engineering Aspects. **390**(1-3): p. 62-66.

134. Cunningham, M.F., *Microsuspension Polymerization of Methyl Methacrylate.* Polymer Reaction Engineering, 1999. **7**(2): p. 231-257.

135. Okubo, M., H. Yonehara, and T. Kurino, *Influence of viscosity within polymerizing particle on the morphology of micron-sized, monodisperse composite polymer particles produced by seeded polymerization for the dispersion of highly monomer-swollen polymer particles.* Colloid & Polymer Science, 2003. **281**(10): p. 1002-1005.

136. Chaiyasat, P., et al., *Synthesis of micrometer-sized poly(methyl methacrylate) particles by microsuspension iodine transfer polymerization (ms ITP).* RSC Adv., 2016. **6**(97): p. 95062-95066.

137. Werts, M.P.L., et al., *Titanium Dioxide−Polymer Core–Shell Particles Dispersions as Electronic Inks for Electrophoretic Displays.* Chemistry of Materials, 2008. **20**(4): p. 1292-1298.

138. Shao-Hai, F. and F. Kuan-Jun, *Preparation of styrene-maleic acid copolymers and its application in encapsulated pigment red 122 dispersion.* Journal of Applied Polymer Science, 2007. **105**(2): p. 317-321.

139. Chaiyasat, P., et al., *Influence of water domain formed in hexadecane core inside cross-linked capsule particle on thermal properties for heat storage application.* Colloid and Polymer Science, 2008. **286**(6): p. 753-759.

140. Qiu, J., B. Charleux, and K. Matyjaszewski, *Controlled/living radical polymerization in aqueous media: homogeneous and heterogeneous systems.* Prog. Polym. Sci., 2001. **26**(10): p. 2083-2134.

141. McDonald, C.J., et al., *Emulsion Polymerization of Voided Particles by Encapsulation of a Nonsolvent.* Macromolecules, 2000. **33**(5): p. 1593-1605.

142. Sarı, A., C. Alkan, and A. Karaipekli, *Preparation, characterization and thermal properties of PMMA/n-heptadecane microcapsules as novel solid–liquid microPCM for thermal energy storage.* Applied Energy, 2010. **87**(5): p. 1529-1534.

143. Yin, D., et al., *Pickering emulsion: A novel template for microencapsulated phase change materials with polymer–silica hybrid shell.* Energy, 2014. **64**: p. 575-581.

144. Luo, Y. and F.J. Schork, *Emulsion and miniemulsion polymerizations with an oil-soluble initiator in the presence and absence of an aqueous-phase radical scavenger.* J. Polym. Sci., Part A: Polym. Chem., 2002. **40**(19): p. 3200-3211.

145. Hawlader, M.N.A., M.S. Uddin, and M.M. Khin, *Microencapsulated PCM thermal-energy storage system.* Appl. Energy, 2003. **74**(1-2): p. 195-202.

146. Konuklu, Y., M. Unal, and H.O. Paksoy, *Microencapsulation of caprylic acid with different wall materials as phase change material for thermal energy storage.* Solar Energy Materials and Solar Cells, 2014. **120**: p. 536-542.

147. Yang, R., et al., *Preparation of n-tetradecane-containing microcapsules with different shell materials by phase separation method.* Solar Energy Materials and Solar Cells, 2009. **93**(10): p. 1817-1822.

148. Zhang, H., X. Wang, and D. Wu, *Silica encapsulation of n-octadecane via sol–gel process: A novel microencapsulated phase-change material with enhanced thermal conductivity and performance.* Journal of Colloid and Interface Science, 2010. **343**(1): p. 246-255.

149. He, F., X. Wang, and D. Wu, *New approach for sol–gel synthesis of microencapsulated n-octadecane phase change material with silica wall using sodium silicate precursor.* Energy, 2014. **67**: p. 223-233.

150. Li, M., Z. Wu, and J. Tan, *Properties of form-stable paraffin/silicon dioxide/expanded graphite phase change composites prepared by sol–gel method.* Applied Energy, 2012. **92**: p. 456-461.

151. Chen, Z., et al., *Preparation and characteristics of microencapsulated stearic acid as composite thermal energy storage material in buildings.* Energy and Buildings, 2013. **62**: p. 469-474.

152. Bungenberg de Jong, H. and H. Kruyt, *Coacervation (partial miscibility in colloid systems).* Proc Koninklijke Nederlandse Akademie Wetenschappen, 1929. **32**: p. 849-856.

153. Arshady, R., *Microspheres and microcapsules, a survey of manufacturing techniques Part II: Coacervation.* Polymer Engineering & Science, 1990. **30**(15): p. 905-914.

154. Bayes-Garcia, L., et al., *Phase Change Materials (PCM) microcapsules with different shell compositions: Preparation, characterization and thermal stability.* Solar Energy Materials and Solar Cells. **94**(7): p. 1235-1240.

155. Bhattacharyya, A. and J. Argillier, *Microencapsulation by complex coacervation: effect of cationic surfactants.* Journal of Surface Science and Technology, 2005. **21**(3/4): p. 161.

156. Kaibara, K., et al., *pH-Induced Coacervation in Complexes of Bovine Serum Albumin and Cationic Polyelectrolytes.* Biomacromolecules, 2000. **1**(1): p. 100-107.

157. Kizilay, E., A.B. Kayitmazer, and P.L. Dubin, *Complexation and coacervation of polyelectrolytes with oppositely charged colloids.* Adv Colloid Interface Sci, 2011. **167**(1-2): p. 24-37.

158. Mayya, K.S., A. Bhattacharyya, and J.F. Argillier, *Micro-encapsulation by complex coacervation: influence of surfactant.* Polymer International, 2003. **52**(4): p. 644-647.

159. Remuñán-López, C. and R. Bodmeier, *Effect of formulation and process variables on the formation of chitosan-gelatin coacervates.* International Journal of Pharmaceutics, 1996. **135**(1–2): p. 63-72.

160. Shin, Y., K. Son, and E. Cho, *Preparation and characterization of microcapsules by coacervation for development of thermoregulating textile materials with microencapsulated phase change materials.* J. Korean Fiber Soc., 2002. **39**(2): p. 224-232.

161. Takenaka, H., Y. Kawashima, and S.Y. Lin, *Micromeritic properties of sulfamethoxazole microcapsules prepared by gelatin–acacia coacervation.* Journal of Pharmaceutical Sciences, 1980. **69**(5): p. 513-516.

162. Tokumitsu, H., H. Ichikawa, and Y. Fukumori, *Chitosan-gadopentetic acid complex nanoparticles for gadolinium neutron-capture therapy of cancer: preparation by novel emulsion-droplet coalescence technique and characterization.* Pharm Res, 1999. **16**(12): p. 1830-5.

163. Pesa, H.S. and S. Lowell, *Pressure sensitive transfer record sheet*. 1960, Google Patents.

164. Teixeira, C.S.N.R., et al., *Characterization and evaluation of commercial fragrance microcapsules for textile application.* The Journal of The Textile Institute. **103**(3): p. 269-282.

165. Mi, F.-L., H.-W. Sung, and S.-S. Shyu, *Drug release from chitosan–alginate complex beads reinforced by a naturally occurring cross-linking agent.* Carbohydrate Polymers, 2002. **48**(1): p. 61-72.

166. Loxley, A. and B. Vincent, *Preparation of poly(methyl methacrylate) microcapsules with liquid cores.* J. Colloid Interface Sci., 1998. **208**(1): p. 49-62.

167. Zhang, Y., et al., *Preparation and Thermal Property of Phase Change Material Microcapsules by Phase Separation.* Materials Science Forum, 2007. **561-565**: p. 2293-2296.

168. Ciriminna, R., et al., *From molecules to systems: Sol− gel microencapsulation in silica-based materials.* Chemical reviews, 2010. **111**(2): p. 765-789.

169. Sasaguchi, K. and R. Viskanta, *Phase Change Heat Transfer During Melting and Resolidification of Melt Around Cylindrical Heat.* Journal of energy resources technology, 1989. **111**: p. 43.

170. Fang, G., Z. Chen, and H. Li, *Synthesis and properties of microencapsulated paraffin composites with SiO2 shell as thermal energy storage materials.* Chemical Engineering Journal, 2010. **163**(1): p. 154-159.

171. Gelderblom, H., et al., *Cremophor EL: the drawbacks and advantages of vehicle selection for drug formulation.* European Journal of Cancer, 2001. **37**(13): p. 1590-1598.

172. Kasaai, M.R., J. Arul, and G. Charlet, *Intrinsic viscosity–molecular weight relationship for chitosan.* Journal of Polymer Science Part B: Polymer Physics, 2000. **38**(19): p. 2591-2598.

173. Ho, K.M., et al., *Mechanistic study of the formation of amphiphilic core–shell particles by grafting methyl methacrylate from polyethylenimine through emulsion polymerization.* Polymer, 2010. **51**(15): p. 3512-3519.

174. Ye, W., et al., *Novel core-shell particles with poly(n-butyl acrylate) cores and chitosan shells as an antibacterial coating for textiles.* Polymer, 2005. **46**(23): p. 10538-10543.

175. Ye, W., et al., *Durable antibacterial finish on cotton fabric by using chitosan-based polymeric core-shell particles.* Journal of Applied Polymer Science, 2006. **102**(2): p. 1787-1793.

176. Ho, K.M., et al., *Amphiphilic polymeric particles with core–shell nanostructures: emulsion-based syntheses and potential applications.* Colloid and Polymer Science, 2010. **288**(16): p. 1503-1523.

177. *Glass Transition*, in *Encyclopedia of Polymer Science and Technology*.

178. Kaptay, G., *On the equation of the maximum capillary pressure induced by solid particles to stabilize emulsions and foams and on the emulsion stability diagrams.* Colloids and Surfaces A: Physicochemical and Engineering Aspects, 2006. **282-283**: p. 387-401.

179. Tang, J., et al., *Dual Responsive Pickering Emulsion Stabilized by Poly[2-(dimethylamino)ethyl methacrylate] Grafted Cellulose Nanocrystals.* Biomacromolecules, 2014. **15**(8): p. 3052-3060.

180. Monteiro, O.A.C. and C. Airoldi, *Some studies of crosslinking chitosan–glutaraldehyde interaction in a homogeneous system.* International Journal of Biological Macromolecules, 1999. **26**(2): p. 119-128.

181. Migneault, I., et al., *Glutaraldehyde: behavior in aqueous solution, reaction with proteins, and application to enzyme crosslinking.* Biotechniques, 2004. **37**(5): p. 790-6, 798-802.

182. Rietjens, M. and P.A. Steenbergen, *Crosslinking Mechanism of Boric Acid with Diols Revisited.* European Journal of Inorganic Chemistry, 2005. **2005**(6): p. 1162-1174.

183. Manna, U. and S. Patil, *Borax Mediated Layer-by-Layer Self-Assembly of Neutral Poly(vinyl alcohol) and Chitosan.* The Journal of Physical Chemistry B, 2009. **113**(27): p. 9137-9142.

184. Jia, W.-T., et al., *Novel borate glass/chitosan composite as a delivery vehicle for teicoplanin in the treatment of chronic osteomyelitis.* Acta biomaterialia, 2010. **6**(3): p. 812-819.

185. Saita, K., et al., *Preparation and characterization of dispersible chitosan particles with borate crosslinking and their antimicrobial and antifungal activity.* Carbohydrate research, 2012. **349**: p. 52-58.

186. Chudzikowski, R., *Guar gum and its applications.* J Soc Cosmet Chem, 1971. **22**: p. 43-60.

187. Sreedhar, B., et al., *Thermal, mechanical, and surface characterization of starch–poly(vinyl alcohol) blends and borax-crosslinked films.* Journal of Applied Polymer Science, 2005. **96**(4): p. 1313-1322.

188. Sabarudin, A., et al., *Synthesis of cross-linked chitosan possessing N-methyl-d-glucamine moiety (CCTS-NMDG) for adsorption/concentration of boron in water samples and its accurate measurement by ICP-MS and ICP-AES.* Talanta, 2005. **66**(1): p. 136-144.

189. Mi, F.-L., et al., *Chitosan–polyelectrolyte complexation for the preparation of gel beads and controlled release of anticancer drug. II. Effect of pH-dependent ionic crosslinking or interpolymer complex using tripolyphosphate or polyphosphate as reagent.* Journal of Applied Polymer Science, 1999. **74**(5): p. 1093-1107.

190. Shu, X. and K. Zhu, *Chitosan/gelatin microspheres prepared by modified emulsification and ionotropic gelation.* Journal of microencapsulation, 2001. **18**(2): p. 237-245.

191. Hasanovic, A., et al., *Chitosan-tripolyphosphate nanoparticles as a possible skin drug delivery system for aciclovir with enhanced stability.* J Pharm Pharmacol, 2009. **61**(12): p. 1609-16.

192. Bhumkar, D.R. and V.B. Pokharkar, *Studies on effect of pH on cross-linking of chitosan with sodium tripolyphosphate: A technical note.* AAPS PharmSciTech, 2006. **7**(2): p. E138-E143.

193. *More about bulk and tapped density*. 2017/8/08]; Available from: http://particle.dk/methods-analytical-laboratory/bulk-and-tapped-density/more-about-bulk-and-tapped-density/.

194. Wang, Q.Z., et al., *Protonation constants of chitosan with different molecular weight and degree of deacetylation.* Carbohydrate Polymers, 2006. **65**(2): p. 194-201.

195. Ho, B.-C., Y.-D. Lee, and W.-K. Chin, *Thermal degradation of polymethacrylic acid.* Journal of Polymer Science Part A: Polymer Chemistry, 1992. **30**(11): p. 2389-2397.

196. Schild, H.G., *Thermal degradation of poly(methacrylic acid): Further studies applying TGA/FTIR.* Journal of Polymer Science Part A: Polymer Chemistry, 1993. **31**(9): p. 2403-2405.

197. Roberts, G.A. and K.E. Taylor, *Chitosan gels, 3. The formation of gels by reaction of chitosan with glutaraldehyde.* Macromolecular Chemistry and Physics, 1989. **190**(5): p. 951-960.

198. Beppu, M., et al., *Crosslinking of chitosan membranes using glutaraldehyde: Effect on ion permeability and water absorption.* Journal of membrane science, 2007. **301**(1): p. 126-130.

199. Kil'deeva, N.R., et al., *Mechanism of the reaction of glutaraldehyde with chitosan.* Bioorg Khim, 2009. **35**(3): p. 397-407.

200. Monteiro, O.A. and C. Airoldi, *Some studies of crosslinking chitosan–glutaraldehyde interaction in a homogeneous system.* International Journal of Biological Macromolecules, 1999. **26**(2): p. 119-128.

201. Zhang, X.-x., et al., *Crystallization and prevention of supercooling of microencapsulated n-alkanes.* J. Colloid Interface Sci., 2005. **281**(2): p. 299-306.

202. Nan, G.-h., et al., *Preparation and properties of nanoencapsulated phase change materials containing polyaniline.* Wuli Huaxue Xuebao, 2014. **30**(2): p. 338-344.

203. Fan, Y.F., et al., *Super-cooling prevention of microencapsulated phase change material.* Thermochim. Acta, 2004. **413**(1-2): p. 1-6.

204. Alvarado, J.L., et al., *Characterization of supercooling suppression of microencapsulated phase change material by using DSC.* J. Therm. Anal. Calorim., 2006. **86**(2): p. 505-509.

205. Hopwood, D., C. Allen, and M. McCabe, *The reactions between glutaraldehyde and various proteins. An investigation of their kinetics.* The Histochemical Journal, 1970. **2**(2): p. 137-150.

206. Jiang, K., et al., *Effect of Geometrical Confinement on the Nucleation and Crystallization Behavior of n-Alkane Mixtures.* The Journal of Physical Chemistry B, 2008. **112**(51): p. 16485-16489.

207. Hu, Y., et al., *Synthesis and characterization of chitosan–poly(acrylic acid) nanoparticles.* Biomaterials, 2002. **23**(15): p. 3193-3201.

208. Ahn, J.-S., H.-K. Choi, and C.-S. Cho, *A novel mucoadhesive polymer prepared by template polymerization of acrylic acid in the presence of chitosan.* Biomaterials, 2001. **22**(9): p. 923-928.

209. Jeong, S.-G., et al., *Optimal preparation of PCM/diatomite composites for enhancing thermal properties.* International Journal of Heat and Mass Transfer, 2013. **62**: p. 711-717.

210. Ford, T.J., *Liquid-phase thermal decomposition of hexadecane: reaction mechanisms.* Industrial & Engineering Chemistry Fundamentals, 1986. **25**(2): p. 240-243.

211. Alisetti, E.L. and S.K. Roy, *Forced convection heat transfer to phase change material slurries in circular ducts.* J. Thermophys. Heat Transfer, 2000. **14**(1): p. 115-118.

212. Alvarado, J.L., et al., *Thermal performance of microencapsulated phase change material slurry in turbulent flow under constant heat flux.* International Journal of Heat and Mass Transfer, 2007. **50**(9-10): p. 1938-1952.

213. Wu, W., et al., *Jet impingement and spray cooling using slurry of nanoencapsulated phase change materials.* Int. J. Heat Mass Transfer, 2011. **54**(13-14): p. 2715-2723.

214. Keblinski, P., J.A. Eastman, and D.G. Cahill, *Nanofluids for thermal transport.* Mater. Today (Oxford, U. K.), 2005. **8**(6): p. 36-44.

215. Sukhorukov, G., A. Fery, and H. Moehwald, *Intelligent micro- and nanocapsules.* Prog. Polym. Sci., 2005. **30**(8-9): p. 885-897.

216. Karlberg, A.T., K. Magnusson, and U. Nilsson, *Air oxidation of d -limonene (the citrus solvent) creates potent allergens.* Contact Dermatitis, 1992. **26**(5): p. 332-340.